ABSTRACT

NOVEL MULTIUSER DETECTION AND MULTI-RATE SCHEMES FOR MULTI-CARRIER CDMA

by
Pingping Zong

A large variety of services is expected for wireless systems, in particular, high data rate services, such as wireless Internet access. Users with different data rates and quality of service (QoS) requirements must be accommodated. A suitable multiple access scheme is key to enabling wireless systems to support both the high data rate and the integrated multiple data rate transmissions with satisfactory performance and flexibility. A multi-carrier code division multiple access (MC-CDMA) scheme is a promising candidate for emerging broadband wireless systems. MC-CDMA is a hybrid of orthogonal frequency division multiplexing (OFDM) and code division multiple access (CDMA). The most salient feature of MC-CDMA is that the rate of transmission is not limited by the wireless channel's frequency-selective fading effects caused by multipath propagation. In MC-CDMA, each chip of the desired user's spreading code, multiplied by the current data bit, is modulated onto a separate subcarrier. Therefore, each subcarrier has a narrow bandwidth and undergoes frequency-flat fading. Two important issues for an MC-CDMA wireless system, multiuser detection and multi-rate access, are discussed in this dissertation.

Several advanced receiver structures capable of suppressing multiuser interference in an uplink MC-CDMA system, operating in a frequency-selective fading channel, are studied in this dissertation. One receiver is based on a so-called multi-shot structure, in which the interference introduced by the asynchronous reception of different users is successfully suppressed by a receiver based on the minimum mean-square error (MMSE) criterion with a built-in de-biasing feature. Like many other multiuser schemes, this receiver is very sensitive to a delay estimation error. A

blind adaptive two-stage decorrelating receiver based on the "bootstrap algorithm" is developed to combat severe performance degradation due to a delay estimation error. It is observed that in the presence of a delay estimation error the blind adaptive bootstrap receiver is more near-far resistant than the MMSE receiver. Furthermore, a differential bootstrap receiver is proposed to extend the limited operating range of the two-stage bootstrap receiver which suffers from a phase ambiguity problem.

Another receiver is based on a partial sampling (PS) demodulation structure, which further reduces the sensitivity to unknown user delays in an uplink scenario. Using this partial sampling structure, it is no longer necessary to synchronize the receiver with the desired user. Following the partial sampling demodulator, a minimum mean-square error combining (MMSEC) detector is applied. The partial sampling MMSEC (PS-MMSEC) receiver is shown to have strong interference suppression and timing acquisition capabilities. The complexity of this receiver can be reduced significantly, with negligible performance loss, by choosing a suitable partial sampling rate and using a structure called reduced complexity PS-MMSEC (RPS-MMSEC). The adaptive implementation of these receivers yields a superior rate of convergence and symbol error rate performance in comparison to a conventional MMSEC receiver with known timing.

All the above receiver structures are for a single-rate MC-CDMA. Three novel multi-rate access schemes for multi-rate MC-CDMA, fixed spreading length (FSL), coded FSL (CFSL) and variable spreading length (VSL), have been developed. These multi-rate access schemes enable users to transmit information at different data rates in one MC-CDMA system. Hence, voice, data, image and video can be transmitted seamlessly through a wireless infrastructure. The bit error rate performance of these schemes is investigated for both low-rate and high-rate users.

NOVEL MULTIUSER DETECTION AND MULTI-RATE SCHEMES FOR MULTI-CARRIER CDMA

by
Pingping Zong

A Dissertatation
Submitted to the Faculty of
New Jersey Institute of Technology
in Partial Fulfillment of the Requirements for the Degree of
Doctor of Philosophy in Electrical Engineering

Department of Electrical and Computer Engineering

May 2001

APPROVAL PAGE

NOVEL MULTIUSER DETECTION AND MULTI-RATE SCHEMES FOR MULTI-CARRIER CDMA

Pingping Zong

Dr. Yeheskel Bar-Ness, Dissertation Advisor — Date
Distinguished Professor of Electrical and Computer Engineering, NJIT

Dr. Leonard Cimini, Jr, Committee Member — Date
Member of Technical Staff, AT&T Labs Research

Dr. Hongya Ge, Committee Member — Date
Assistant Professor of Electrical and Computer Engineering, NJIT

Dr. Alexander Haimovich, Committee Member — Date
Associate Professor of Electrical and Computer Engineering, NJIT

Dr. Zoi-Heleni Michalopoulou, Committee Member — Date
Associate Professor of Mathematics, NJIT

BIOGRAPHICAL SKETCH

Author: Pingping Zong

Degree: Doctor of Philosophy

Date: May, 2001

Undergraduate and Graduate Education:

- Doctor of Philosophy in Electrical Engineering,
  New Jersey Institute of Technology, Newark, NJ, 2001
- Master of Science in Electrical Engineering,
  New Jersey Institute of Technology, Newark, NJ, 1998
- Bachelor of Science in Electrical Engineering,
  Beijing University of Posts and Telecommunications, Beijing, China, 1995

Major: Electrical Engineering

Presentations and Publications:

Pingping Zong, Kunjie Wang and Yeheskel Bar-Ness
"Partial Sampling MMSE Interference Suppression in Asynchronous Multi-Carrier CDMA System," to appear in the IEEE Journal on Selected Areas in Communications.

Pingping Zong and Yeheskel Bar-Ness
"Performance of a Variable Spreading Length (VSL) Dual-Rate MC-CDMA System," proceeding of the 35th Annual Conference on Information Sciences and Systems (CISS2001), Baltimore, MD, March, 2001.

Pingping Zong, Kunjie Wang and Yeheskel Bar-Ness
"A Novel Partial-Symbol MMSE Receiver for Uplink Multi-Carrier CDMA," proceeding of the IEEE Vehicular Technology Conference 2001 (VTC2001 spring), Rhodes Island, Greece, May 6-9, 2001.

Pingping Zong, Yeheskel Bar-Ness and James K. Chen
"Performance Analysis of a Dual-rate Synchronous MC-CDMA System," proceeding of the IEEE Global Telecommunications Conference (Globecom'2000), San Francisco, CA, U.S.A., Nov. 27-Dec. 3,2000.

Pingping Zong, Yeheskel Bar-Ness and James K. Chen

"Adaptive Blind Time Tracking and Multi-user Detection for Asynchronous MC-CDMA System," proceeding of the 34th Annual Conference on Information Sciences and Systems (CISS2000), Princeton, NJ, March, 2000.

Pingping Zong, Yeheskel Bar-Ness and James K. Chen

"Adaptive Multi-shot Multi-user Detection for Asynchronous MC-CDMA Using Bootstrap Algorithm," proceeding of the 2nd International Workshop on Multi-carrier Spread Spectrum (MC-SS99), Oberpfaffenhofen, Germany, Sept. 15-17, 1999.

Matthijs A. Visser, Pingping Zong and Yeheskel Bar-Ness

"A Novel Method for Blind Frequency Offset Correction in an OFDM System," proceedings of the 9th IEEE International Symposium on Personal, Indoor and Mobile Radio Communications (PIMRC'98), Boston, MA, U.S.A., pp. 816-820, Sept. 8-11, 1998.

Pingping Zong, Kunjie Wang and Yeheskel Bar-Ness

"Performance Improvement for Low-Rate Signal in a Dual-Rate MC-CDMA System with Frequency-Selective Rayleigh Fading Channel," submitted to the 4th International Symposium on Wireless Personal Multimedia Communications.

Kunjie Wang, Pingping Zong and Yeheskel Bar-Ness

"A Reduced Complexity Partial Sampling MMSE Receiver for Asynchronous MC-CDMA Systems," submitted to the IEEE Global Telecommunications Conference 2001.

To my parents

ACKNOWLEDGMENT

I would like to express my deepest gratitude to my advisor, Dr. Yeheskel Bar-Ness. His advice, guidance and insight helped me enormously throughout this research.

My gratitude is extended to Dr. Cimini, Dr. Hongya Ge, Dr. Alexander Haimovich and Dr. Michalopoulou for serving as members on the thesis committee and for their comments.

I had the pleasure of working with my colleagues at the Center for Communications and Signal Processing Research at NJIT. Their help and suggestions are appreciated and acknowledged.

Finally, I sincerely thank my parents, my brother and my sister for their support, encouragement and love. This work could not have been possible if it were not for them.

TABLE OF CONTENTS

Chapter **Page**

TABLE OF CONTENTS
(Continued)

Chapter **Page**

LIST OF FIGURES

Figure **Page**

LIST OF FIGURES
(Continued)

Figure **Page**

CHAPTER 1

INTRODUCTION

The traditional wireline system has been extended from primarily voice traffic to high data rate applications. The trend in wireless communications is to provide an infrastructure that is also capable of offering a broad range of services with the quality of the wireline system. The upcoming 3G technology, for example, has specified four generic types of services: basic and enhanced voice services, low-rate data message services, medium-rate Internet services (64-144 kb/s) and high-rate packet/circuit based network services up to 2 Mb/s [1, 2]. Higher-speed standards, IEEE802.11 and HIPERLAN for wireless local area networks (WLAN), target data rates up to 54 Mb/s and up to 150 Mb/s respectively [3, 4]. To provide such a range of services, there is a need for a new wireless system that is able to support the emerging wireless personal communication services (PCS) at both higher and multiple rates. In this dissertation, a multiple access technique that suits this concept, termed multicarrier code-division multiple access (MC-CDMA), is studied. Specifically, several multiuser detection schemes and multi-rate access structures are proposed for this MC-CDMA system.

1.1 Multicarrier Code-Division Multiple Access

Several multiple access schemes exist that allow multiple users to share a finite radio resource. Frequency division multiple access (FDMA), time division multiple access (TDMA) and code division multiple access (CDMA) are the three major multiple access techniques. In FDMA and TDMA, different users are distinguished by their frequency channel and time slot, respectively. Thus, both FDMA and TDMA have the disadvantage of a fixed system capacity due to the channel/slot preassignment.

In a CDMA system, different users are assigned orthogonal speading codes and share the same frequency spectrum all the time. The receiver performs a time correlation operation to detect the desired user by multiplying the received signal with the corresponding speading code. Due to the noise-like cross-correlation property of the speading codes, increasing the number of users in a CDMA system only raises the noise floor. Thus, this code division technique enables a soft system capacity provided that enough speading codes are available [5]. If the speading code is used in conjunction with phase-shift keying (PSK) modulation, the resulting modulated signal is called direct-sequence CDMA (DS-CDMA). DS-CDMA, however, is not suitable for very high data rate transmissions. For instance, when the data rate is in the order of 100 Mb/s, as in the asynchronous transfer mode (ATM), DS-CDMA techniques will be impractical due to severe inter-chip interference, caused by multipath propagation, and the difficulty to synchronize such a fast speading code [6].

A multi-carrier modulation (MCM) scheme was proposed for high-rate transmission. In MCM, a bit stream is converted into parallel substreams and transmitted simultaneously on different subcarriers [7]. Each substream is transmitted at a much lower rate, making the system less sensitive to the physical channel's delay spread. The overall scheme however, still maintains the original high-rate transmission rate. For a high data rate wireless system, when the signal's bit duration is comparable to the channel's delay spread, MCM is a promising approach for combating inter-symbol interference (ISI). A special form of MCM, orthogonal frequency division multiplexing (OFDM), was adopted earlier for digital audio broadcasting (DAB) and digital terrestrial television broadcasting (dTTb) in Europe [7, 8, 9]. Recently, several WLAN standards, IEEE802.11a and HIPERLAN2, have selected OFDM as their physical layer standard. In an OFDM system, parallel substreams are modulated onto subcarriers using an inverse discrete Fourier transform (IDFT) [10]. The OFDM

subcarriers are separated by the reciprocal of the symbol duration. Thus, the mutual orthogonality between subcarriers is ensured despite their overlapping spectra [11]. The densely spaced subcarriers make OFDM very spectrally efficient [12, 13].

By combining MCM and DS-CDMA techniques, various schemes, such as multi-carrier DS-CDMA (MC-DS-CDMA) [14] and multi-tone CDMA (MT-CDMA) [15] have been proposed. A hybrid of OFDM and DS-CDMA, termed multi-carrier CDMA (MC-CDMA) [16], which also has efficient frequency utilization, is considered in this dissertation. A block diagram of an MC-CDMA system is shown in Figure 1.1. In an MC-CDMA system, the original data of different users are multiplied in parallel by the chips of speading codes preassigned to the corresponding users, then added (multiplexed) together. All multiplexed chips are modulated onto different subcarriers, as in OFDM, and transmitted simultaneously. This process can be viewed as direct-sequence spreading in the frequency domain. An MC-CDMA signal has a similar frequency utilization as an OFDM signal, where each subcarrier's bandwidth is sufficiently narrow so that each subcarrier experiences frequency non-selective fading. Thus, there is no need for channel equalization in MC-CDMA. Also, by despreading the received signal in the frequency domain, an MC-CDMA receiver exploits the complete channel diversity. Conversely, in a DS-CDMA system, a RAKE receiver's capability of taking advantage of the diversity in the time domain is limited by the number of fingers in the RAKE receiver. With these prominent features, MC-CDMA becomes a promising multiple access scheme for future broadband wireless communications.

1.2 Multiuser Detection

The performance of a multiple access system is limited by the presence of multiuser interference (MUI). In a CDMA system, for example, MUI arises because of the non-zero cross-correlation between different transmitted signals. A conventional CDMA

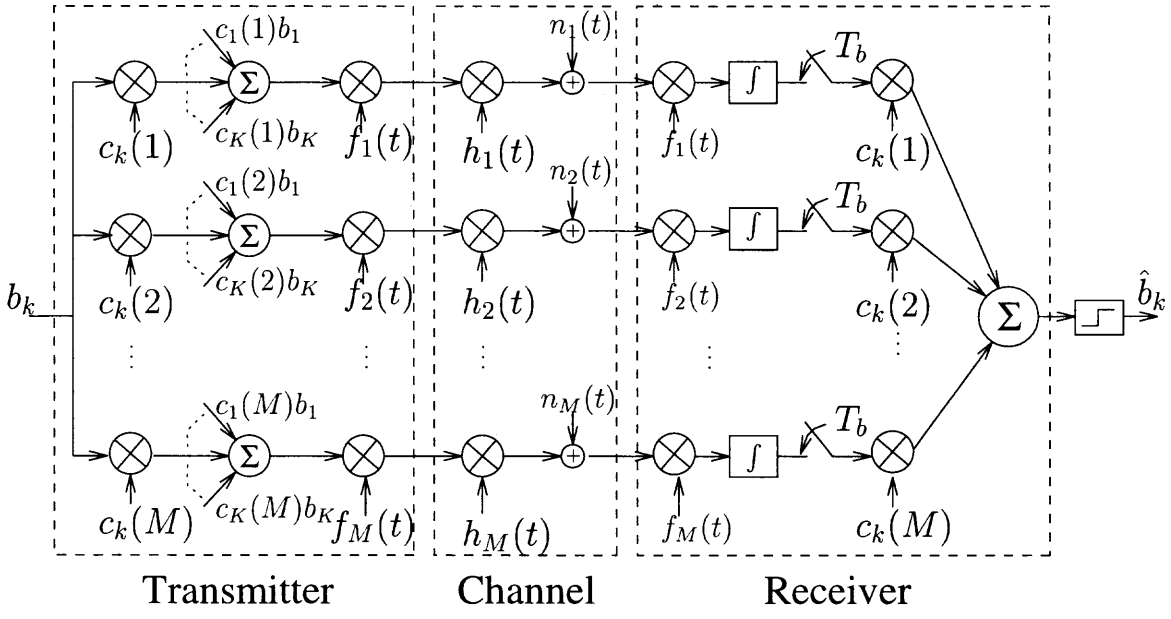

Figure 1.1 Block diagram of an MC-CDMA system.

system using a RAKE receiver requires accurate power control of all users in order to avoid the so-called near-far problem, i.e. the desired signal being buried by MUI. Sensitivity of the conventional RAKE receiver to MUI has stimulated research on enhanced multiuser receivers, which perform MUI suppression by exploiting the structure of the interference. An optimal maximum likelihood sequence detector (MLSD) was proposed in [17]. Due to its high complexity, several sub-optimal linear and non-linear multiuser detectors have been studied. In this dissertation, linear multiuser detection schemes are studied. One of the simplest linear multiuser detectors is the conventional decorrelating detector [18, 19], which uses the inverse of the correlation matrix. Another popular linear multiuser detector is based on a minimum mean-square error (MMSE) criterion [20, 21]. The MMSE multiuser detector has attracted the most interest due to the possible adaptive implementation [22, 23, 24, 25] and its ability to achieve a performance close to the single-user bound (SUB). An alternative decorrelating detector based on the "bootstrap algorithm" was proposed in [26]. The blind adaptive version of the bootstrap detector

has been shown to behave similar to the MMSE detector [27, 28]. Many of these linear multiuser detection schemes have been applied successfully to DS-CDMA or the downlink of MC-CDMA. They are adapted to function in the uplink of an MC-CDMA system for the scope of this dissertation.

Two different types of MC-CDMA receivers have been considered in the literature. One receiver first demultiplexes the received signal with a speading code to extract the transmitted information of the corresponding user. A multiuser detection stage is added to further suppress MUI [29, 30, 31]. Another receiver performs demultiplexing and multiuser detection jointly to achieve more degrees of freedom [32, 33, 34, 35, 36]. This receiver, however, requires higher complexity, as the number of coefficients is the same as the number of subcarriers, which is always greater than the number of users. Both receiver types are studied in this dissertation.

In this dissertation, the multiuser detectors are applied to an uplink scenario, where different users have different channels and asynchronous arrivals. The uplink is chosen for two reasons. First, the multiuser detection in the uplink channel is a more general and challenging problem. Second, the processing capability of the base station allows for the employment of more powerful multiuser detection techniques.

1.3 Multi-Rate Access

Wireless PCS is required to provide various data and multimedia services in addition to voice services. At the present time, most of these services are available only through wireline connections. As mentioned earlier, the 3G standard specifies four types of services with different data rates and quality of service (QoS) requirements. In order to successfully integrate these services into one seamless wireless infrastructure, it is necessary to develop a system that can operate at multiple data rates. There are several multi-rate access methodologies, such as fixed chip rate [37], fixed

processing gain [38], multi-code [39, 40] and multi-modulation [37], that have been proposed for a DS-CDMA system. These methods achieve multi-rate transmission through different means: chip rate, processing gain, number of codes and modulation format. The linear decorrelating and MMSE receivers, originally proposed for single-rate systems, have been extended to multi-rate DS-CDMA systems [41, 42, 43, 44, 45, 46].

Two different modes of multi-rate detectors, low-rate and high-rate, were proposed and investigated in [42, 43] for DS-CDMA. The detection interval of the low-rate and high-rate mode detectors are the low-rate symbol duration and the high-rate symbol duration, respectively. They perform differently for the low-rate and high-rate users and require different implementation complexity. Even though the MC-CDMA system and the DS-CDMA system have different signal structures, a multi-rate MC-CDMA system is introduced in this dissertation based on the aforementioned techniques. Three novel multi-rate access schemes are proposed and investigated for an MC-CDMA system.

1.4 Scope of the Dissertation

An MC-CDMA system is considered in this dissertation, due to its applicability to high-rate transmission, which is needed for the growing area of wireless communications. However, in comparison to DS-CDMA, MC-CDMA is more sensitive to a timing synchronization error and carrier frequency offset. Because of the densely spaced subcarriers, a small timing/frequency shift causes intercarrier interference (ICI), and hence severe performance degradation. Furthermore, as a result of a rotation of the constellation, the received signal may contain severe inter-rail interference. Previous research for multiuser detection for MC-CDMA dealt solely with a synchronous transmission scenario [16, 47, 48, 49, 50, 51]. In this dissertation, several

multiuser detection schemes, based on linear decorrelating and MMSE detectors, are studied for an asynchronous MC-CDMA system.

First, a multi-shot receiver is studied. The multi-shot structure with a finite observation window length was first proposed for an asynchronous DS-CDMA receiver [52, 53, 54, 55]. It has been shown that the performance of a multi-shot receiver asymptotically approaches that of an IIR detector. The performance of a truncated (i.e. ignoring edge-effect) and an optimal (i.e. considering edge-effect) multi-shot receiver is similar under moderate signal-to-noise ratio conditions. In this dissertation, for feasibility of implementation, only the truncated version is considered. This structure, combined with an MMSE detector, is used to combat MUI, ISI and ICI caused by the multipath channel, asynchronous reception and frequency offset. Another multi-shot structure based on a blind adaptive decorrelating detector, using the bootstrap algorithm, is also implemented. This blind multiuser detector contains two stages, which perform both interference cancellation and constellation rotation. The robustness of performance and convergence of this blind adaptive scheme is described in the presence of a delay estimation error and phase ambiguity.

Second, a partial sampling (PS) demodulation structure for the asynchronous MC-CDMA system is proposed to eliminate the timing acquisition requirement. The partial sampling method samples the received signal at a rate, which is faster than the symbol rate. It is analogous to the fractionally spaced equalizer for a single-user single-carrier system [20]. An MMSE combining (MMSEC) detector, is applied after the PS demodulation to perform robust interference suppression. In addition, the MMSEC detector may be used for timing acquisition. This receiver is termed partial sampling MMSEC (PS-MMSEC) receiver. The PS-MMSEC receiver needs an expanded observation interval to capture a complete desired symbol, because the receiver does not know the starting point of the desired symbol, which is similar

to a chip-MMSE detector for an asynchronous DS-CDMA system [56, 57]. The PS-MMSEC receiver first quantifies the observation interval into a finite set of sub-intervals regardless of the timing uncertainty of the starting point of the desired user, and then weights these sub-intervals to minimize the mean-square error of the output. In other words, the PS-MMSEC receiver finds the MMSE solution from a finite set of hypotheses. The PS-MMSEC receiver is shown to have better interference suppression capability than a conventional MMSE receiver with known timing, which samples the received signal at the symbol rate. However, the complexity of the PS-MMSEC receiver increases significantly with the number of subcarriers in comparison to the conventional symbol MMSEC receiver. In order to avoid an excessive number of taps required by the PS-MMSEC receiver, a reduced complexity PS-MMSEC (RPS-MMSEC) receiver, is proposed. This RPS-MMSEC receiver first combines the outputs of the partial sampling demodulator into several groups. As a result, the receiver complexity can be independent of the number of subcarriers, and hence be reduced dramatically. The flexible choice of complexity provides a trade-off with the performance and makes the RPS-MMSEC receiver more convenient and suitable for practical applications. Both receivers can be implemented adaptively using the least mean square (LMS) algorithm, aided by a training sequence.

The structure of the MC-CDMA signal also provides sufficient flexibility to enable multiple data rate transmission. In this dissertation, three dual-rate access methods for the MC-CDMA system are proposed and compared through their bit error rate (BER) performance. The fixed spreading length (FSL) method is a straightforward adaptation of the fixed processing gain method of DS-CDMA applied to MC-CDMA. With the FSL, users with different rates are spread by orthogonal speading codes of the same length and multicarrier modulated onto a same set of subcarriers. The subcarriers are spaced by the reciprocal of the high-rate users' bit duration, which maintains subcarrier orthogonality for both high-rate and low-rate

users. As a result, the FSL scheme does not suffer form ICI. However, this scheme introduces a loss of spectrum efficiency for the low-rate users, because the frequency separation of the adjacent subcarriers is not as small as possible. Therefore, the FSL scheme degrades the system capacity.

To improve the bandwidth efficiency, i.e. system capacity, two other dual-rate access schemes are proposed: coded FSL (CFSL) and variable spreading length (VSL). These two schemes achieve a higher system capacity through different means. The CFSL scheme increases capacity through processing in the time domain. One low-rate bit is encoded into several high-rate coded bits, hence the coding gain for the low-rate users compensates for the bandwidth efficiency loss. The VSL scheme, on the other hand, spreads and modulates users of different rates onto different sets of subcarriers with speading codes of different lengths. This introduces ICI as the subcarriers of the low-rate and high-rate users are no longer orthogonal. However, it is shown in this dissertation that a set of orthogonal speading codes with different length will remain orthogonal after being transformed by a nonorthogonal demodulator, if any sub-block of a longer speading codes is orthogonal to a shorter speading code with the same length. The performance of FSL, CFSL and VSL is evaluated, using an MMSEC receiver.

1.5 Outline

In Chapter 2, the asynchronous uplink MC-CDMA signal model is described. Also, the structures of a multi-shot MMSE receiver and a multi-shot bootstrap receiver for asynchronous MC-CDMA are developed. The effects of a timing mismatch, frequency offset and phase ambiguity of the proposed multiuser receivers are also discussed. A summary of the results has been published in conference proceedings [58, 59].

In Chapter 3, an improved MC-CDMA multiuser receiver is developed using partial sampling demodulation with an MMSEC receiver for an asynchronous

scenario. A reduced complexity structure for this scheme is also proposed. The performance of the proposed receivers is compared with the performance of the conventional symbol receiver with known timing. Issues related to the adaptive implementation of the receivers are also discussed. Results are included in [60, 61, 62].

In Chapter 4, a dual-rate MC-CDMA system with three different dual-rate access schemes mentioned in the previous section are presented. The dual-rate scheme and system can easily be adapted to fit into a multi-rate scheme and system with some small modifications. The low-rate/high-rate mode MMSEC receivers for the suggested dual-rate access schemes are illustrated together with performance comparisons. These results are included in papers [63, 64, 65].

Finally, Chapter 5 concludes the dissertation. The main results and contributions are summarized.

CHAPTER 2

MULTI-SHOT MULTIUSER DETECTION FOR ASYNCHRONOUS MC-CDMA

2.1 Signal Structure

An MC-CDMA system with K active users is considered. The same data rate is assumed for all active users, and each user's information symbol has duration T and is Ma-ary QAM modulated. For each user k, its symbol $b_k(i)$ is multiplexed with a corresponding spreading code, $\mathbf{c}_k = [c_{k1}, c_{k2}, \ldots, c_{kM}]$, $k = 1, 2, \ldots, K$. In this dissertation, the number of subcarriers is assumed to be equal to the length of the spreading code, M. That is, M multiplexed chips are modulated onto M subcarriers by a bank of oscillators. The adjacent subcarriers are separated by $\Delta f = \frac{F}{T}$, where F, which is a positive integer, is a dimensionless system parameter that determines the spacing of the subcarriers by an integer multiple of the inverse of the symbol duration. Subcarriers with this separation are orthogonal to each other:

$$\int_0^T e^{j2\pi f_m t} e^{j2\pi f_n t} = \delta(m-n). \tag{2.1}$$

When $F = 1$, the adjacent subcarriers are spaced by $\frac{1}{T}$, which represents the minimum frequency separation for orthogonality of the subcarriers. In that case, the multicarrier modulation and demodulation can be implemented by an inverse discrete Fourier transform (IDFT) and DFT operation, respectively.

In an asynchronous system, such as in uplink communications, different users will transmit their symbols with different delays, τ_k. As the symbol has duration T, any delay value larger than T can be equivalently treated by $\text{mod}(\tau_k)_T$ as a delay of value less than T that is associated with another symbol. Thus, the delays can be assumed to be uniformly distributed in $[0, T)$. Without loss of generality, the K active users are assumed to be numbered according to their transmission delays, i.e. $0 \leq \tau_1 \leq \tau_2 \leq \ldots \leq \tau_K < T$. A block diagram of an uplink MC-CDMA system is shown in Figure 2.1.

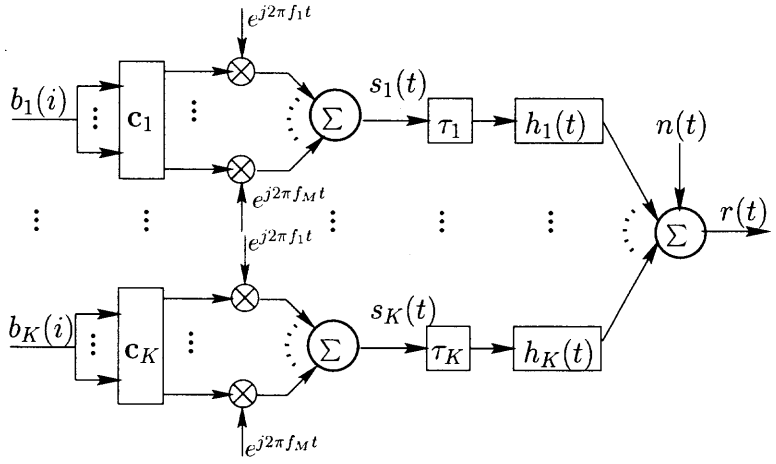

Figure 2.1 Block diagram of an uplink MC-CDMA system.

The continuous baseband waveform of the received signal can be described by

$$r(t) = \sum_{i=-\infty}^{+\infty} \sum_{k=1}^{K} \sqrt{a_k} b_k(i) P(t - iT - \tau_k) \sum_{m=1}^{M} c_{km} h_{km} e^{j2\pi f_m (t-\tau_k)} + n(t) \tag{2.2}$$

where $b_k(i)$ denotes the kth user's ith information symbol, a_k is its transmission power, $c_{km} = \pm\frac{1}{\sqrt{M}}$, $m = 1, \ldots, M$, is the mth chip of the kth user's spreading code $\mathbf{c}_k$, $n(t)$ is a complex white Gaussian noise process with zero mean and variance σ_n^2 and $P(t)$ is a normalized rectangular pulse shape waveform shown as,

$$P(t) = \begin{cases} \frac{1}{\sqrt{T}} & 0 \leq t < T \\ 0 & otherwise \end{cases} \tag{2.3}$$

Also, in equation (2.2),

$$h_{km} = \beta_{km} e^{j\theta_{km}} \tag{2.4}$$

is the channel fading factor of the kth user's mth subcarrier, where β_{km} and θ_{km} are the amplitude and phase response, respectively, resulting from the multipath fading channel. As the bandwidth of each subcarrier is assumed sufficiently small, the fading on each subcarrier is frequency-flat. The random amplitude is assumed Rayleigh distributed, corresponding to the worst propagation scenario of no line of sight, while the random phase θ_{km} is uniformly distributed over the interval $[-\pi, \pi)$. Due

to the nature of uplink transmission, which originates at different mobile locations, the fading processes for different users,

$$\mathbf{h}_k = [h_{k1}, h_{k2}, \ldots, h_{kM}]^T, \; k = 1, 2, \ldots, K \tag{2.5}$$

is independent. The correlation between the random fading factors on different subcarriers of the same user k, h_{km} and h_{kn}, is given by the spaced-frequency correlation function $\rho(\Delta f_{mn})$. In a wide-sense stationary uncorrelated scattering (WSSUS) channel, the spaced-frequency correlation function can be derived using the Fourier transform of the exponentially decaying power-delay profile of the channel [51, 66]:

$$\rho(\Delta f_{mn}) = \frac{1 - j2\pi\tau_d \Delta f_{mn}}{1 + (2\pi\tau_d \Delta f_{mn})^2} \tag{2.6}$$

where τ_d is the rms channel delay spread, which is defined as the square root of the second central moment of the channel's power-delay profile, and Δf_{mn} is the frequency separation of subcarriers m and n:

$$\Delta f_{mn} = \frac{(m-n)F}{T} \tag{2.7}$$

2.2 Multi-Shot Receiver

When K active user's information streams are received with different transmission delays, a receiver with K branches, each synchronized to the corresponding user, must be used to exploit the received asynchronous signal $r(t)$. Each branch of the receiver consists of M oscillators followed by the integrate and dump filter sampled at the symbol rate $\frac{1}{T}$ as demodulators. The outputs of the M filters are fed into a demultiplexer, which contains the spreading code of the corresponding user, $\boldsymbol{c}_k$. As the amplitude of all code elements is equal (i.e. $|c_{km}| = \frac{1}{\sqrt{M}}$), the demultiplexing can be viewed as an equal gain combining (EGC) of the energy, which was distributed on the different subcarriers, for the corresponding user. The block diagram of the multi-shot receiver is shown in Figure 2.2.

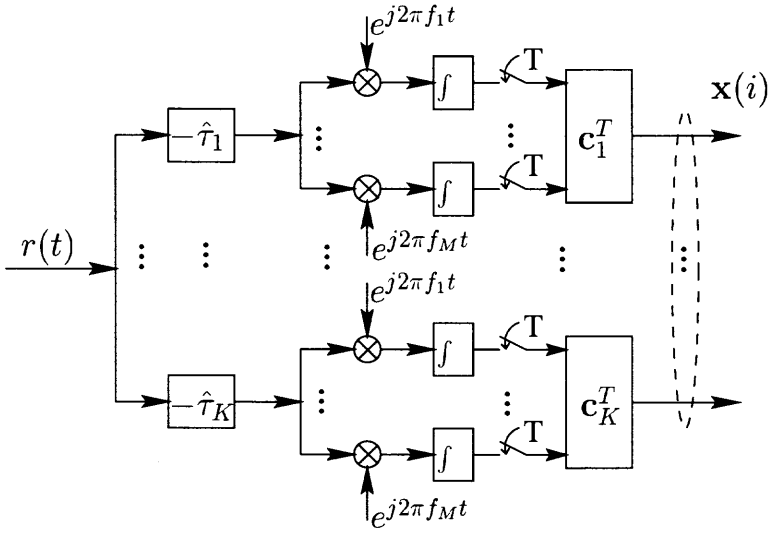

Figure 2.2 Block diagram of a multi-shot receiver.

This so-called multi-shot receiver has a similar structure to an asynchronous DS-CDMA receiver proposed in [54]. Notice that in order to apply the multi-shot structure, timing acquisition must be accomplished for all active users.Furthermore, a frequency offset, ϵ, between the transmitter's and receiver's carrier oscillator is also taken into consideration. Thus, the ith instant output of the lth branch, $x_l(i)$, contains the ith symbol of the lth user as shown in the following equation

$$x_l(i) = \rho_{ll}\sqrt{a_l}b_l(i) + \sum_{\substack{k=1 \\ k\neq l}}^{K} \rho_{lk}\sqrt{a_k}b_k(i) + \sum_{k=l+1}^{K} \rho_{lk}^L \sqrt{a_k}b_k(i-1) + \sum_{k=1}^{l-1} \rho_{lk}^R \sqrt{a_k}b_k(i+1) + \eta_l(i) \quad (2.8)$$

where,

$$\rho_{lk} = \frac{1}{T}\sum_{m=1}^{M}\sum_{p=1}^{M} h_{km}c_{km}c_{lp}e^{-j2\pi f_m \tau_{lk}} \int_0^{T-|\tau_{lk}|} e^{j2\pi(f_m - f_p + \epsilon)t}dt \quad (2.9)$$

$$\rho_{lk}^L = \frac{1}{T}\sum_{m=1}^{M}\sum_{p=1}^{M} h_{km}c_{km}c_{lp}e^{-j2\pi f_m \tau_{lk}} \int_0^{\tau_{lk}} e^{j2\pi(f_m - f_p + \epsilon)t}dt \quad (2.10)$$

$$\rho_{lk}^R = \frac{1}{T}\sum_{m=1}^{M}\sum_{p=1}^{M} h_{km}c_{km}c_{lp}e^{-j2\pi f_m \tau_{lk}} \int_{T-\tau_{lk}}^{T} e^{j2\pi(f_m - f_p + \epsilon)t}dt \quad (2.11)$$

$$\eta_l = \frac{1}{T}\sum_{p=1}^{M} c_{lp} \int_0^T n(t+\tau_l)e^{-j2\pi(f_p - \epsilon)t}dt \quad (2.12)$$

and $\tau_{lk} = \tau_k - \tau_l$. Note that η_l, $l = 1, \ldots, K$, is a sequence of colored Gaussian noise samples with zero mean and covariance

$$\mathrm{E}\left[\eta_l \eta_k^*\right] = \sigma_n^2 \frac{1}{T^2} \sum_{m=1}^{M} \sum_{p=1}^{M} c_{km} c_{lp} e^{-j2\pi(f_m - \epsilon)\tau_{lk}} \int_0^{T-|\tau_{lk}|} e^{j2\pi(f_m - f_p)t} dt \tag{2.13}$$

The first term in equation (2.8) corresponds to the desired user's current transmitted symbol, while the other terms represent interference from other users, termed multiuser interference (MUI). Note that the third and the fourth terms in equation (2.8) vanish when all τ_k are zero, i.e. for synchronous transmission. Therefore, in asynchronous reception, the desired user suffers MUI from other users not only through the current symbol but also the previous and next symbols. Intercarrier interference (ICI) is also introduced after the demodulation due to the frequency offset, ϵ. Thus, the performance of the multi-shot receiver in the asynchronous MC-CDMA system is limited by the presence of MUI and ICI.

The ith interval of the multi-shot receiver's outputs, $x_l(i)$, $l = 1, \ldots, K$ shown in equation (2.8), are stacked into a vector containing information at the ith instant of all of the active users, $\mathbf{x}(i) = [x_1(i), x_2(i), \ldots, x_K(i)]^T$, as,

$$\begin{aligned} \mathbf{x}(i) &= \mathbf{P}\mathbf{A}\mathbf{b}(i) + \mathbf{P}_L\mathbf{A}\mathbf{b}(i-1) + \mathbf{P}_R\mathbf{A}\mathbf{b}(i+1) + \boldsymbol{\eta}(i) \\ &= \begin{bmatrix} \mathbf{P}_L & \mathbf{P} & \mathbf{P}_R \end{bmatrix} \begin{bmatrix} \mathbf{A}\mathbf{b}(i-1) \\ \mathbf{A}\mathbf{b}(i) \\ \mathbf{A}\mathbf{b}(i+1) \end{bmatrix} + \boldsymbol{\eta}(i) \end{aligned} \tag{2.14}$$

where,

$$\mathbf{A} = \mathrm{diag}\left[\sqrt{a_1}, \sqrt{a_2}, \ldots, \sqrt{a_K}\right] \quad \mathbf{b}(i) = [b_1(i), b_2(i), \ldots, b_K(i)]^T$$

$$\boldsymbol{P}_L = \begin{bmatrix} 0 & \rho_{12}^L & \cdots & \rho_{1K}^L \\ 0 & 0 & \cdots & \rho_{2K}^L \\ \vdots & \vdots & \ddots & \vdots \\ 0 & 0 & \cdots & 0 \end{bmatrix} \qquad \boldsymbol{P}_R = \begin{bmatrix} 0 & 0 & \cdots & 0 \\ \rho_{21}^R & 0 & \cdots & 0 \\ \ddots & \vdots & \ddots & \vdots \\ \rho_{K1}^R & \rho_{K2}^R & \cdots & 0 \end{bmatrix}$$

$$\boldsymbol{P} = \begin{bmatrix} \rho_{11} & \rho_{12} & \cdots & \rho_{1K} \\ \rho_{21} & \rho_{22} & \cdots & \rho_{2K} \\ \vdots & \vdots & \ddots & \vdots \\ \rho_{K1} & \rho_{K2} & \cdots & \rho_{KK} \end{bmatrix}$$

2.3 Multiuser Detection

Since part of the interference to the current desired information in equation (2.8) is caused by adjacent symbols, it is intuitive to process the outputs of the multi-shot receiver in an IIR multiuser detector with infinite memory length. As a complete structure of the interference can be captured during infinite observation interval, such an IIR detector can effectively suppress the interference caused by neighboring symbols. However, it has impractically high computational complexity because the observation window length is infinite. It has been shown in [53, 54] that a conventional FIR decorrelator with a moderate finite observation window length can asymptotically achieve the performance of the IIR detector for asynchronous DS-CDMA system. In this section, FIR multiuser detectors based on both the MMSE criterion and the bootstrap decorrelating scheme are designed for an asynchronous MC-CDMA system.

The outputs of the multi-shot receiver, shown in equation (2.14), will be processed by an FIR multiuser detector with processing window of length NT, where N is a positive odd integer: N continuous outputs $\mathbf{x}(n)$ around the ith symbol interval ($n = i - \frac{N-1}{2}, \ldots, i, \ldots, i + \frac{N-1}{2}$) are arranged into an $NK \times 1$ vector to estimate the current symbol vector $\mathbf{b}(i)$:

$$
\begin{aligned}
\boldsymbol{\mathcal{X}}(i) &= \left[\mathbf{x}^T(i - \tfrac{N-1}{2}) \quad \mathbf{x}^T(i - \tfrac{N-1}{2} + 1) \quad \ldots \quad \mathbf{x}^T(i + \tfrac{N-1}{2}) \right]^T \\
&= \begin{bmatrix} \mathbf{P} & \mathbf{P}_R & \mathbf{0} & \ldots & \mathbf{0} \\ \mathbf{P}_L & \mathbf{P} & \mathbf{P}_R & \ldots & \mathbf{0} \\ \vdots & \vdots & \vdots & \ddots & \vdots \\ \mathbf{0} & \mathbf{0} & \mathbf{0} & \ldots & \mathbf{P} \end{bmatrix} \begin{bmatrix} \boldsymbol{A} & & & \\ & \boldsymbol{A} & & \\ & & \vdots & \\ & & & \boldsymbol{A} \end{bmatrix} \begin{bmatrix} \mathbf{b}(i - \frac{N-1}{2}) \\ \mathbf{b}(i - \frac{N-1}{2} + 1) \\ \vdots \\ \mathbf{b}(i + \frac{N-1}{2}) \end{bmatrix} + \begin{bmatrix} \mathbf{P}_L \mathbf{A} \mathbf{b}(i - \frac{N-1}{2} - 1) \\ \mathbf{0} \\ \vdots \\ \mathbf{P}_R \mathbf{A} \mathbf{b}(i + \frac{N-1}{2} + 1) \end{bmatrix} \\
&\quad + \begin{bmatrix} \boldsymbol{\eta}(i - \frac{N-1}{2}) \\ \boldsymbol{\eta}(i - \frac{N-1}{2} + 1) \\ \vdots \\ \boldsymbol{\eta}(i + \frac{N-1}{2}) \end{bmatrix} \\
&= \boldsymbol{\mathcal{P}} \boldsymbol{\mathcal{A}} \boldsymbol{\mathcal{B}}(i) + \mathbf{bias} + \boldsymbol{\mathcal{N}}(i)
\end{aligned} \tag{2.15}
$$

When $N \to \infty$, the FIR detector becomes an ideal IIR multiuser detector. Figure 2.3 shows the block diagram of this FIR multiuser detector.

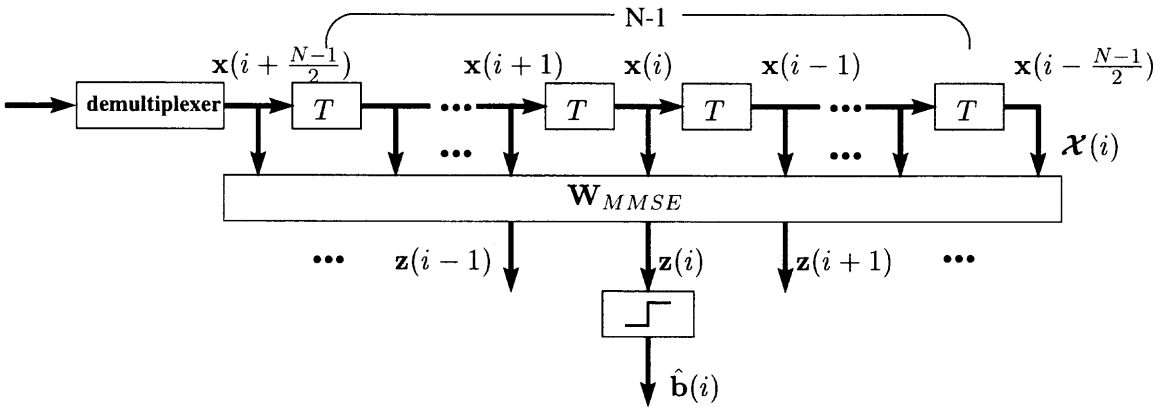

Figure 2.3 Block diagram of Multi-shot MMSE multiuser detector

Notice that the matrix $\mathcal{P}$ in equation (2.15) has a block-tridiagonal structure. Since $\boldsymbol{P}$ is a Hermitian positive definite matrix, $\boldsymbol{P}_L$ is an upper triangle matrix and $\boldsymbol{P}_R$ is a lower triangle matrix, and $\boldsymbol{P}_L = \boldsymbol{P}_R^H$, the matrix $\mathcal{P}$ is a Hermitian positive definite matrix of full rank. Of most importance is the fact that this matrix $\mathcal{P}$ and $\mathcal{P}^{-1}$ are diagonal dominant matrices as shown in Figure 2.4.

The term **bias**, is due to the matrix truncation, i.e. the edge-effects. If the operation matrix of a multiuser detector is diagonal dominant, the term **bias** can be ignored as shown in [54]. It can be seen that the center block of the **bias** term in equation (2.15) is a zero vector. Therefore, if only the current symbols, which are located at the center block of the first term, are of interest, the performance of a multiuser detector will be minimally degraded by ignoring the **bias** term, under the condition that the multiuser receiver's linear operation matrix is diagonally dominant. This feature is called de-biasing. A decorrelating detector and an MMSE detector have the de-biasing feature. Because of this de-biasing feature, $N = 3$ is a reasonable approximation to estimate only the middle symbols of $\boldsymbol{\mathcal{B}}(i)$, $\boldsymbol{b}(i)$. This approximation dramatically reduces computational complexity. When $N = 3$,

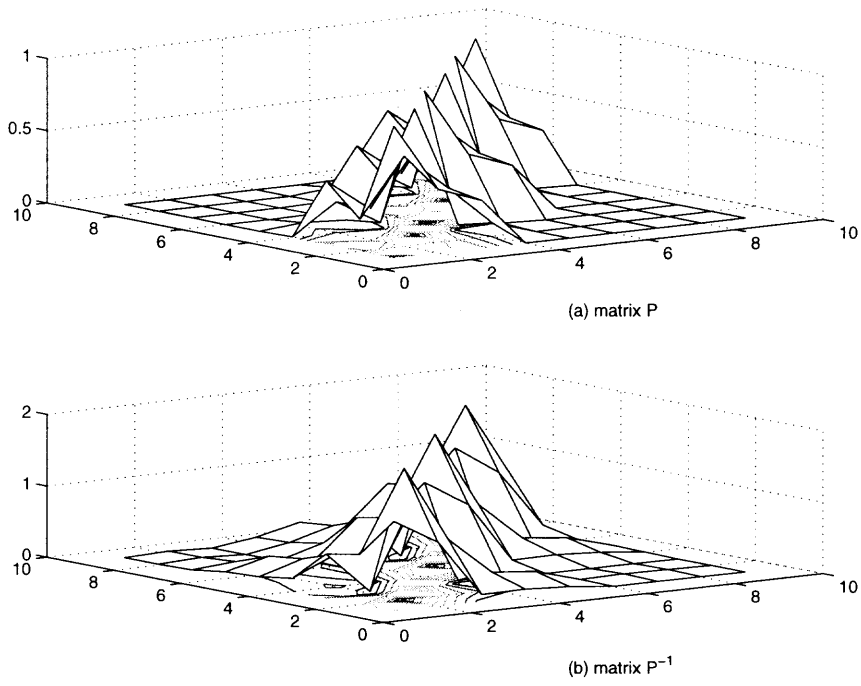

Figure 2.4 Diagonal dominance of matrices $\mathcal{P}$ and $\mathcal{P}^{-1}$

equation (2.15) can be rewritten as:

$$\begin{aligned}
\boldsymbol{\mathcal{X}}(i) &= \begin{bmatrix} \mathbf{x}(i-1) \\ \mathbf{x}(i) \\ \mathbf{x}(i+1) \end{bmatrix} \\
&= \begin{bmatrix} \mathbf{P} & \mathbf{P}_R & \mathbf{0} \\ \mathbf{P}_L & \mathbf{P} & \mathbf{P}_R \\ \mathbf{0} & \mathbf{P}_L & \mathbf{P} \end{bmatrix} \begin{bmatrix} \boldsymbol{A} & & \\ & \boldsymbol{A} & \\ & & \boldsymbol{A} \end{bmatrix} \begin{bmatrix} \mathbf{b}(i-1) \\ \mathbf{b}(i) \\ \mathbf{b}(i+1) \end{bmatrix} \\
&\quad + \begin{bmatrix} \boldsymbol{\eta}(i-1) \\ \boldsymbol{\eta}(i) \\ \boldsymbol{\eta}(i+1) \end{bmatrix} \\
&= \boldsymbol{\mathcal{P}}\boldsymbol{\mathcal{A}}\boldsymbol{\mathcal{B}}(i) + \boldsymbol{\mathcal{N}}(i)
\end{aligned} \tag{2.16}$$

The noise vector, $\boldsymbol{\mathcal{N}}(i)$, in equation (2.16) has zero mean and covariance matrix $\boldsymbol{R}_{\mathcal{N}}$, where

$$\begin{aligned}
\boldsymbol{R}_{\mathcal{N}} &= \mathrm{E}\left[\boldsymbol{\mathcal{N}}(i)\boldsymbol{\mathcal{N}}(i)^H\right] = \begin{bmatrix} \boldsymbol{K} & \boldsymbol{K}_+ & \mathbf{0} \\ \boldsymbol{K}_- & \boldsymbol{K} & \boldsymbol{K}_+ \\ \mathbf{0} & \boldsymbol{K}_- & \boldsymbol{K} \end{bmatrix} \\
\boldsymbol{K}(l,k) &= \mathrm{E}\left[\eta_l(i)\eta_k^*(i)\right] = \frac{\sigma_n^2}{T^2}\sum_{m=1}^{M}\sum_{p=1}^{M} c_{km}c_{lp}e^{-j2\pi(f_m-\epsilon)\tau_{lk}}\int_0^{T-|\tau_{lk}|} e^{j2\pi(f_m-f_p)t}dt \\
\boldsymbol{K}_+(l,k) &= \mathrm{E}\left[\eta_l(i-1)\eta_k^*(i)\right] = \frac{\sigma_n^2}{T^2}\sum_{m=1}^{M}\sum_{p=1}^{M} c_{km}c_{lp}e^{-j2\pi(f_m-\epsilon)\tau_{lk}}\int_0^{\tau_{lk}} e^{j2\pi(f_m-f_p)t}dt \\
\boldsymbol{K}_-(l,k) &= \mathrm{E}\left[\eta_l(i)\eta_k^*(i-1)\right] = \boldsymbol{K}_+(k,l)^*
\end{aligned} \tag{2.17}$$

Notice that as the delays are assumed to be less than T, the noise vectors $\boldsymbol{\eta}(i-1)$ and $\boldsymbol{\eta}(i+1)$ are uncorrelated.

2.3.1 MMSE Multiuser Detection

Equation (2.16) shows that the basic problem is to design a near-far resistant multiuser detector to separate and detect multiuser information symbols $\mathbf{b}(i)$ from outputs $\boldsymbol{\mathcal{X}}(i)$. In other words, design a detector that diagonalizes the correlation matrix $\boldsymbol{\mathcal{P}}$. The conventional decorrelator uses the inverse of $\boldsymbol{\mathcal{P}}$ to separate different users and cancel MUI completely. Therefore, the conventional decorrelator is near-far resistant. However, the use of the conventional decorrelator will enhance the noise variance. In the low interference region, this noise enhancement increases the symbol error rate dramatically.

An MMSE detector is optimal in a mean-squared error sense with respect to both noise and interference. It achieves the single-user bound (SUB), which is defined as,

$$\mathrm{Pe}_{2,\mathrm{SUB}} = \mathrm{E}_{\boldsymbol{H}}\left[\mathrm{Q}\left(\sqrt{\frac{a_2}{\sigma_n^2}\frac{1}{M}\sum_{m=1}^{M} {h_{km}}^2}\right)\right] \tag{2.18}$$

in the low interference region. It is also near-far resistant, as the performance is the same as that of the conventional decorrelator when the interference becomes

sufficiently high. The MMSE decision variable for the kth user's ith symbol is

$$z_k(i) = \boldsymbol{w}_k^H \boldsymbol{\mathcal{X}}(i), \quad k = 1, 2, \ldots, K \tag{2.19}$$

where the $(3K \times 1)$ weight vector $\boldsymbol{w}_k$ is chosen to minimize the mean square error (MSE) conditioned on the random delays

$$\boldsymbol{\tau} = [\tau_1, \tau_2, \ldots, \tau_K]^T \tag{2.20}$$

and the multipath channel's fading factors

$$\boldsymbol{H} = [\boldsymbol{h}_1, \boldsymbol{h}_2, \ldots, \boldsymbol{h}_K] \tag{2.21}$$

Using equation (2.16), the conditional MSE is derived as follows,

$$\begin{aligned} \mathrm{MSE}_k(\boldsymbol{\tau}, \boldsymbol{H}) &= \mathrm{E}\left[\left(\hat{b}_k - b_k\right)^2\right] \\ &= \boldsymbol{w}_k^H \left(\boldsymbol{\mathcal{P}}_{K+k} \boldsymbol{\mathcal{A}}_{K+k}^2 \boldsymbol{\mathcal{P}}_{K+k}^H + a_k \boldsymbol{p}_{K+k} \boldsymbol{p}_{K+k}^H + \boldsymbol{R}_{\mathcal{N}}\right) \boldsymbol{w}_k \\ &- 2\sqrt{a_k} \boldsymbol{w}_k^H \boldsymbol{p}_{K+k} + 1 \end{aligned} \tag{2.22}$$

where $\boldsymbol{\mathcal{P}}_{K+k}$ denotes the matrix $\boldsymbol{\mathcal{P}}$ without the $(K+k)$th column, $\boldsymbol{p}_{K+k}$ denotes the $(K+k)$th column of $\boldsymbol{\mathcal{P}}$ and $\boldsymbol{\mathcal{A}}_{K+k}$ denotes the matrix $\boldsymbol{\mathcal{A}}$ without the $(K+k)$th column and row. The index $(K+k)$ refers to the location of the current symbol from the kth user in matrix $\boldsymbol{\mathcal{X}}(i)$. By taking the gradient of the MSE with respect to $\boldsymbol{w}_k$ and applying the following well-known matrix inversion rule,

$$(\boldsymbol{D} + \alpha \boldsymbol{x} \boldsymbol{y}^H)^{-1} = \boldsymbol{D}^{-1} - \frac{1}{\alpha^{-1} + \boldsymbol{y}^H \boldsymbol{D}^{-1} \boldsymbol{x}} \boldsymbol{D}^{-1} \boldsymbol{x} \boldsymbol{y}^H \boldsymbol{D} - 1 \tag{2.23}$$

the optimum weights conditioned on $\boldsymbol{H}$ and $\boldsymbol{\tau}$ can be obtained as,

$$\begin{aligned} \boldsymbol{w}_{k,\mathrm{MMSE}} &= \frac{\sqrt{a_k}}{1 + a_k \boldsymbol{p}_{K+k}^H \left(\boldsymbol{\mathcal{P}}_{K+k} \boldsymbol{\mathcal{A}}_{K+k}^2 \boldsymbol{\mathcal{P}}_{K+k}^H + \boldsymbol{R}_{\mathcal{N}}\right)^{-1} \boldsymbol{p}_{K+k}} \\ &\times \left(\boldsymbol{\mathcal{P}}_{K+k} \boldsymbol{\mathcal{A}}_{K+k}^2 \boldsymbol{\mathcal{P}}_{K+k}^H + \boldsymbol{R}_{\mathcal{N}}\right)^{-1} \boldsymbol{p}_{K+k} \end{aligned} \tag{2.24}$$

As a result, the conditional MMSE achieved by the MMSE detector is given by,

$$\begin{aligned} \mathrm{MMSE}_{k,\boldsymbol{\tau},\boldsymbol{H}} &= 1 - \sqrt{a_k} \boldsymbol{w}_{k,\mathrm{MMSE}}^H \boldsymbol{p}_{K+k} \\ &= \left[1 + a_k \boldsymbol{p}_{K+k}^H \left(\boldsymbol{\mathcal{P}}_{K+k} \boldsymbol{\mathcal{A}}_{K+k}^2 \boldsymbol{\mathcal{P}}_{K+k}^H + \boldsymbol{R}_{\mathcal{N}}\right)^{-1} \boldsymbol{p}_{K+k}\right]^{-1} \end{aligned} \tag{2.25}$$

The corresponding maximum signal to noise plus interference ratio (MSNIR) of the kth user conditioned on the given delays and channel is described by:

$$\mathrm{MSNIR}_{k,\boldsymbol{\tau},\boldsymbol{H}} = a_k \boldsymbol{p}_{K+k}^H \left(\boldsymbol{\mathcal{P}}_{K+k}\boldsymbol{\mathcal{A}}_{K+k}^2\boldsymbol{\mathcal{P}}_{K+k}^H + \boldsymbol{R}_{\mathcal{N}}\right)^{-1} \boldsymbol{p}_{K+k} \tag{2.26}$$

The theoretical symbol error rate of the MMSE detector for the kth user averaged over the delays and fading can be evaluated as,

$$\mathrm{Pe}_k = \mathrm{E}_{\boldsymbol{\tau},\boldsymbol{H}} \left| \mathrm{Q}\left(\sqrt{\mathrm{MSNIR}_{k,\boldsymbol{\tau},\boldsymbol{H}}}\right)\right| \tag{2.27}$$

The expectation in equation (2.27) is performed by averaging a number of Monte-Carlo runs with independent random channel fading factors $\boldsymbol{H}$ and delays $\boldsymbol{\tau}$.

2.3.2 Blind Adaptive Bootstrap Multiuser Detection

For the MMSE multiuser detector presented in the previous section, the following are required to be known at the receiver: the spreading codes of all active users, $\boldsymbol{C}$, the timing of all active users, $\boldsymbol{\tau}$, the received users' amplitudes, $\boldsymbol{A}$, and the channel, $\boldsymbol{H}$. Additionally, the MMSE detector has a high computational complexity, since matrix inversions need to be performed. As applied to a DS-CDMA system, some adaptive MMSE detectors were proposed in [22, 24], in which training sequences are used to eliminate some required knowledge. The reliance on a training sequence is cumbersome in a time-variant environment, as data transmission has to switch to training sequence retransmission frequently. Thus, in this section, a blind adaptive multiuser detection scheme, the bootstrap algorithm, is implemented to avoid some of the above requirements. The bootstrap algorithm separates the different signals by adaptively adjusting the weight matrix to reduce the correlation between detected data of different users. It has been shown that, similar to an MMSE detector, the adaptive detector using the bootstrap algorithm has better performance than the conventional decorrelator in the low interference region and approaches the performance of the conventional decorrelator in the high interference region [27].

The use of this bootstrap algorithm in the multi-shot receiver for the asynchronous MC-CDMA system is shown in the following sections.

2.3.2.1 Steady State of Bootstrap Algorithm In the bootstrap algorithm, the decision variables of K active users' current symbols are generated as

$$\mathbf{z}(:,i) = (\mathbf{I} - \mathbf{W})^H \boldsymbol{\mathcal{X}}(i) \tag{2.28}$$

where $\boldsymbol{I}$ is a $3K \times 3K$ identity matrix and $\mathbf{W}$ is a weight matrix with zeros on the diagonal,

$$\mathbf{W} = \begin{bmatrix} 0 & w_{1,2} & \dots & w_{1,3K} \\ w_{2,1} & 0 & \dots & w_{2,3K} \\ \vdots & \vdots & \ddots & \vdots \\ w_{3K,1} & w_{3K,2} & \dots & 0 \end{bmatrix}$$

The desired kth user's decision variable $z_k(i)$ can therefore be written as

$$z_k(i) = x_{K+k}(i) - \mathbf{w}_{K+k}^H \boldsymbol{\mathcal{X}}_{K+k}(i) \tag{2.29}$$

where $x_{K+k}(i)$ denotes the $(K+k)$th element of vector $\boldsymbol{\mathcal{X}}(i)$, $\boldsymbol{\mathcal{X}}_{K+k}(i)$ denotes the vector without the $(K+k)$th element and $\mathbf{w}_{K+k}$ denotes the $(K+k)$th column of matrix $\boldsymbol{W}$ without the $(K+k)$th element. In order to separate the different users' symbols, the matrix $\boldsymbol{W}$ is chosen such that the correlations between the desired kth user's decision variable and others are equal to zero,

$$E[z_k(i)\hat{\boldsymbol{\mathcal{B}}}_{K+k}(i)] = \mathbf{0} \tag{2.30}$$

When the interference-to-signal ratio (ISR) is very high, $\hat{\boldsymbol{\mathcal{B}}}_{K+k}(i) = \boldsymbol{\mathcal{B}}_{K+k}(i)$, where $\boldsymbol{\mathcal{B}}_{K+k}(i)$ denotes the vector $\boldsymbol{\mathcal{B}}(i)$ without the $(K+k)$th element and $\mathbf{0}$ is a vector of zeros with length $3K-1$. This is called the limiting condition. Under this condition, equation (2.30) can be expanded with the use of equation (2.29) as

$$\begin{aligned} E[z_k(i)\boldsymbol{\mathcal{B}}_{K+k}(i)] &= E\left[\left(x_{K+k}(i) - \mathbf{w}_{K+k}^H \boldsymbol{\mathcal{X}}_{K+k}(i)\right)\boldsymbol{\mathcal{B}}_{K+k}(i)\right] \\ &= \bar{\boldsymbol{q}}_{K+k}\boldsymbol{\mathcal{A}}_{K+k} - \boldsymbol{w}_{K+k}^H \bar{\boldsymbol{\mathcal{P}}}_{K+k}\boldsymbol{\mathcal{A}}_{K+k} \end{aligned} \tag{2.31}$$

where $\bar{\mathbf{q}}_{K+k}$ denotes the $(K+k)$th row of matrix $\boldsymbol{\mathcal{P}}$ without the $(K+k)$th element and $\bar{\boldsymbol{\mathcal{P}}}_{K+k}$ denotes the matrix $\boldsymbol{\mathcal{P}}$ without the $(K+k)$th column and row. To obtain equation (2.31), the information symbols of different users are assumed uncorrelated. Using equation (2.31), the steady state of the different columns of the weight matrix $\boldsymbol{W}$ can be derived as follows,

$$\mathbf{w}_{K+k} = \left(\bar{\boldsymbol{\mathcal{P}}}_{K+k}^{-1}\right)^{H} \bar{\boldsymbol{q}}_{K+k}^{H} \tag{2.32}$$

In Appendix A, it is shown that with these weight vectors, the bootstrap detector has the same performance as that of the conventional decorrelating detector. The adaptive bootstrap converges to the steady state weights shown in equation (2.32) in the high interference region. In the case of low interference, the steady state weights cannot be found analytically because of the nonlinear nature of the control algorithm. However, simulations show that the adaptive bootstrap detector performs similar to the MMSE detector.

2.3.2.2 Inter-Rail Interference Cancellation The bootstrap detector shown in the previous section cancels MUI by minimizing the correlation between different users' detected signals. However, the inter-rail interference in each of these detected signals, caused by the frequency offset, is left uncompensated. The inter-rail interference can be viewed as the result of a rotation in the constellation. An example of this inter-rail interference caused by a frequency offset is depicted in Figure 2.5. The rotated constellation at the output of the first bootstrap stage is shown in Figure 2.5(c). This constellation is rotated back as shown in Figure 2.5(d) with the aid of a second stage.

The phase rotation under the limiting condition can be found analytically. Using the steady state of the limiting weight $\boldsymbol{W}$, as defined in equation (2.32), the kth user's decision variable can be expressed as (see Appendix A),

$$z_k(i) = \alpha_k \sqrt{a_k} b_k(i) + n_k(i) \tag{2.33}$$

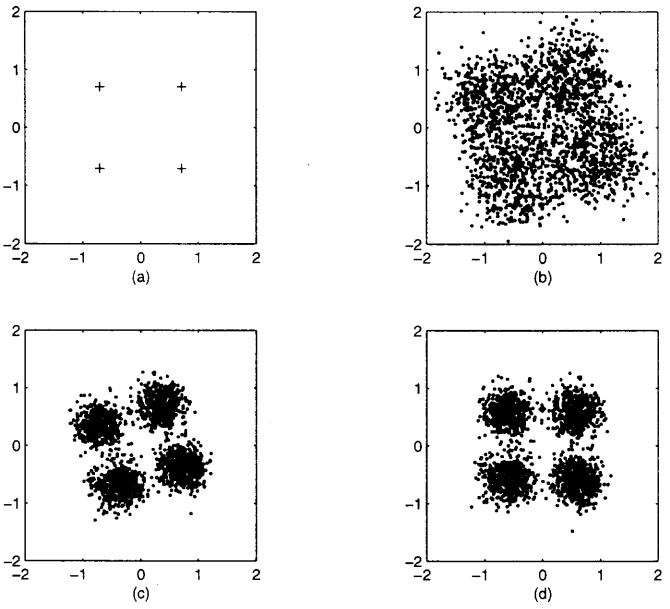

Figure 2.5 Constellations of 4-QAM for $M = 7, K = 3, \epsilon = 0.1\Delta f$, SNR = 10 dB and ISR = -5 dB, (a) Transmitted constellation, (b) Matched filter output, (c)First stage output, (d)Second stage output

where

$$\alpha_k = p_{K+k,K+k} - \bar{\mathbf{q}}_{K+k}\bar{\boldsymbol{\mathcal{P}}}^{-1}_{K+k}\bar{\mathbf{p}}_{K+k} \tag{2.34}$$

$p_{K+k,K+k}$ is the $(K+k, K+k)$th element of $\boldsymbol{\mathcal{P}}$ and $\bar{\mathbf{p}}_{K+k}$ denotes the vector $\mathbf{p}_{K+k}$ without the $(K+k)$th element. When a frequency offset is present, α_k as shown in equation (2.34) becomes a complex number. Thus, the phase of α_k, $\angle\alpha_k$, is the phase rotation of the decision variable, $z_k(i)$. A second stage bootstrap detector is needed to cancel the inter-rail interference due to $\angle\alpha_k$. The bootstrap implementation of this stage is similar to the first stage except that K weight matrices of size 2×2, $\mathbf{W}_{rot_k}, k = 1, 2, \ldots, K$, are needed to separate the in-phase and quadrature components of the K active users individually. The steady state of the limiting weight value of the second stage bootstrap detector was shown in [31] to satisfy,

$$\boldsymbol{W}_{rot_k} = \begin{bmatrix} 0 & -\frac{\Im\{\alpha_k\}}{\Re\{\alpha_k\}} \\ \frac{\Im\{\alpha_k\}}{\Re\{\alpha_k\}} & 0 \end{bmatrix} \tag{2.35}$$

2.3.2.3 Implementation of the Adaptive Bootstrap Algorithm A blind adaptive multiuser detector applying the bootstrap algorithm is implemented. This adaptive detector, which has been proposed in [51] for the synchronous case, consists of two stages to jointly perform multiuser interference cancellation and inter-rail interference cancellation. As QAM-modulated information symbols are considered, a complex bootstrap algorithm [28] is used in the implementation of the first stage. This complex algorithm takes into account information from both the real and imaginary parts. The following recursive equation is used to update the weights of the bootstrap detector in the first stage,

$$\mathbf{w}_{K+k}(i+1) = \mathbf{w}_{K+k}(i) + \mu z_k(i)^* \text{csgn}(\mathbf{z}(:,i)_{K+k}(i)) \tag{2.36}$$

where i denotes the update iteration, μ denotes the step-size parameter of the adaptation process and csgn denotes the complex signum operation:

$$\text{csgn}(.) = \text{sgn}(\Re(.)) + j \times \text{sgn}(\Im(.)) \tag{2.37}$$

In the second stage, K real bootstrap detectors with weight matrix of size 2×2 are used to cancel the inter-rail interference for the K active users. The recursive weight update equation for the kth user is,

$$w_{rot_{12}}(i+1) = w_{rot_{12}}(i) + \mu_{rot} \Im\{z_k(i)\} \text{sgn}(\Re\{z_k(i)\}) \tag{2.38}$$

where μ_{rot} denotes the step-size parameter. The block diagram of this two-stage adaptive bootstrap multi-shot multiuser detector is shown in Figure 2.6 for the kth user.

It has been shown in [67] that sufficient conditions for the convergence of this adaptive bootstrap algorithm are:

1. The cross-correlation matrix $\boldsymbol{\mathcal{P}}$ is diagonally dominant;

2. The step-size μ is smaller than the reciprocal of the maximal signal amplitude.

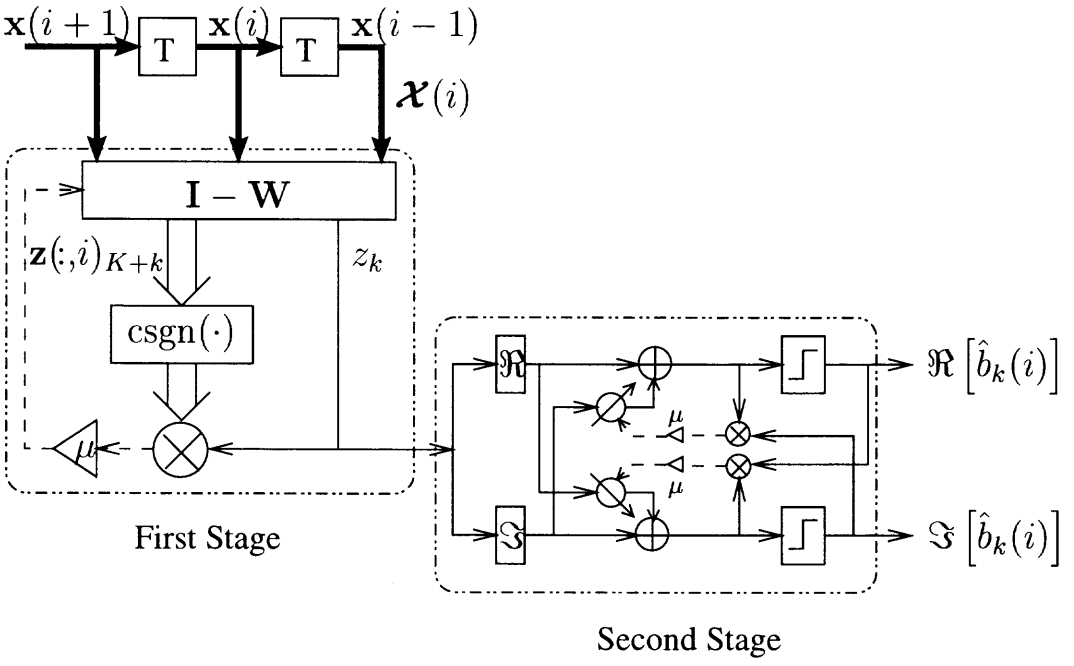

Figure 2.6 Block diagram of two-stage bootstrap multi-shot multiuser detector

As shown in Figure 2.4, $\mathcal{P}$ is a diagonal dominant matrix, therefore, with a proper step-size, the weights of this blind adaptive multi-shot multiuser detector will always converge.

2.4 Multiuser Detection with Timing Estimation Error

The previous discussions were based on the assumption of perfect timing knowledge for all active users at the multi-shot receiver. This may not be true in reality. Due to movement of the mobile users, the transmission delays of the users are time-varying. If the tracking rate of a timing estimation scheme is not fast enough, an erroneous delay estimation, $\hat{\tau}_l \neq \tau_l, l = 1, 2, \ldots, K$, is made. In fact, both a conventional decorrelation detector and an MMSE detector, which rely on some manipulations of the correlation matrix $\mathcal{P}$, are sensitive to this timing estimation error. One of the advantages of using an adaptive multiuser detector is that the detector will automatically adjust the weights whenever there is a timing variation

of the desired signal's arrival, and converge to a new correct steady state. Therefore, the blind adaptive bootstrap detector proposed in the previous section is expected to be more robust to timing estimation errors. However, when frequency offset and timing estimation error are present, the adaptation of the second stage of the proposed bootstrap may break down due to possible phase ambiguity. Thus, in order to avoid a severe system performance degradation particularly for higher order M-ary QAM modulated information symbols, a differential one-stage bootstrap detector is also proposed in this section.

2.4.1 Effects of Erroneous Timing Estimation

With the erroneous transmission delays $\hat{\tau}_l$, the outputs of the multi-shot receiver $\boldsymbol{\mathcal{X}}(i)$ in equation (2.15) can be rewritten as[1]

$$\begin{aligned}\hat{\boldsymbol{\mathcal{X}}}(i) &= \begin{bmatrix} \hat{\mathbf{P}} & \hat{\mathbf{P}}_R & \mathbf{0} \\ \hat{\mathbf{P}}_L & \hat{\mathbf{P}} & \hat{\mathbf{P}}_R \\ \mathbf{0} & \hat{\mathbf{P}}_L & \hat{\mathbf{P}} \end{bmatrix} \begin{bmatrix} \boldsymbol{A} & & \\ & \boldsymbol{A} & \\ & & \boldsymbol{A} \end{bmatrix} \begin{bmatrix} \mathbf{b}(i-1) \\ \mathbf{b}(i) \\ \mathbf{b}(i+1) \end{bmatrix} + \begin{bmatrix} \hat{\boldsymbol{\eta}}(i-1) \\ \hat{\boldsymbol{\eta}}(i) \\ \hat{\boldsymbol{\eta}}(i+1) \end{bmatrix} \\ &= \hat{\boldsymbol{\mathcal{P}}}\boldsymbol{\mathcal{A}}\boldsymbol{\mathcal{B}}(i) + \hat{\boldsymbol{\mathcal{N}}}(i) \end{aligned} \tag{2.39}$$

where

$$\hat{\boldsymbol{P}}(l,k) = \frac{1}{T}\sum_{m=1}^{M}\sum_{p=1}^{M} h_{km}c_{km}c_{lp}e^{-j2\pi f_m\hat{\tau}_{lk}}\int_0^{T-|\hat{\tau}_{lk}|} e^{j2\pi(f_m-f_p+\epsilon)t}dt \tag{2.40}$$

$$\hat{\mathbf{P}}_L(l,k) = \frac{1}{T}\sum_{m=1}^{M}\sum_{p=1}^{M} h_{km}c_{km}c_{lp}e^{-j2\pi f_m\hat{\tau}_{lk}}\int_0^{\hat{\tau}_{lk}} e^{j2\pi(f_m-f_p+\epsilon)t}dt \tag{2.41}$$

$$\hat{\mathbf{P}}_R(l,k) = \frac{1}{T}\sum_{m=1}^{M}\sum_{p=1}^{M} h_{km}c_{km}c_{lp}e^{-j2\pi f_m\hat{\tau}_{lk}}\int_{T-\hat{\tau}_{lk}}^{T} e^{j2\pi(f_m-f_p+\epsilon)t}dt \tag{2.42}$$

Notice that $\hat{\tau}_{lk}$ is defined as $\hat{\tau}_{lk} = \tau_k - \hat{\tau}_l$, in which $\hat{\tau}_{ll} \neq 0$. Thus, the diagonal elements of $\hat{\mathbf{P}}_L$ and $\hat{\mathbf{P}}_R$ are no longer zero, and the received desired signal, presented by $\hat{\boldsymbol{P}}(l,l)$ in equation (2.40), suffers amplitude reduction and larger constellation rotation as compared to the perfect timing estimation case shown in the first term of equation (2.8). If the timing estimation error is sufficiently small, i.e., $|\hat{\tau}_{ll}| << |\tau_l|$, which is

[1]for brevity, the term **bias** is omitted in this equation.

reasonable in the time tracking stage, the correlation matrix $\hat{\boldsymbol{\mathcal{P}}}$ is still diagonally dominant. This justifies ignoring the **bias** term in equation (2.39). The noise vector $\hat{\boldsymbol{\mathcal{N}}}(i)$ has zero mean and covariance matrix $\boldsymbol{R}_{\hat{\mathcal{N}}}$ as

$$\boldsymbol{R}_{\hat{\mathcal{N}}} = \mathrm{E}\left[\hat{\boldsymbol{\mathcal{N}}}(i)\hat{\boldsymbol{\mathcal{N}}}(i)^H\right] = \begin{bmatrix} \hat{\boldsymbol{K}} & \hat{\boldsymbol{K}}_+ & \mathbf{0} \\ \hat{\boldsymbol{K}}_- & \hat{\boldsymbol{K}} & \hat{\boldsymbol{K}}_+ \\ \mathbf{0} & \hat{\boldsymbol{K}}_- & \hat{\boldsymbol{K}} \end{bmatrix} \tag{2.43}$$

$$\hat{\boldsymbol{K}}(l,k) = \mathrm{E}\left[\hat{\eta}_l(i)\hat{\eta}_k^*(i)\right] = \frac{\sigma_n^2}{T^2}\sum_{m=1}^{M}\sum_{p=1}^{M} c_{km}c_{lp}e^{-j2\pi(f_m-\epsilon)\hat{\tau}_{lk}}\int_0^{T-|\hat{\tau}_{lk}|} e^{j2\pi(f_m-f_p)t}dt \tag{2.44}$$

$$\hat{\boldsymbol{K}}_+(l,k) = \mathrm{E}\left[\hat{\eta}_l(i-1)\hat{\eta}_k^*(i)\right] = \frac{\sigma_n^2}{T^2}\sum_{m=1}^{M}\sum_{p=1}^{M} c_{km}c_{lp}e^{-j2\pi(f_m-\epsilon)\hat{\tau}_{lk}}\int_0^{\hat{\tau}_{lk}} e^{j2\pi(f_m-f_p)t}dt \tag{2.45}$$

where $\hat{\tau}_{lk} = \hat{\tau}_k - \hat{\tau}_l$.

With erroneous timing estimations $\hat{\tau}_l, l = 1, 2, \ldots, K$, the steady state of the bootstrap's weights vector for the kth user under the limiting condition (compare to equation (2.32)), becomes

$$\mathbf{w}_{K+k} = \left(\hat{\bar{\boldsymbol{\mathcal{P}}}}_{K+k}^{-1}\right)^H \hat{\bar{\boldsymbol{q}}}_{K+k}^H \tag{2.46}$$

where, as before, $\hat{\bar{\boldsymbol{q}}}_{K+k}$ is the $(K+k)$th row of that matrix without the $(K+k)$th element and $\hat{\bar{\boldsymbol{\mathcal{P}}}}_{K+k}$ is matrix $\hat{\boldsymbol{\mathcal{P}}}$ without the $(K+k)$th row and column. Based on the output SNR (SNR^o), the performance of the adaptive bootstrap multiuser detector is compared to that of the conventional decorrelating detector in the high interference region (i.e. the limiting condition)[2]. With erroneous timing estimation, the desired kth user's decision variable $z_k(i)$ of the bootstrap detector (compare to equation (2.33)) becomes

$$z_k(i) = \hat{\alpha}_k\sqrt{a_k}b_k(i) + n_{b,k}(i) \tag{2.47}$$

where, $\hat{\alpha}_k$, using equation (2.34), is shown to be

$$\hat{\alpha}_k = \hat{p}_{K+k,K+k} - \hat{\bar{\mathbf{q}}}_{K+k}\hat{\bar{\boldsymbol{\mathcal{P}}}}_{K+k}^{-1}\hat{\bar{\mathbf{p}}}_{K+k} \tag{2.48}$$

[2]With accurate timing estimation, the bootstrap detector under the limiting condition has the same SNR^o as the conventional decorrelating detector.

and $n_{b,k}(i)$ has zero mean and variance $\hat{\sigma}^2_{b,k}$ defined in Appendix A as,

$$\hat{\sigma}^2_{b,k} = r_{K+k,K+k} - 2\hat{\tilde{\boldsymbol{q}}}_{K+k}\hat{\tilde{\boldsymbol{\mathcal{P}}}}^{-1}_{K+k}\boldsymbol{r}_{K+k} + \hat{\tilde{\boldsymbol{q}}}_{K+k}\hat{\tilde{\boldsymbol{\mathcal{P}}}}^{-1}_{K+k}\boldsymbol{R}_{K+k}(\hat{\tilde{\boldsymbol{q}}}_{K+k}\hat{\tilde{\boldsymbol{\mathcal{P}}}}^{-1}_{K+k})^H \qquad (2.49)$$

where, $\hat{\tilde{\mathbf{p}}}_{K+k}$ denotes the $(K+k)$th column of matrix $\hat{\boldsymbol{\mathcal{P}}}$ without the $(K+k)$th element, $r_{K+k,K+k}$ denotes the $(K+k,K+k)$th element of matrix $\boldsymbol{R}_{\hat{\mathcal{N}}}$, $\boldsymbol{r}_{K+k}$ denotes the $(K+k)$th column of matrix $\boldsymbol{R}_{\hat{\mathcal{N}}}$ without the $(K+k)$th element and $\boldsymbol{R}_{K+k}$ denotes the matrix without the $(K+k)$th row and column. Thus, the SNR^o of the bootstrap detector under limiting condition can be described by,

$$\text{SNR}^o{}_{bootstrap} = \frac{|\hat{\alpha}_k|^2 a_k}{\hat{\sigma}^2_{b,k}} \qquad (2.50)$$

Equation (2.50) shows that the output SNR of the adaptive bootstrap multiuser detector for the kth user does not depend on the power of interfering users. Thus, even with an erroneous timing estimation, the adaptive bootstrap multiuser detector is near-far resistant.

On the other hand, the decision variable of the kth user, using the conventional decorrelator with erroneous timing estimation is

$$z_k(i) = \beta_{K+k}\sqrt{a_k}b_k(i) + \boldsymbol{\beta}_{K+k}\boldsymbol{A}_{K+k}\boldsymbol{\mathcal{B}}_{K+k}(i) + n_{d,k}(i) \qquad (2.51)$$

where

$$\begin{aligned}\beta_{K+k} &= \boldsymbol{\mathcal{P}}^{-1}\hat{\boldsymbol{\mathcal{P}}}|_{(K+k,K+k)} \\ &= (p_{K+k,K+k} - \bar{\mathbf{q}}_{K+k}\bar{\boldsymbol{\mathcal{P}}}^{-1}_{K+k}\bar{\mathbf{p}}_{K+k})^{-1}(\hat{p}_{K+k,K+k} - \bar{\mathbf{q}}_{K+k}\bar{\boldsymbol{\mathcal{P}}}^{-1}_{K+k}\hat{\bar{\mathbf{p}}}_{K+k})\end{aligned} \qquad (2.52)$$

and $\boldsymbol{\beta}_{K+k}$ denotes the $(K+k)$th row of $\boldsymbol{\mathcal{P}}^{-1}\hat{\boldsymbol{\mathcal{P}}}$ without the $(K+k)$th element. Noise sample $n_{d,k}(i)$ has zero mean and variance $\sigma^2_{d,k} = \boldsymbol{R}_\eta(k,k)$ defined in Appendix A as

$$\sigma^2_{d,k} = |\alpha_k|^{-2}\left[r_{K+k,K+k} - 2\bar{\boldsymbol{q}}_{K+k}\bar{\boldsymbol{\mathcal{P}}}^{-1}_{K+k}\boldsymbol{r}_{K+k} + \bar{\boldsymbol{q}}_{K+k}\bar{\boldsymbol{\mathcal{P}}}^{-1}_{K+k}\boldsymbol{R}_{K+k}(\bar{\boldsymbol{q}}_{K+k}\bar{\boldsymbol{\mathcal{P}}}^{-1}_{K+k})^H\right] \qquad (2.53)$$

Thus, the SNR^o of the decorrelating detector can be described as,

$$\text{SNR}^o{}_{decorrelator} = \frac{|\beta_{K+k}|^2 a_k}{\boldsymbol{\beta}_{K+k}\boldsymbol{A}_{K+k}\boldsymbol{\beta}^H_{K+k} + \sigma^2_{d,k}} \qquad (2.54)$$

If the timing estimation errors for all active users are assumed sufficiently small ($|\hat{\tau}_{ll}| << |\tau_l|$), $\boldsymbol{\mathcal{P}} \approx \hat{\boldsymbol{\mathcal{P}}}$. Then, terms $\beta_{K+k} \approx 1$, $\alpha_k \approx \hat{\alpha}_k$ and $\sigma^2_{d,k} \approx |\alpha_k|^{-2}\hat{\sigma}^2_{b,k}$. Thus, equation (2.54) can be reduced to

$$\mathrm{SNR}^o{}_{decorrelator} = \frac{|\hat{\alpha}_k|^2 a_k}{|\hat{\alpha}_k|^2 \boldsymbol{\beta}_{K+k} \boldsymbol{A}_{K+k} \boldsymbol{\beta}^H_{K+k} + \hat{\sigma}^2_{b,k}} \tag{2.55}$$

Equations (2.55) shows that, with an erroneous timing estimations, the output SNR of the conventional decorrelator for the kth user does depend on the power of interfering users. The performance of the conventional decorrelator deteriorates significantly due to the severe MUI. Thus, the near-far resistant property of this detector is impaired.

2.4.2 Differential Bootstrap Detector

It has been shown in section 2.3.2.2 that the received desired signal not only suffers from amplitude reduction and MUI, but also inter-rail interference, which results in rotation of the transmitted symbol constellation. The phase rotation is caused by channel fading, frequency offset, timing estimation error, etc. To handle this problem, a two-stage bootstrap multiuser detector [31], in which the multiuser detection is followed by a phase rotation process, was utilized in the previous sections. However, the second stage, which cancels inter-rail interference, only works correctly when the phase rotation is limited to,

$$|\angle\hat{\alpha}_k| < \frac{\pi}{M_a}, \quad k = 1, 2, \ldots, K \tag{2.56}$$

where M_a denotes the order of the QAM modulation of the transmitted information symbol. Otherwise, it results in symbol errors caused by phase ambiguity. Caused by random phenomena, the $\angle\hat{\alpha}_k$'s are random variables, whose statistics are very difficult to obtain analytically. To obtain some insight into the statistics of the $\angle\hat{\alpha}_k$, several histograms of the $\angle\hat{\alpha}_k$ are shown in Figure 2.7, in which the values on the x-axis are normalized by π. The histograms of $\angle\hat{\alpha}_k$ are shown for two different values

of the frequency offset ϵ and timing estimation error $\hat{\tau}_{kk}$. It can be seen that the mean of the phase rotation is shifted mostly by the frequency offset. The variance of the $\angle\hat{\alpha}_k$ depends on the random timing estimation error: the variation of the phase rotation becomes larger as the timing estimation error increases and smaller as the timing estimation error decreases. Therefore, the two-stage bootstrap scheme cannot be applied to the case where a moderate timing estimation error occurs, since the large variation of the phase rotation results in a severe phase ambiguity problem. As a result, the adaptation of the second stage would converge to an incorrect steady state.

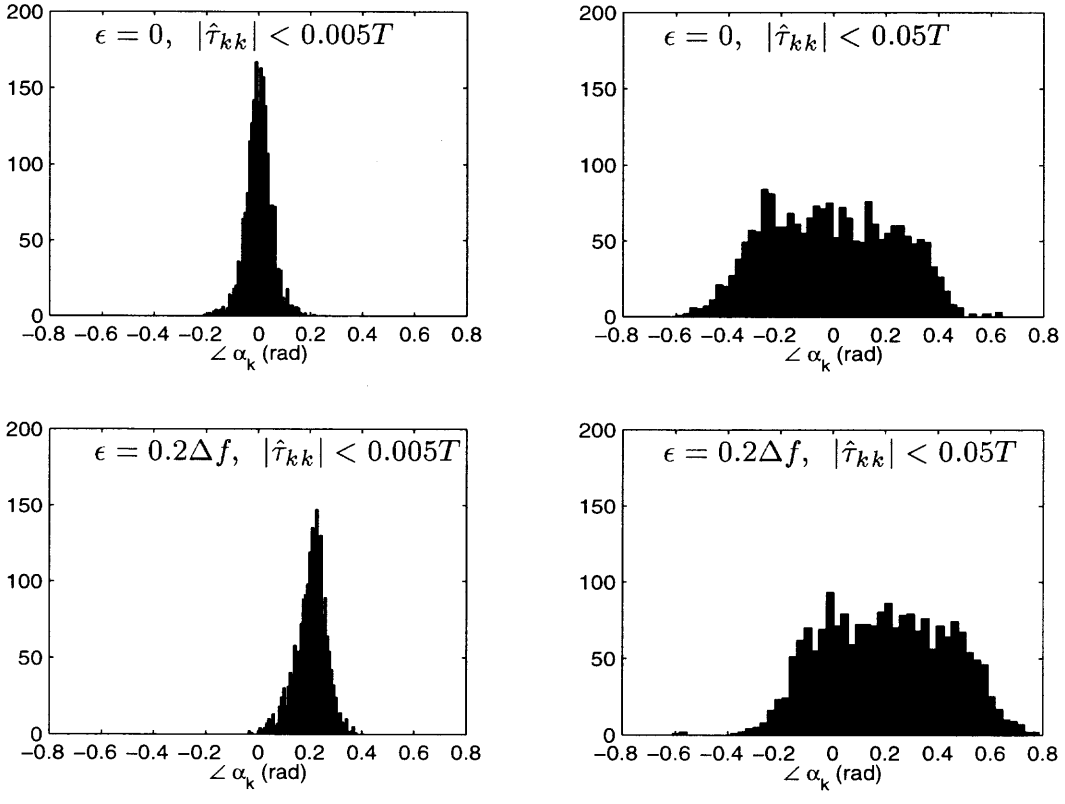

Figure 2.7 Histogram of the phase rotation with different ϵ and $\hat{\tau}_{kk}$.

To avoid incorrect convergence caused by the phase ambiguity, a differential bootstrap detection scheme is proposed. In this scheme, the second stage of the proposed coherent bootstrap multiuser detector is removed. Instead, the infor-

mation symbol is differentially encoded before being multiplexed by the spreading code. With such modulation, the information is embedded in the phase difference between two successive received signals. Therefore, if the transmission environment does not change much during two successive symbols, the phase rotation will not affect the performance of a bootstrap multiuser detector followed by a differential decoder. Hence, this differential bootstrap scheme is robust in the presence of a phase rotation resulting from channel fading, frequency offset, timing estimation error, etc. However, due to the non-coherent reception, the symbol error rate performance has a 3dB loss.

2.5 Simulation Results

The symbol error rate performance of the proposed multi-shot multiuser detector over a Rayleigh fading channel is examined through simulations. An MC-CDMA system with $M = 7$ subcarriers and $K = 3$ active users is considered. The spreading code sequences are chosen from a normalized Gold code with length 7. The transmission delays of the three users are chosen as random variables with a uniform distribution on $[0, T)$. The information symbols are generated by a normalized 4-QAM source. The SNR is defined as $\text{SNR}_k = \frac{a_k}{\sigma_n^2}$. Assuming the desired user is the second user, i.e. SNR_2 is used to indicate the desired user's SNR. The interference-to-signal ratio (ISR) is defined as $\text{ISR} = \frac{a_i}{a_2}, \quad i \neq 2$. In the simulations, the probability density function (pdf) of the normalized amplitude of the fading factor β_{km} is defined as,

$$p(\beta_{km}) = \frac{\beta_{km}}{\sigma^2} \exp\left(-\frac{\beta_{km}^2}{2\sigma^2}\right) \tag{2.57}$$

with $\text{E}[\beta_{km}^2] = 2\sigma^2 = 1$. Since the symbol error rate of the receiver is dependent on the channel realization, all the symbol error rate results are obtained by averaging over 100 Monte-Carlo runs.

In this section, uncorrelated flat Rayleigh fading per subcarrier is assumed. Some scenarios may be developed for which this assumption is realistic. One solution comes at the expense of a loss of bandwidth efficiency: the frequency separation between adjacent subcarriers can be increased to exceed the coherent bandwidth. Another scheme that does not suffer the loss in bandwidth efficiency was developed in [35]. This scheme can be explained by several simultaneous MC-CDMA transmissions in parallel where the subcarriers are interleaved over frequency to guarantee uncorrelated fading per subcarrier for each MC-CDMA transmission. This parallel MC-CDMA transmission can be generated by transmitting several information symbols per user in parallel, transmitting one information symbol per user from several independent user groups in parallel, or a combination of the previous two.

The uncorrelated fading channel model is widely used in the literature for comparisons between various detection schemes, due to the ease of implementation, computationally efficient system simulation, and simple reproduction of the simulation results. Although a correlated fading channel does not provide as much frequency diversity as the uncorrelated fading channel, it will not change the relative performance of these schemes qualitatively. The intention of this chapter is to propose and evaluate the performance of several detectors. Hence, using the uncorrelated fading channel model is reasonable for comparing the proposed detectors with other detectors in the literature, and presenting the results as reference curves for further investigations.

Figure 2.8 compares the near-far performance of different detectors with perfect timing estimation, i.e. $\hat{\tau}_{kk} = 0, \quad k = 1, 2, \ldots, K$. The symbol error rate is shown for the desired user with $\mathrm{SNR}_2 = 10\mathrm{dB}$ as a function of ISR, with SNR_i the same for all $i \neq 2$. It can be seen that the performance of the proposed two-stage adaptive bootstrap detector has almost the same performance as the MMSE detector, which is an optimal linear detector in the mean squared error sense. In the high interference

region (ISR $\rightarrow \infty$dB), the adaptive bootstrap and MMSE detectors' performance approaches that of the decorrelating detector. The adaptive bootstrap detector is also considered as a near-far resistant detector since its performance is bounded by the performance of the near-far resistant decorrelating detector. In the low interference region (ISR $\rightarrow -\infty$dB) the conventional decorrelating detector has a worse performance, due to noise enhancement, than the MMSE and bootstrap schemes. It can also be seen that both adaptive bootstrap and MMSE detectors can not reach the SUB defined in equation (2.18) in the low interference region. This performance loss is a result of a non-optimal signal combining performed by the EGC weighted demultiplexers preceding the multiuser detector (see Figure 2.2). When the power of the received signals on the subcarriers are not the same due to the selective fading attenuation [20], a maximum ratio combining (MRC) is the optimal signal combining scheme. For comparison, the performance of a multi-shot MMSE receiver with a MRC weighted demultiplexer, $[h_{k1}c_{k1}, h_{k2}c_{k2}, \ldots, h_{kM}c_{kM}]^T$, is shown in Figure 2.8. The MMSE-MRC receiver outperforms the receivers with an EGC weighted demultiplexer. However, the MMSE-MRC scheme needs knowledge of the channel response, which requires channel estimation process.

Figure 2.9 shows the robustness of the two-stage adaptive bootstrap detector in the presence of small timing estimation errors, i.e., $|\hat{\tau}_{22}| \leq 0.005T$. Due to the erroneous timing estimation, both MMSE and decorrelating detectors become non-resistant to the near-far effects, as shown in this figure. The performance of the proposed adaptive bootstrap detector, however, shows near-far resistance with such timing estimation error as the performance does not further degrade when ISR $\rightarrow \infty$dB. This is because the bootstrap detector does not depend on the channel/timing estimation for the interference cancellation. Instead, the bootstrap separates the desired signals from interference by adaptively adjusting the weight matrix according to the residual correlation between desired and interfering signals.

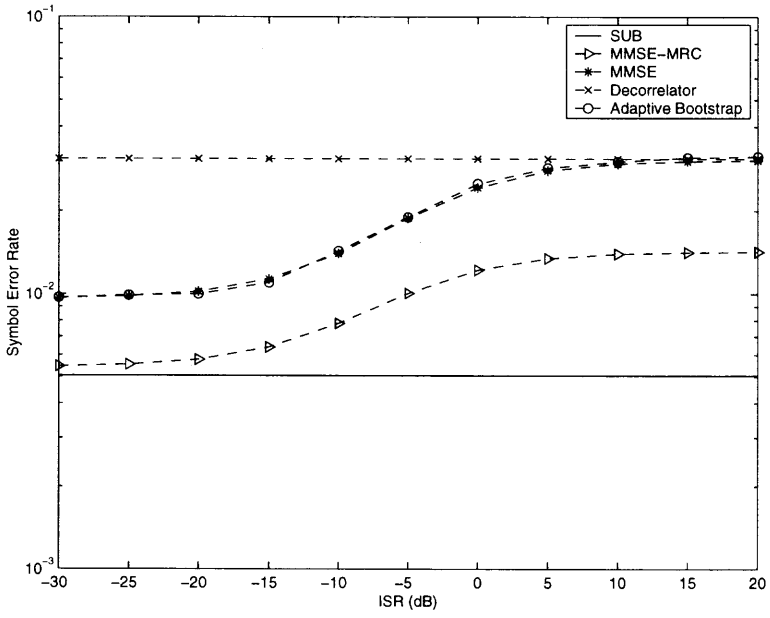

Figure 2.8 Symbol error rate vs. interference power for $M = 7, K = 3, \epsilon = 0.1\Delta f$ with perfect timing estimation, SNR_2=10dB.

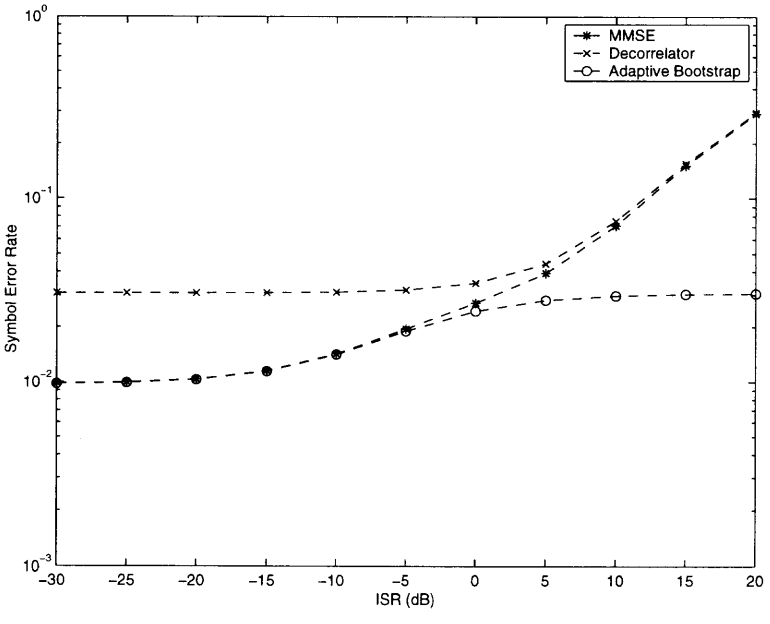

Figure 2.9 Symbol error rate vs. interference power for $M = 7, K = 3, \epsilon = 0.1\Delta f$ with small timing estimation error, $|\hat{\tau}_{kk}| < 0.005T$ SNR_2=10dB.

In Figure 2.10, the adaptive bootstrap output SNIR, for the desired user 2, is plotted versus the iteration. At iterations of 10000 and 25000, different delay estimation errors are introduced into the system. It can be seen that the adaptive bootstrap detector will automatically adjust the detection weight matrix and converge to the right SNIR value. For comparison, the results obtained with an MMSE detector without erroneous timing estimation, i.e., $\tau_{22} = 0$, is also shown in Figure 2.10. The adaptive bootstrap detector results in a slight performance loss due to partial energy loss, since part of the desired signal falls outside of the demodulator's sample interval. The performance gap in Figure 2.10 between the adaptive bootstrap and MMSE without timing estimation error shows this performance loss.

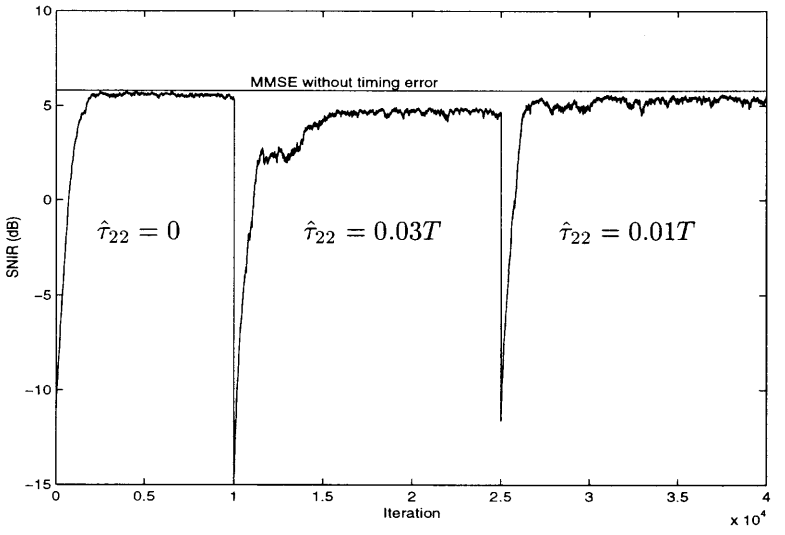

Figure 2.10 SNIR vs. time for adaptive bootstrap with $M = 7, K = 3, \epsilon = 0.1\Delta f$, SNR_2=6dB and ISR=20dB. Erroneous delay estimation happens at time 10000 and 25000.

This figure also shows that the bootstrap algorithm needs at least a few thousand iterations to reach convergence, which will not be suitable for the current package data transmission. The slow convergence speed is partially due to the asynchronous reception of different users. For example, with the same number of

active users, the cross-correlation matrix $\mathcal{P}$, for the multi-shot receiver with $N = 3$ for asynchronous MC-CDMA system, has a matrix size nine times as large as for a synchronous MC-CDMA system (compare $3K \times 3K$ with $K \times K$, respectively). In addition, the bootstrap algorithm suffers decreased diagonal dominance, as more interference, i.e. non-zero off-diagonal elements, is introduced. Thus, compared to a synchronous scenario, the convergence will be much slower, as a smaller step size is needed to avoid overshoot in the adaptation. If the number of active users increases, the convergence of the bootstrap algorithm will slow down further as an even smaller step size is required for convergence.

As mentioned in section 2.4.2, when the phase rotation caused by channel, frequency offset or erroneous timing estimation exceeds a certain range, the second stage of the bootstrap detector will not work properly due to possible phase ambiguity. To mitigate this problem, a differential bootstrap was introduced. Figures 2.11 and 2.12 show the performance of this differential bootstrap detector with low-interference (ISR=-20dB) and high-interference (ISR=20dB), respectively. The frequency offset is set to $\epsilon = 0.2\Delta f$ and the delay estimation errors are chosen as a uniformly distributed random variable with $|\hat{\tau}_{22}| < 0.05T$, with which a severe phase ambiguity problem will be introduced for 4-QAM modulated symbols (as shown in Figure 2.7 that the phase rotation $\angle\alpha_k$ exceeds $\frac{\pi}{4}$ very often). In these figures, the performance of the differential bootstrap detector is compared to a coherent two-stage bootstrap detector and an MMSE detector. It can be seen that due to phase ambiguity, the performance of the coherent bootstrap is severely deteriorated. The performance of the MMSE detector with erroneous delay estimation is also degraded significantly due to the high interference level. The differential bootstrap detector, however, is robust in the presence of both phase ambiguity and interference. The performance of an MMSE detector with perfect delay estimation is also shown in these figures as a benchmark. This represents the best performance

the adaptive bootstrap can achieve. It can be seen that the differential bootstrap detector has approximately a 3dB SNR loss, which is due to the non-coherent reception.

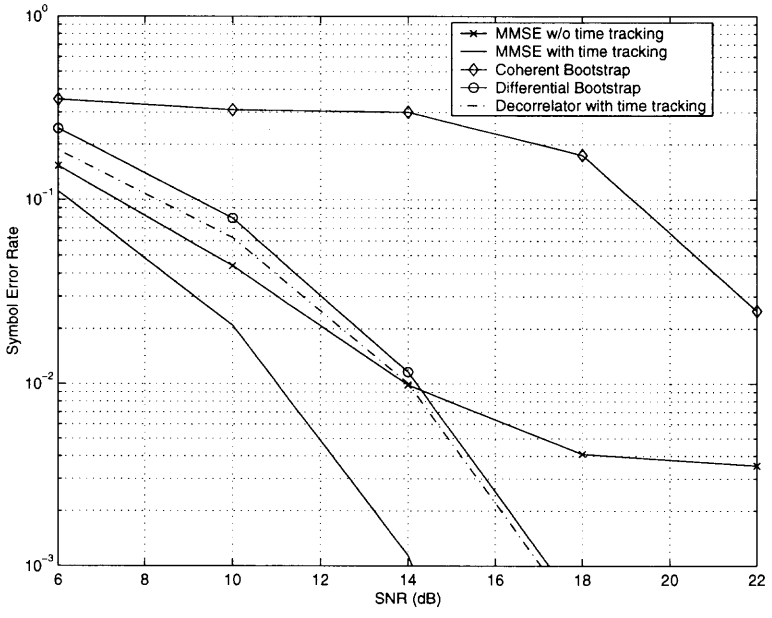

Figure 2.11 Symbol error rate vs. SNR with $M = 7, K = 3, \epsilon = 0.2\Delta f$, ISR=$-$20dB and $|\hat{\tau}_{kk}| < 0.05T$.

2.6 Discussion

FIR MMSE and adaptive bootstrap multiuser detectors with the multi-shot structure for an asynchronous MC-CDMA system were studied in this chapter. The performance of these detectors was evaluated under uncorrelated Rayleigh fading channel. The multi-shot structure, with a built-in de-biasing feature, effectively provides sufficient information about the interference caused by asynchronous receptions of active users. As a result, the MMSE and adaptive bootstrap multiuser detectors with a multi-shot structure successfully perform multiuser interference cancellation as shown in the simulation results. Also, it was shown that the performance of these two detection schemes is effected by the demultiplexing

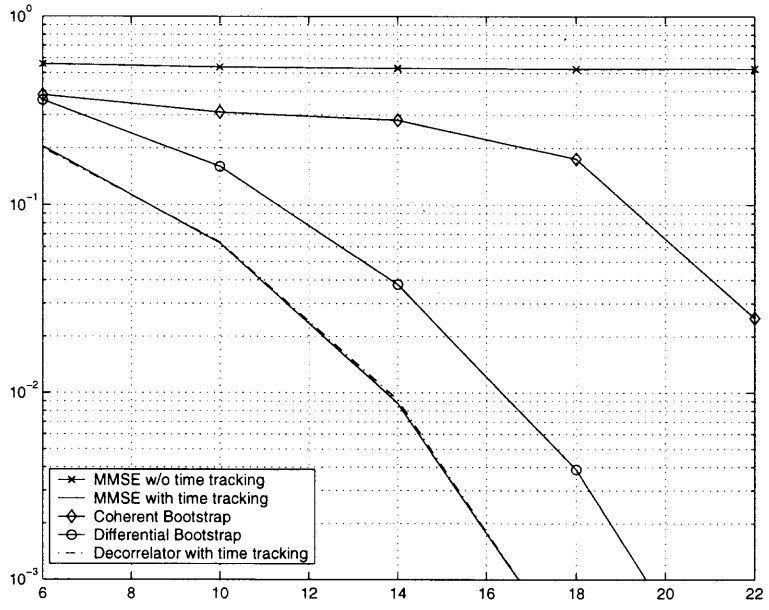

Figure 2.12 Symbol error rate vs. SNR with $M = 7, K = 3, \epsilon = 0.2\Delta f$, ISR=20dB and $|\hat{\tau}_{kk}| < 0.05T$.

scheme. The detector preceded by an MRC weighted demultiplexer achieves better performance than the one preceded by an EGC weighted demultiplexer. The near-far resistance of these detectors in the presence of a timing estimation error is also studied. The blind adaptive bootstrap detector shows a time tracking and interference suppression capability in comparison to the MMSE detector and the conventional decorrelating receiver. Furthermore, a differential bootstrap detector was proposed to combat phase ambiguity.

CHAPTER 3

PARTIAL SAMPLING MULTIUSER DETECTION FOR ASYNCHRONOUS MC-CDMA

In the previous chapter, a multi-shot receiver for an asynchronous MC-CDMA system was discussed. For this receiver, the delay of the desired signal must be found with small error in order to correctly demodulate information carried by different subcarriers. That is, the receiver's observation interval should be accurately matched with the desired signal's timing to avoid self ISI and ICI. Since all users are of interest for the uplink, this multi-shot receiver requires timing knowledge of all active users to perform multiuser detection. Therefore, timing acquisition must be accomplished for all users prior to the multiuser detection, which significantly increases the system complexity.

In [56, 57], a chip-MMSE interference suppression scheme is presented for asynchronous DS-CDMA. A sufficient statistic of the desired signal is formed by sampling the received signal at the chip rate. Thus, the timing uncertainty is quantized into a finite set of hypotheses. Then, an adaptive demodulator based on the MMSE criterion is run for each hypothesis. The hypothesis that yields the best estimated mean square error (MSE) is used to obtain timing acquisition and demodulation. Inspired by this idea, as long as the timing uncertainty of the MC-CDMA signal can be quantized to build a sufficient statistic for the desired signal, an optimal receiver can also be obtained for an asynchronous MC-CDMA system to jointly perform timing acquisition and multiuser detection.

In this chapter, a method using partial sampling demodulation is discussed, in which the requirement of prior timing knowledge for an uplink MC-CDMA receiver is removed. The partial sampling minimum mean square error combining (PS-MMSEC) receiver is shown to have a stronger interference suppression and near-far resistance capability than that of a regular symbol level receiver, which samples

the received signal at the symbol rate. The adaptive version of this PS-MMSEC receiver can be implemented using the least-mean-square (LMS) algorithm, aided by a training sequence. The only knowledge assumed by this adaptive receiver is the spreading code of the desired user. Furthermore, compared to a chip-level receiver proposed for the DS-CDMA system in [22, 24, 56, 57], the PS-MMSEC scheme is more flexible since varying partial sampling rates can be chosen as a compromise between system complexity and performance. Also, a less complex scheme termed reduced complexity partial sampling MMSEC (RPS-MMSEC) receiver, which has fewer MMSEC coefficients, is discussed in this chapter.

3.1 Partial Sampling (PS) Demodulator

The continuous baseband waveform of the received asynchronous MC-CDMA signal is repeated from equation (2.2):

$$r(t) = \sum_{i=-\infty}^{+\infty} \sum_{k=1}^{K} \sqrt{a_k} b_k(i) P(t - iT - \tau_k) \sum_{m=1}^{M} c_{km} h_{km} e^{j2\pi f_m (t-\tau_k)} + n(t) \qquad (3.1)$$

As shown in Chapter 2, for an MC-CDMA system, the received signal needs to be demodulated by a bank of correlators with a sampling interval of T. In the uplink scenario, in order to avoid ICI and partial energy loss of the desired user, such symbol interval demodulators require prior timing knowledge of all active users. As shown in Figure 2.10, a small timing error will degrade the performance of the non-adaptive decorrelating and MMSE detectors dramatically. In addition, even the adaptive bootstrap detector suffers a performance loss in case of a timing offset between the receiver's observation interval and the received signal's arrival time, because the receiver cannot capture the complete energy of the desired user. To mitigate this problem, a partial sampling demodulator is proposed. Unlike the regular demodulator used in Chapter 2, which samples the received signal at the symbol rate, the partial sampling demodulator consists of an integrate-and-dump filter with a

sampling rate of T_s followed by an L-tap tapped delay line for each subcarrier, where $T_s = \frac{2T}{L}$ and L is a positive integer indicating the partial sampling rate. The block diagram of this partial sampling demodulator is shown in Figure 3.1.

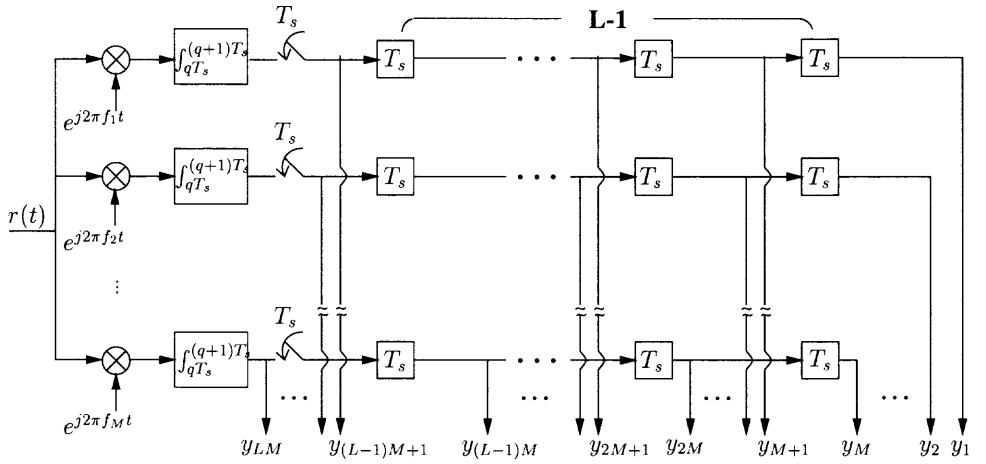

Figure 3.1 Block diagram of the partial sampling demodulator

Increasing the value of L gives the receiver more degrees of freedom to choose its weights and, thus, provides better interference suppression capability. In order to have uncorrelated noise samples at different sampling instants, the sampling rate must be less than the total bandwidth of the MC-CDMA signal, i.e. $\frac{1}{T_s} \leq \frac{2+(M-1)F}{T}$, where a positive integer F, as defined in Chapter 2, is the system parameter that determines the spacing of the subcarriers by an integer multiple of the inverse of the symbol duration. Hence, $1 \leq L \leq 2\left((M-1)F+2\right)$. Since the receiver does not know the delay of the desired user, the observation interval can not be aligned with the received desired signal. To fully utilize the desired user's signal energy, the observation interval must be long enough to capture one complete desired symbol for any unknown delay. To satisfy this requirement, given that the random delay is no more than T as in Chapter 2, $2T$ is the minimum observation length required. Within this expanded observation interval, a finite set of hypotheses on different subcarriers are generated for different subintervals, $[qT_s, (q+1)T_s]$, regardless of the uncertainty of the starting time of the desired symbol. The qth discrete time sample

on the nth subcarrier can be written as

$$y_{qM+n}(i) = \frac{1}{T}\int_{iT+qT_s}^{iT+(q+1)T_s} r(t)e^{-j2\pi f_n t}dt$$
$$= \sum_{k=1}^{K}\sqrt{a_k}\left[p_{qM+n,k}b_k(i) + p^L_{qM+n,k}b_k(i-1) + p^R_{qM+n,k}b_k(i+1)\right] + \eta_{qM+n}(i) \quad (3.2)$$

where

$$p^L_{qM+n,k} = \frac{1}{T}\sum_{m=1}^{M} c_{km}h_{km}e^{-j2\pi f_m\tau_k}\int_{\min[qT_s,\tau_k]}^{\min[(q+1)T_s,\tau_k]} e^{j2\pi(f_m-f_n)t}dt \quad (3.3)$$

$$p_{qM+n,k} = \frac{1}{T}\sum_{m=1}^{M} c_{km}h_{km}e^{-j2\pi f_m\tau_k}\int_{\max[qT_s,\tau_k]}^{\min[(q+1)T_s,T+\tau_k]} e^{j2\pi(f_m-f_n)t}dt \quad (3.4)$$

$$p^R_{qM+n,k} = \frac{1}{T}\sum_{m=1}^{M} c_{km}h_{km}e^{-j2\pi f_m\tau_k}\int_{\max[qT_s,T+\tau_k]}^{\min[(q+1)T_s,2T]} e^{j2\pi(f_m-f_n)t}dt \quad (3.5)$$

and $q = 0, 1, \ldots, L-1$, $n = 1, 2, \ldots, M$ and $k = 1, 2, \ldots, K$. Notice that $p^L_{qM+n,k}, p_{qM+n,k}$ and $p^R_{qM+n,k}$ are zero when the upper limit of the integration is smaller than the lower limit. Also, the noise sample $\eta_{qM+n} = \frac{1}{T}\int_{qT_s}^{(q+1)T_s} n(t)e^{-j2\pi f_n t}dt$ is a colored Gaussian r.v. with zero mean and covariance

$$\gamma_{qM+n,pM+m} = \mathrm{E}\left[\eta_{qM+n}\eta^*_{pM+m}\right] = \frac{1}{T^2}\int_{qT_s}^{(q+1)T_s} n(t)e^{-j2\pi f_n t}dt\int_{pT_s}^{(p+1)T_s} n(\tau)^* e^{j2\pi f_m\tau}d\tau$$
$$= \delta(q-p)\frac{1}{T^2}\int_{qT_s}^{(q+1)T_s}\int_{qT_s}^{(q+1)T_s}\mathrm{E}\left[n(t)n(\tau)^*\right]e^{-j2\pi f_n t}e^{j2\pi f_m\tau}d\tau dt$$
$$= \delta(q-p)\frac{2\sigma^2}{LT}\mathrm{sinc}\left(2T\frac{f_m-f_n}{L}\right)e^{j2\pi\frac{(f_m-f_n)T}{L}(2q+1)} \quad (3.6)$$

The function $\delta(q-p)$ represents the independence of the noise samples at different sampling instants q and p. Due to the asynchronous character of the uplink transmission, there are, as described by equation (3.2), three consecutive symbols within the observation interval $2T$ for each user. In contrast to the output of a symbol demodulator, the output of this partial sampling demodulator contains ICI due to a shorter integration duration, which causes a loss of orthogonality between different subcarriers:

$$\frac{1}{T}\int_{iT+qT_s}^{iT+(q+1)T_s} e^{j2\pi(f_m-f_p)t}dt \neq \delta(m-p), \quad m,p = 1,2,\ldots,M \quad (3.7)$$

Furthermore, the output of the partial sampling demodulator contains only partial information for all active users. As a result, a demultiplexer, which was used in the previous chapter to extract the user information before the multiuser detection, cannot be applied after the partial sampling demodulator to form a sufficient statistic of the users' information. Instead, a new receiver structure, which is appropriate for this situation will be shown in the next section.

An equivalent synchronous discrete time model is developed by stacking the outputs of the partial sampling demodulator into an $(ML \times 1)$ vector in the order of the sample's time index q and subcarrier index n as shown in Figure 3.1,

$$\boldsymbol{y}(i) = [y_1(i), y_2(i), \ldots, y_{ML}(i)]^T \tag{3.8}$$

This equivalent synchronous vector is used to make a decision on the ith symbol of the desired user. $\boldsymbol{y}(i)$ can be described in matrix notation as

$$\boldsymbol{y}(i) = \boldsymbol{PAB}(i) + \boldsymbol{\eta}(i) \tag{3.9}$$

where

$$\boldsymbol{P} = \begin{bmatrix} p^L_{1,1} & \cdots & p^L_{1,K} & p_{1,1} & \cdots & p_{1,K} & p^R_{1,1} & \cdots & p^R_{1,K} \\ p^L_{2,1} & \cdots & p^L_{2,K} & p_{2,1} & \cdots & p_{2,K} & p^R_{2,1} & \cdots & p^R_{2,K} \\ \vdots & \ddots & \vdots & \vdots & \ddots & \vdots & \vdots & \ddots & \vdots \\ p^L_{ML,1} & \cdots & p^L_{ML,K} & p_{ML,1} & \cdots & p_{ML,K} & p^R_{ML,1} & \cdots & p^R_{ML,K} \end{bmatrix}$$

$$\boldsymbol{A} = \text{diag}\left[\sqrt{a_1}, \ldots, \sqrt{a_K}, \sqrt{a_1}, \ldots, \sqrt{a_K}, \sqrt{a_1}, \ldots, \sqrt{a_K}\right]$$

$$\boldsymbol{B}(i) = [b_1(i-1), \ldots, b_K(i-1), b_1(i), \ldots, b_K(i), b_1(i+1), \ldots, b_K(i+1)]^T$$

and $\boldsymbol{\eta}(i)$ is a colored Gaussian noise vector with covariance matrix $\boldsymbol{\Gamma} = \mathrm{E}\left[\boldsymbol{\eta}(i)\boldsymbol{\eta}(i)^H\right]$. The $(qM+n, pM+m)$th element of $\boldsymbol{\Gamma}$ was defined in equation (3.6).

3.2 Partial Sampling MMSE Combining (PS-MMSEC) Receiver

In an MC-CDMA system, the energy of the transmitted signal is divided over different subcarriers. Thus, for each user, an MC-CDMA receiver needs to combine

the received signal in the frequency domain and then make a decision. In Chapter 2, a demultiplexer, which essentially performs EGC or MRC, was applied to combine the energy distributed over different subcarriers before the multiuser detection. Such demultiplexer provides the detector with the information per user. This is particularly important for the adaptive bootstrap algorithm, since the mechanism of this algorithm is to separate active users by forcing decorrelation at the detector's output. However, the demultiplexer cannot be used together with the partial sampling demodulator, since the output of the partial sampling demodulator contains ICI and only partial user information.

An MMSE combining (MMSEC) scheme [32, 33], which jointly performs combining and multiuser detection, is applied to the receiver with the partial sampling structure. This receiver is termed partial sampling MMSEC (PS-MMSEC). The block diagram of the PS-MMSEC receiver is shown in Figure 3.2.

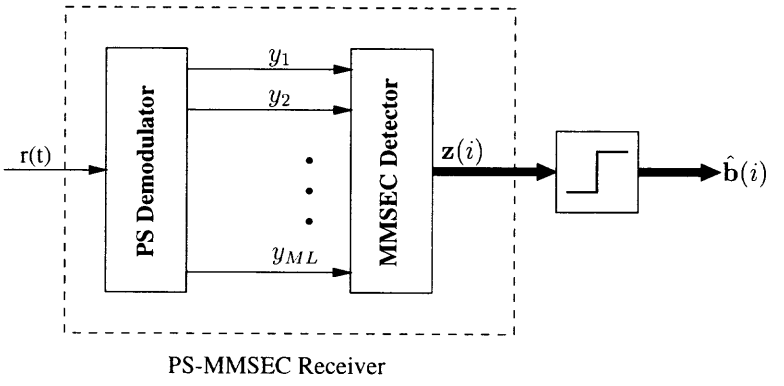

Figure 3.2 Block diagram of the PS-MMSEC receiver

The MMSEC detector calculates the mean-square error for each active user directly from the statistics provided by the partial sampling demodulator,

$$\mathrm{MSE}_k = \mathrm{E}\left[\left(\sqrt{a_k}b_k - \boldsymbol{w}_k^H \boldsymbol{y}\right)^2\right] \tag{3.10}$$

This detector works similar to the chip-MMSE detector in the DS-CDMA system proposed in [22]. Compared to an MMSE detector preceded by a demultiplexer, the MMSEC detector performs the same or better, because the MMSEC detector

with dimension $M \times 1$ has more degrees of freedom than the MMSE detector with dimension $K \times 1$, since $M \geq K$ in an MC-CDMA system. Because the partial sampling demodulator samples the received signal L times as fast as a regular symbol demodulator, the dimension of the MMSEC detector in a PS-MMSEC receiver is $ML \times 1$. The ML coefficients of the MMSEC detector, for the desired user k, in the PS-MMSEC receiver can be derived similarly to those of an MMSE detector as shown in section 2.3.1 [61]. Following the derivation, the $ML \times 1$ weight vector becomes

$$\boldsymbol{w}_{k,\text{mmsec}} = \arg\min_{\boldsymbol{w}_k} \text{MSE}_k = \frac{\sqrt{a_k}}{1 + a_k \boldsymbol{p}_{K+k}^H \left(\boldsymbol{P}_{K+k}\boldsymbol{A}_{K+k}^2\boldsymbol{P}_{K+k}^H + \boldsymbol{\Gamma}\right)^{-1}\boldsymbol{p}_{K+k}} \times \left(\boldsymbol{P}_{K+k}\boldsymbol{A}_{K+k}^2\boldsymbol{P}_{K+k}^H + \boldsymbol{\Gamma}\right)^{-1}\boldsymbol{p}_{K+k} \tag{3.11}$$

where $\boldsymbol{P}_{K+k}$ denotes the matrix $\boldsymbol{P}$ without the $(K+k)$th column, $\boldsymbol{p}_{K+k}$ denotes the $(K+k)$th column of $\boldsymbol{P}$ and $\boldsymbol{A}_{K+k}$ denotes the matrix $\boldsymbol{A}$ without the $(K+k)$th column and row. Notice that the MMSEC coefficients can be determined using a decision-directed least mean square (LMS) gradient algorithm. Thus, the PS-MMSEC receiver only needs to know the spreading code of the desired user and a training sequence to initialize adaptation. Also, after the adaptation has reached to a steady state value, the MMSEC coefficients in the PS-MMSEC receiver can be used to extract timing information, given that the partial sampling duration is the same or smaller than the minimum resolvable delay.

In Figure 3.3, the MMSEC coefficients of the 7th subcarrier at different partial sampling instants are shown for an asynchronous $M = 7$ subcarriers MC-CDMA system. The random delays are assume to be discrete values, which are multiples of $\frac{T}{M}$. The partial sampling parameter is $L = 2M = 14$. Thus, the minimum resolvable delay, $\frac{T}{M}$, is equal to the partial sampling duration T_s. It can be seen from the figure that the start of M successive large-valued coefficients on the 7th subcarrier indicates the length of delay τ_k.

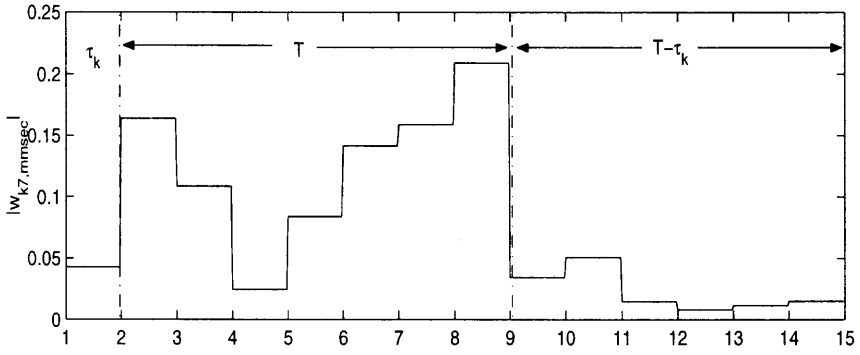

Figure 3.3 Timing of the MMSEC coefficients

The partial sampling demodulator's ith output vector is multiplied by these MMSEC coefficients for the kth user to form a test statistic,

$$\hat{b}_k(i) = \text{csgn}(z(i)) = \text{csgn}(\boldsymbol{w}_{k,\text{mmsec}}^H \boldsymbol{y}(i)) \tag{3.12}$$

The MSNIR of the kth user conditioned on the random delays $\boldsymbol{\tau}$ and the channel's fading $\boldsymbol{H}$ is described by:

$$\text{MSNIR}_{k,\boldsymbol{\tau},\boldsymbol{H}} = a_k \boldsymbol{p}_{K+k}^H \left(\boldsymbol{P}_{K+k} \boldsymbol{A}_{K+k}^2 \boldsymbol{P}_{K+k}^H + \boldsymbol{\Gamma} \right)^{-1} \boldsymbol{p}_{K+k} \tag{3.13}$$

where $\boldsymbol{\tau}$ and $\boldsymbol{H}$ were defined in equations (2.20) and (2.21), respectively. The theoretical 4-QAM symbol error rate of the kth user averaged over the delays and fading can be evaluated as

$$\text{Pe}_k = 2\text{E}_{\boldsymbol{\tau},\boldsymbol{H}} \left[\text{Q} \left(\sqrt{\text{MSNIR}_{k,\boldsymbol{\tau},\boldsymbol{H}}} \right) \right] \tag{3.14}$$

The expectation in equation (3.14) can be obtained by averaging over a number of Monte-Carlo runs with random fading $\boldsymbol{H}$ and delays $\boldsymbol{\tau}$.

As mentioned before, the partial sampling parameter L provides a trade-off between performance and complexity. Figures 3.4 depicts the dependence of the performance of a PS-MMSEC receiver on the parameter L in an asynchronous MC-CDMA system with $K = 3$ users and $M = 7$ subcarriers, while 3.5 shows the result

obtained in a system with $K = 10$ and $M = 15$. The random delays are assumed to be quantized values with a minimum increment of $\frac{T}{M}$ in these systems, i.e. $\frac{T}{7}$ in the former system and $\frac{T}{15}$ in the latter. These two figures show that for both systems, the performance of the PS-MMSEC receiver improves dramatically with L increasing up to a certain value, i.e. $L = 4$ for the former system and $L = 10$ for the latter. Beyond this value, the performance improvement becomes less significant. Therefore, there is a great possibility of reducing system complexity by using a proper small value of L. Furthermore, the results shown in these figures can also be viewed as follow. A PS-MMSEC receiver with a certain partial sampling rate achieves satisfactory performance even when the values of the random delays are much finer quantized by an increment smaller than the reciprocal of the partial sampling rate.

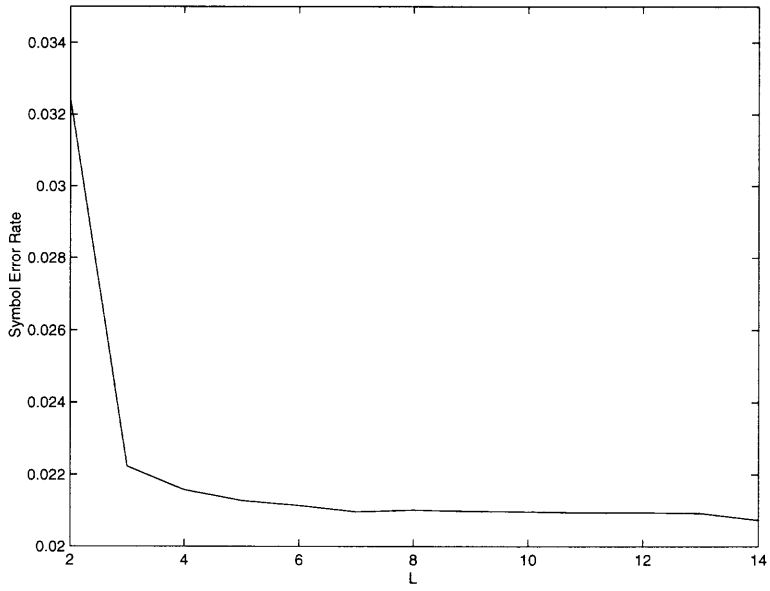

Figure 3.4 Symbol error rate vs. PS-MMSEC's sampling parameter L, SNR=10dB, ISR=5dB, $M = 7$, $K = 3$

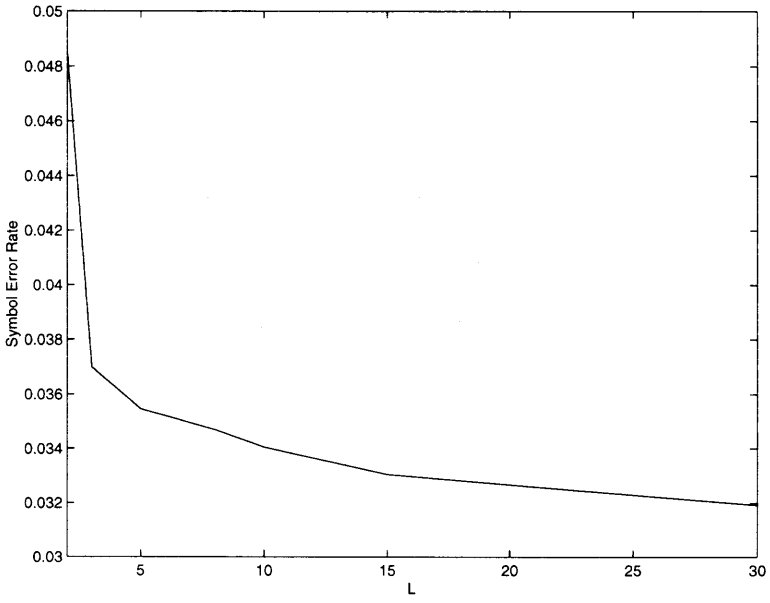

Figure 3.5 Symbol error rate vs. PS-MMSEC's sampling parameter L, SNR=10dB, ISR=5dB, $M = 15$, $K = 10$

3.3 Reduced Complexity PS-MMSEC (RPS-MMSEC) Receiver

The PS-MMSEC receiver requires ML coefficients, which is L times as many coefficients as a regular symbol MMSEC detector. Even for a possible small L, as discussed in the previous section, the complexity of the PS-MMSEC receiver increases significantly with the number of subcarriers M. To avoid excessive complexity, a simpler structure, termed reduced complexity PS-MMSEC (RPS-MMSEC) receiver, is proposed. In this receiver, the outputs of the partial sampling demodulator are first combined, with the aid of the corresponding user's spreading code, into several groups before the MMSEC multiuser detection. As a result, the number of MMSEC coefficients can be reduced from ML to NL ($N < M$). This RPS-MMSEC receiver allows one to implement an MMSEC detector with fewer coefficients than a PS-MMSEC receiver and without significant performance loss. The choice of grouping parameter N in the proposed RPS-MMSEC receiver is influenced by the trade-off

between performance and implementation considerations. The block diagram of the proposed RPS-MMSEC receiver is shown in Figure 3.6[1].

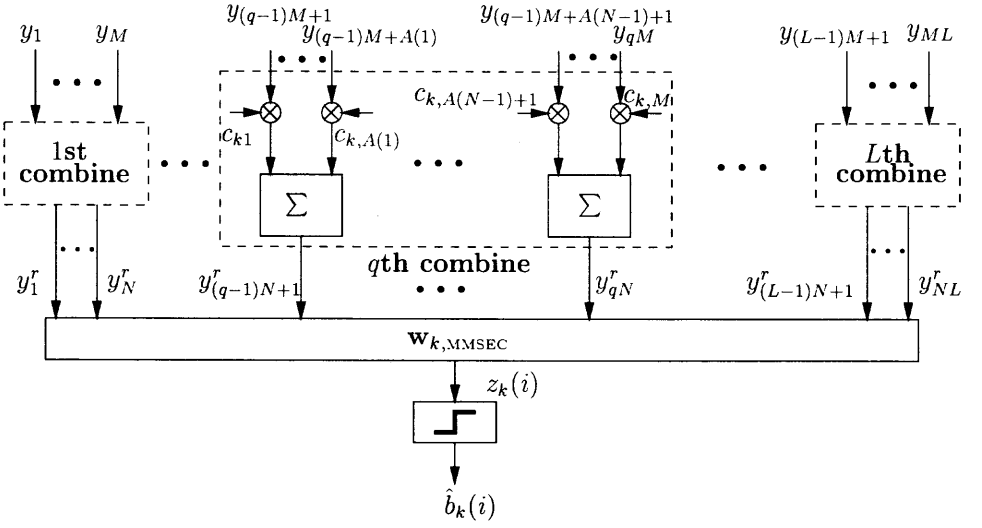

Figure 3.6 Block diagram of the RPS-MMSEC receiver for the kth user

The ML partial sampling demodulator outputs at time instant i, $\boldsymbol{y}(i)$ in equation (3.9), are combined into NL groups as,

$$y^r_{k,qN+n}(i) = \sum_{p=A(n-1)+1}^{A(n)} y_{qM+p}(i)c_{kp}$$

$$= \sum_{k'=1}^{K} \sqrt{a_{k'}} \left[p_{r_{qN+n,k'}} b_{k'}(i) + p^L_{r_{qN+n,k'}} b_{k'}(i-1) + p^R_{r_{qN+n,k'}} b_{k'}(i+1) \right] + \eta^r_{qN+n,k}(i) \quad (3.15)$$

where

$$\begin{aligned}
q &= 0, 1, \ldots, L-1; \quad n = 1, 2, \ldots, N \\
A(n) &= \begin{cases} 0 & n = 0 \\ n\lfloor \frac{M}{N} \rfloor + \sum_{s=1}^{n} U\left(M - N\lfloor \frac{M}{N} \rfloor - s\right) & n = 1, 2, \ldots, N \end{cases} \\
U(x) &= \begin{cases} 1 & x = 0, 1, \ldots \\ 0 & otherwise \end{cases} \\
p^L_{r_{qN+n,k'}} &= \frac{1}{T} \sum_{p=A(n-1)+1}^{A(n)} \sum_{m=1}^{M} c_{kp} c_{k'm} h_{k'm} e^{-j2\pi f_m \tau_{k'}} \int_{\min[qT_s, \tau_{k'}]}^{\min[(q+1)T_s, \tau_{k'}]} e^{j2\pi(f_m - f_p)t} dt \\
p_{r_{qN+n,k'}} &= \frac{1}{T} \sum_{p=A(n-1)+1}^{A(n)} \sum_{m=1}^{M} c_{kp} c_{k'm} h_{k'm} e^{-j2\pi f_m \tau_{k'}} \int_{\max[qT_s, \tau_{k'}]}^{\min[(q+1)T_s, T+\tau_{k'}]} e^{j2\pi(f_m - f_p)t} dt
\end{aligned} \quad (3.16)$$

[1]The block of the partial sampling demodulator, which was shown in Figure 3.2, is omitted for brevity.

$$p^R_{r_{qN+n,k'}} = \frac{1}{T}\sum_{p=A(n-1)+1}^{A(n)}\sum_{m=1}^{M} c_{kp}c_{k'm}h_{k'm}e^{-j2\pi f_m\tau_{k'}}\int_{\max[qT_s,T+\tau_{k'}]}^{\min[(q+1)T_s,2T]} e^{j2\pi(f_m-f_p)t}dt$$

$$\eta^r_{qN+n,k} = \frac{1}{T}\sum_{p=A(n-1)+1}^{A(n)}\int_{qT_s}^{(q+1)T_s} n(t)e^{-j2\pi f_p t}dt$$

Equation (3.15) shows that the samples of all M subcarriers corresponding to the same qth partial sampling instant are combined into N groups. The combining is performed by grouping the subcarriers with the subcarrier index from $A(n-1)+1$ to $A(n)$ into the nth group. $A(n)$ is defined in equation (3.16). The multiplication with c_{kp}, shown in Figure 3.6 and equation (3.15), does not intend to demultiplex the kth user, but prevents corruption of the desired user's signal by the summation during the grouping. This multiplication can also suppress the MUI to some extent before MMSEC detection. Notice that equation (3.15) is used to estimate the kth user's ith transmitted information symbol.

The NL samples are stacked into a vector in the order of their time instants and subcarrier positions, as

$$\begin{aligned}\boldsymbol{y}^r_k(i) &= \left[y^r_{k,1}(i), y^r_{k,2}(i), \ldots, y^r_{k,NL}(i)\right]^T \\ &= \boldsymbol{P}^r\boldsymbol{A}\boldsymbol{B}(i) + \boldsymbol{\eta}^r_k(i)\end{aligned} \tag{3.17}$$

where

$$\boldsymbol{P}^r = \begin{bmatrix} p^L_{r_{1,1}} & \cdots & p^L_{r_{1,K}} & p_{r_{1,1}} & \cdots & p_{r_{1,K}} & p^R_{r_{1,1}} & \cdots & p^R_{r_{1,K}} \\ p^L_{r_{2,1}} & \cdots & p^L_{r_{2,K}} & p_{r_{2,1}} & \cdots & p_{r_{2,K}} & p^R_{r_{2,1}} & \cdots & p^R_{r_{2,K}} \\ \vdots & \ddots & \vdots & \vdots & \ddots & \vdots & \vdots & \ddots & \vdots \\ p^L_{r_{NL,1}} & \cdots & p^L_{r_{NL,K}} & p_{r_{NL,1}} & \cdots & p_{r_{NL,K}} & p^R_{r_{NL,1}} & \cdots & p^R_{r_{NL,K}} \end{bmatrix}$$

$$\boldsymbol{\eta}^r_k(i) = [\eta^r_{1,k}, \eta^r_{2,k}, \ldots, \eta^r_{NL,k}]^T$$

Notice that the noise sample vector $\boldsymbol{\eta}^r_k(i)$ has zero mean and covariance matrix $\boldsymbol{\Gamma}^r$, whose $(qN+n, pN+m)$th element can be derived similar to equation (3.6) as

$$\gamma^r_{qN+n,pN+m} = \delta(q-p)\frac{2\sigma_n^2}{LT}\sum_{p_1=A(m-1)+1}^{A(m)}\sum_{p_2=A(n-1)+1}^{A(n)} \operatorname{sinc}\left(2T\frac{f_{p_1}-f_{p_2}}{L}\right)e^{j2\pi\frac{(f_{p_1}-f_{p_2})T}{L}(2q+1)} \tag{3.18}$$

The reduced complexity partial sampling demodulator's ith output vector, $\boldsymbol{y}_k^r(i)$, is multiplied by the MMSEC coefficients, which can be calculated using equation (3.11)[2], to form a test statistic for the kth user's ith symbol,

$$\hat{b}_k(i) = \text{csgn}(z_k(i)) = \text{csgn}(\boldsymbol{w}_{k,\text{mmsec}}^H \boldsymbol{y}_k^r(i)) \tag{3.19}$$

The theoretical 4-QAM symbol error rate of the kth user averaged over the delays and fading can be evaluated as

$$\text{Pe}_k^r = 2\text{E}_{\boldsymbol{\tau},\boldsymbol{H}}\left[\text{Q}\left(\sqrt{a_k \boldsymbol{p}_{K+k}^{rH}\left(\boldsymbol{P}_{K+k}^r \boldsymbol{A}_{K+k}^2 \boldsymbol{P}_{K+k}^{rH} + \boldsymbol{\Gamma}^r\right)^{-1} \boldsymbol{p}_{K+k}^r}\right)\right] \tag{3.20}$$

where $\boldsymbol{p}_{K+k}^r$ denotes the $(K+k)$th column of matrix $\boldsymbol{P}^r$ and $\boldsymbol{P}_{K+k}^r$ denotes the matrix without the $(K+k)$th column.

Obviously, like in the PS-MMSEC receiver, the performance of the RPS-MMSEC receiver is dependent on the partial sampling parameter L. Furthermore, the grouping parameter N also affects the performance of the RPS-MMSEC receiver. To examine such dependence, the performance of two systems, which were used in Figure 3.4 and 3.5, as a function of N are presented in Figures 3.7 and 3.8. $L = 4$ and $L = 10$ are used in the 7-subcarrier 3-user and 15-subcarrier 10-user systems, respectively, which were determined as the proper choices from Figures 3.4 and 3.5. Similar to the results shown in Figures 3.4 and 3.5, the performance improvement becomes less significant after N reaches a certain value: $N = 4$ for the 7-subcarrier 3-user system and $N = 5$ for the 15-subcarrier 10-user system. Thus, it is possible to significantly reduce the receiver's complexity by choosing a proper small value for the grouping parameter N.

3.4 Adaptive Implementation

Both the PS-MMSEC and RPS-MMSEC receivers can be implemented using the LMS algorithm. The initial adaptation of the LMS algorithm is performed using a

[2] $\boldsymbol{P}$ is replaced by $\boldsymbol{P}^r$ and $\boldsymbol{\Gamma}$ is replaced by $\boldsymbol{\Gamma}^r$

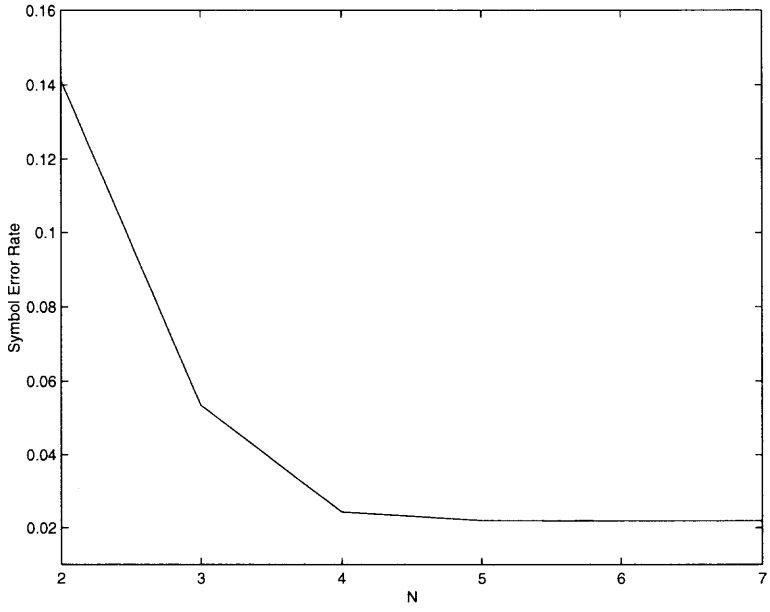

Figure 3.7 Symbol error rate vs. RPS-MMSEC's parameter N, SNR=10dB, ISR=5dB, $M = 7$, $K = 3$, $L = 4$

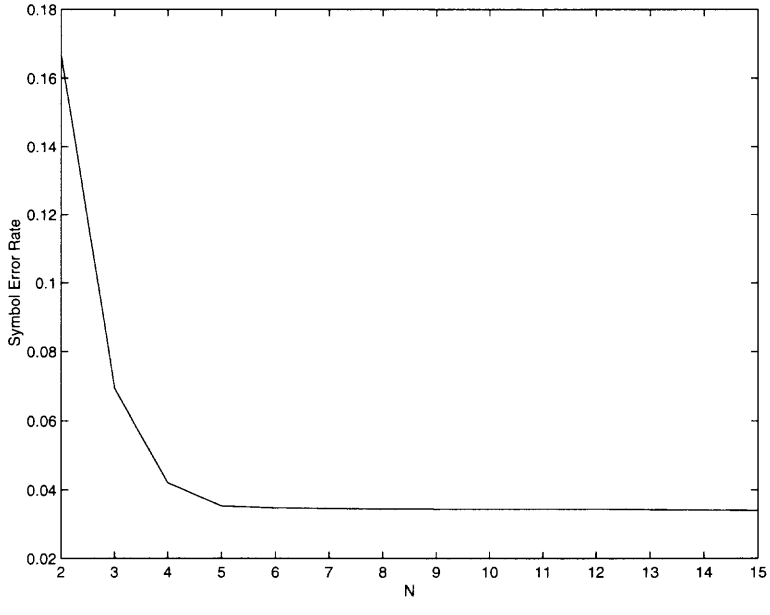

Figure 3.8 Symbol error rate vs. RPS-MMSEC's sampling parameter N, SNR=10dB, ISR=5dB, $M = 15$, $K = 10$, $L = 10$

known training sequence, $\mathbf{d} = [d(1), d(2), \ldots]$, as a reference signal for the algorithm to minimize the output MSE. When the adaptation reaches convergence, the receiver switches to operate in a data driven mode. The reference signal is then provided by the estimated symbols. Notice that the adaptive versions of the PS-MMSEC and RPS-MMSEC receivers provide multiuser detection for an asynchronous MC-CDMA system without requiring knowledge of any timing and interfering users' spreading codes. The recursive relation for updating the MMSEC detector coefficients vector $\boldsymbol{w}(i)$ can be described as

$$\hat{\boldsymbol{w}}_k(i+1) = \hat{\boldsymbol{w}}_k(i) + \mu \boldsymbol{y}(i) \left[\hat{b}_k(i)^* - \boldsymbol{y}(i)^H \hat{\boldsymbol{w}}_k(i)\right] \tag{3.21}$$

where μ is the step-size parameter. As in any LMS adaptive algorithm, the convergence rate of the adaptation depends on μ. With a larger value of μ, the steady state condition is achieved faster but with a higher averaged square error. Another factor that affects the adaptation is the eigenvalue spread of the received signals correlation matrix, because the direction of convergence that takes place may be along the "slow" eigenvector if the input samples are highly correlated. A noise whitening filter $\boldsymbol{D}$ is used preceded the MMSEC to transform the colored Gaussian noise with covariance $\boldsymbol{\Gamma}$ into white noise, where

$$\boldsymbol{D}^H \boldsymbol{D} = \boldsymbol{\Gamma}^{-1} \tag{3.22}$$

The implementation of this whitening filter only depends on L for the PS-MMSEC receiver (see equation (3.6)) or L together with $A(n)$ for the RPS-MMSEC receiver (see equation (3.18)). It can reduce the correlation of the input signal when the SNR is moderate and hence speed up the convergence.

3.5 Performance of the PS-MMSEC and RPS-MMSEC Receivers

In this section, some examples are presented to illustrate the performance of the PS-MMSEC and RPS-MMSEC receivers in an uplink MC-CDMA system. The results

are obtained while operating under both uncorrelated and correlated Rayleigh fading channels. Gold codes with length 7 and 15 are used as spreading code sequences. The random delay τ_k is assumed to be a discrete number, $\frac{p}{M}T$, where integer $p \in [0, M-1]$ with equal probability. Thus, the minimum increment, i.e. resolvable duration, of the random delay is $\frac{T}{M}$. This assumption simplifies the numerical calculation. The uncertainty of the delays is reduced to a set of hypotheses with smaller size, which can be fully experienced without using too many Monte-Carlo runs. Notice that since the proper partial sampling rate of a PS-MMSEC receiver does not depend highly on the delay quantization, which were depicted in Figures 3.4 and 3.5, this quantization does not limit the generality of the proposed PS-MMSEC and RPS-MMSEC receivers. Since the symbol error rate of the receiver is dependent on the channel realization, all the symbol error rate curves shown are obtained by averaging over 200 Monte-Carlo runs.

For comparison, the results obtained with a regular symbol MMSEC receiver with perfect timing acquisition are shown together with the results from the partial sampling receivers. The symbol MMSEC receiver demodulates the received signal in synchronization with the desired user at every symbol interval T and needs an MMSEC detector with M coefficients. Since the partial sampling receivers, with and without the reduced complexity structure, must use information within the $2T$ observation interval, for a fair comparison an observation length $2T$ is also assigned to the symbol MMSEC receiver. Thus, the outputs of the symbol demodulator are stacked in a $2M \times 1$ vector. The desired user's information is extracted by multiplying this vector with $2M \times 1$ MMSEC coefficients. Also, the SUB defined in equation (2.18) is provided as the performance lower bound.

3.5.1 Uncorrelated Rayleigh Fading Channel

In this subsection, uncorrelated frequency flat Rayleigh fading per subcarrier is assumed. As mentioned in Chapter 2, this assumption is realistic for some scenarios. One is spacing the subcarriers greater than or equal to the coherent bandwidth at the expense of a loss in bandwidth efficiency. Another is transmitting several MC-CDMA signal in parallel where the subcarriers are interleaved over the frequency to achieve maximum frequency separation between the subcarriers of the same information symbol. Simulations for the uncorrelated Rayleigh fading channel have been carried out with the following parameters: $M = 7$ subcarriers, $K = 3$ active users.

The averaged symbol error rate versus the ISR for the symbol MMSEC receiver with known timing, and the PS-MMSEC receivers is shown in Figure 3.9. The SNR of the desired user is $\text{SNR}_1 = 10\text{dB}$. It can be seen that in the low interference region, the PS-MMSEC receiver with $L = 2M = 14$, which has the full resolution of the random delays, performs similar to the symbol MMSEC receiver with known timing and approaches the SUB. The PS-MMSEC receiver with $L = 4$ performs slightly worse due to the reduced resolution of the random delays. In the high interference region, the PS-MMSEC receiver with both $L = 4$ and $L = 14$ is shown to perform better than the symbol MMSEC receiver with known timing. The stronger interference suppression capability of the PS-MMSEC can be explained as follows. Although the symbol MMSEC receiver knows the timing of the desired user perfectly, its performance is still limited by MUI. The MUI results from the interfering users' three successive symbols, caused by the timing offset between the desired user and the interfering users. The partial sampling demodulator samples the received signal including the interference more often than the symbol demodulator, which provides more degrees of freedom for the MMSEC multiuser detector to cancel interference. To prove the above statements, the performance of a PS-MMSEC receiver with known timing is also shown. The superior interference suppression capability of this PS-

MMSEC receiver with timing knowledge shows that the performance improvement of the PS-MMSEC receiver in the high interference region is the result of the partial sampling. It is worthwhile to note that with the full timing resolution, i.e. $L = 14$, the PS-MMSEC receivers with and without timing knowledge perform approximately the same.

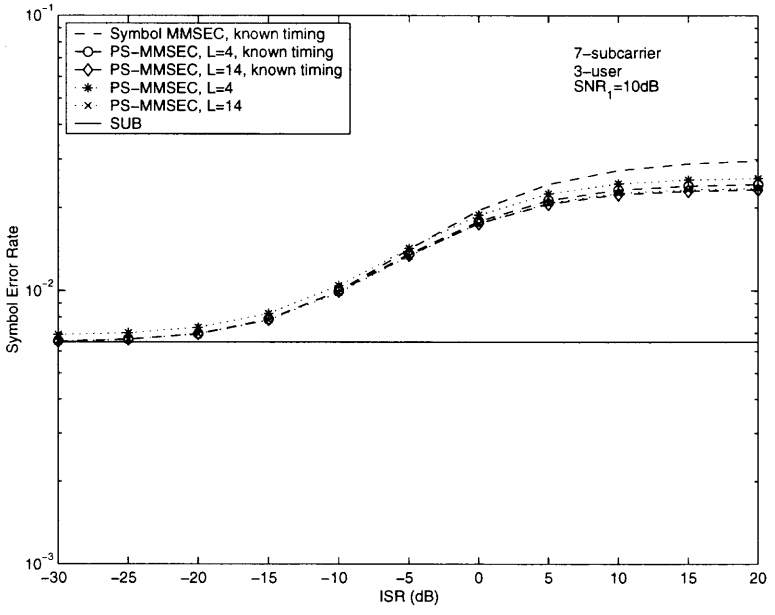

Figure 3.9 Symbol error rate of the PS-MMSEC with $L = 4, 14$ and symbol MMSEC with known timing vs. ISR in uncorrelated Rayleigh fading channel, $\mathrm{SNR}_1 = 10\mathrm{dB}$

The averaged symbol error rate versus the desired user's SNR, SNR_1, for the symbol MMSEC receiver with known timing, the PS-MMSEC, and the RPS-MMSEC receiver, is shown in Figure 3.10. It can be seen that the PS-MMSEC and RPS-MMSEC receivers perform about the same as the symbol MMSEC receiver with known timing. With a similar performance, the complexity of the RPS-MMSEC receiver is comparable to the symbol MMSEC receiver. The symbol MMSEC receiver needs $2M = 14$ coefficients, while the RPS-MMSEC receiver requires $NL = 20$ coefficients. Therefore, the price paid for avoiding a complicated timing estimation block by using the RPS-MMSEC receiver is only a small increase in the number of coefficients (20 instead of 14), which is quite moderate.

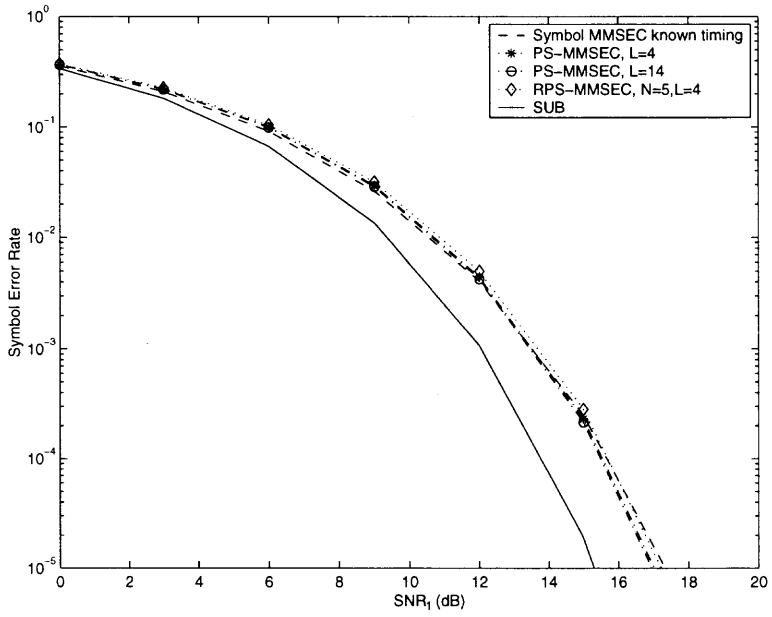

Figure 3.10 Symbol error rate of the PS-MMSEC with $L = 4, 14$, RPS-MMSEC with $N = 5, L = 4$ and symbol MMSEC with known timing vs. SNR_1 in uncorrelated Rayleigh fading channel, ISR=0dB

In Figure 3.11, the output SNIR of the desired user of the adaptive PS-MMSEC, RPS-MMSEC and symbol MMSEC receivers with SNR_1 = 10dB and ISR= 20dB is shown as a function of iterations. This performance is obtained by calculating the output SNIR using the adaptive MMSEC coefficients. The figure illustrates that the PS-MMSEC receiver with $ML = 28$ coefficients and the RPS-MMSEC receiver with $NL = 16$ coefficients has a better SNIR performance and a faster convergence than the symbol MMSEC receiver with known timing. An adaptive PS-MMSEC receiver with the timing knowledge and the same number of coefficients, $ML = 28$, has, as expected, an SNIR performance and rate of convergence similar to the PS-MMSEC receiver without known timing. Thus, the superior behavior of the adaptive PS/RPS-MMSEC receiver in comparison to the adaptive symbol MMSEC receiver with known timing is due to the increase in the degrees of freedom created by the partial sampling demodulator.

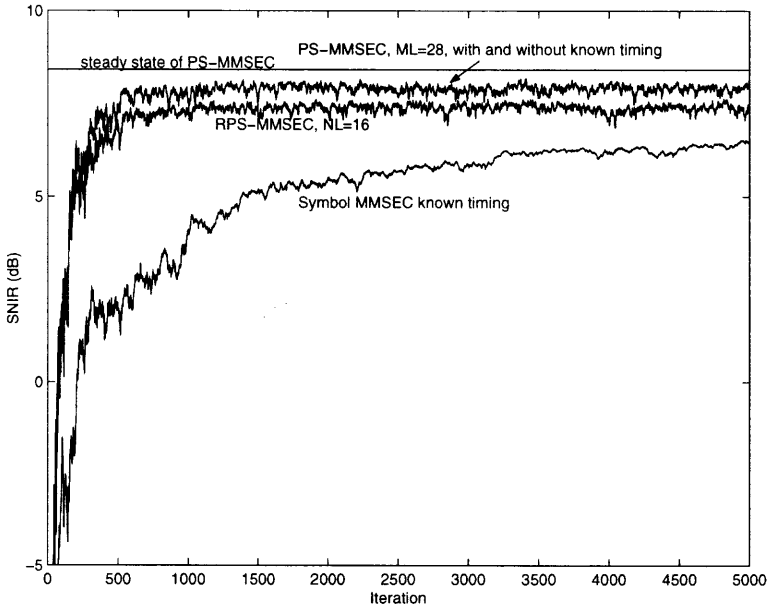

Figure 3.11 SNIR at the output of the adaptive PS-MMSEC, RPS-MMSEC and symbol MMSEC receivers vs. iteration in uncorrelated Rayleigh fading channel, $\text{SNR}_1 = 10\text{dB}$, ISR=20dB

3.5.2 Correlated Rayleigh Fading Channel

In this subsection, a Rayleigh fading channel with a correlation between the subcarriers is assumed. The channel is modeled as a Land-Mobile (LM) channel in an urban environment for which the maximum multipath delay (relative to the first path), τ_{max}, typically is 1-3 μs. As the rms channel delay spread τ_d is always less than τ_{max}, $\tau_d = 0.5\mu s$ is selected. Additionally, it is assumed the total bandwidth $BW = 1\text{MHz}$ and the system parameter $F = 1$, such that for a 15-subcarrier MC-CDMA system the adjacent subcarriers are separated by $\Delta f = \frac{BW}{M+1} = 62.5\text{kHz}$. The correlation between the different subcarriers is calculated using equation (2.6).

Simulations have been carried out with the following parameters: $M = 15$ subcarriers, $N = 5$, $L = 10$, a desired user's SNR is $\text{SNR}_1 = 10\text{dB}$, ISR=20dB and the maximum number of users is 15. The performance of the PS-MMSEC with $ML = 150$ coefficients, the RPS-MMSEC with $NL = 50$ coefficients and the symbol

MMSEC with $2M = 30$ coefficients, in both uncorrelated and correlated Rayleigh fading channels, is shown in Figure 3.12. This figure shows that for both channel types, the PS-MMSEC and RPS-MMSEC receivers outperform the symbol MMSEC receiver with known timing for all number of active users greater than one. This is consistent with the previous explanation that the partial sampling demodulation provides more degrees of freedom, which allows the multiuser detector to perform better interference suppression. The figure also shows that for a low number of active users, all receivers perform considerably better in an uncorrelated fading channel than in a correlated fading channel. This is as expected, because the receivers can utilize more frequency diversity in an uncorrelated fading channel. However, as the number of active users increases, the symbol error rate in the uncorrelated fading channel increases more rapidly than that of the correlated fading channel. This is because the MUI becomes the dominant effect in corrupting the received signal, which is approximately the same for both channel types. As a result, both channel types have almost equal performance for a high number of active users.

3.6 Discussion

In order to eliminate the synchronization process required in regular uplink receivers, a novel partial sampling demodulation scheme for uplink MC-CDMA systems was proposed in this chapter. With a sufficient statistic provided by the partial sampling demodulator, the MMSEC multiuser detector successfully performs joint time acquisition and interference suppression. Simulation results show that the proposed PS-MMSEC receiver outperforms a regular symbol MMSEC receiver with known timing in the presence of strong MUI. This PS-MMSEC receiver requires a number of detector coefficients, which may be prohibitive in a practical system. To reduce the complexity, a lower partial sampling rate can be chosen and/or the RPS-MMSEC receiver can be applied. The RPS-MMSEC receiver significantly reduces

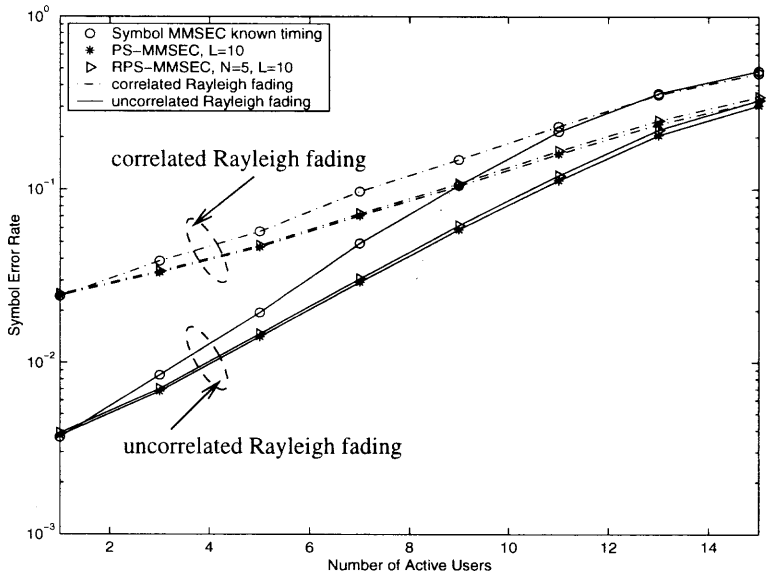

Figure 3.12 Symbol error rate of PS-MMSEC, RPS-MMSEC and symbol MMSEC vs. number of active users in uncorrelated and correlated Rayleigh fading channel, SNR_1 = 10dB, ISR=20dB

the number of detector coefficients without much performance loss, by grouping several subcarriers together. In comparison to the PS-MMSEC receiver, the flexible choice of the detector's coefficient length makes the RPS-MMSEC receiver more convenient and suitable for practical applications. The adaptive implementation of both PS-MMSEC and RPS-MMSEC receiver using the LMS algorithm is shown to have a superior rate of convergence and symbol error rate performance as compared to the regular symbol MMSEC receiver with known timing.

CHAPTER 4

DUAL-RATE ACCESS SCHEMES FOR MC-CDMA SYSTEM

Emerging wireless communication systems will provide not only voice services, but also data services, including facsimile, file transfer and email, etc. Therefore, it is necessary to consider a system which can support multiple data rate communications. This chapter presents a dual-rate synchronous MC-CDMA system wherein users are allowed to transmit information at one of two available rates. Three dual-rate access schemes, fixed spreading length (FSL) [63], coded FSL (CFSL) and variable spreading length (VSL) [64], are proposed.

In the FSL scheme, the same set of subcarriers is used for both high and low-rate signals. The frequency separation between adjacent subcarriers is chosen to be the reciprocal of the high-rate user's bit duration to maintain orthogonality of the subcarriers for both the low-rate and high-rate users. Hence, this scheme prevents ICI with dual-rate transmission. However, the frequency separation is several times wider than the low-rate signals' minimum orthogonal frequency separation. The non-overlapping subcarrier spectra of the low-rate users result in a loss of bandwidth efficiency for these users and consequently a reduction in the system capacity. To alleviate such bandwidth efficiency loss, the VSL scheme is proposed. In this scheme, the low and high-rate users utilize two different sets of subcarriers, which are spaced by the reciprocal of the low-rate and high-rate users' bit duration, respectively. Thus, within the same bandwidth,the low-rate users can be modulated onto more subcarriers in the VSL scheme whose spectra are overlapping, than in the FSL scheme. Since more subcarriers are used, a low-rate user can be assigned with a longer spreading code with a better cross-correlation property, which provides stronger interference suppression capability for the low-rate users. Therefore, the performance of the low-rate users in the VSL scheme is shown superior to the FSL scheme in the presence of interference. Another way to improve the performance of

the low-rate users in the FSL system is to apply channel coding techniques to the low-rate users. This is termed CFSL scheme. The dual-rate MC-CDMA signal has a built-in repetition code structure for the low-rate users, hence, applying the CFSL scheme for the low-rate users will not introduce extra redundancy. The coding gain achieved by the coding techniques compensates for the bandwidth efficiency loss for the low-rate users.

To evaluate the performance of the FSL, CFSL and VSL schemes in a multipath frequency-selective Rayleigh fading channel, an MMSEC multiuser detector, which has been used in the previous chapter for the single-rate MC-CDMA system, is implemented for the dual-rate system. It is worth noting that these dual-rate access schemes can be easily extended to fit into a multi-rate MC-CDMA system with small notational changes.

4.1 Dual-rate MC-CDMA System

A dual-rate synchronous MC-CDMA system, in which the low-rate users and the high-rate users can be transmitted together, is considered. The bit duration of the low-rate and high-rate users is $T^{(l)}$ and $T^{(h)}$, respectively, where $T^{(l)} = NT^{(h)}$ and the rate ratio N is a positive integer. MC-CDMA signals with $K^{(l)}$ low-rate users and $K^{(h)}$ high-rate users are generated in the same manner as a single-rate MC-CDMA signal: each low/high-rate information bit is replicated into $M^{(l)}/M^{(h)}$ parallel copies, multiplied with a corresponding spreading code with length $M^{(l)}/M^{(h)}$, and modulated on $M^{(l)}/M^{(h)}$ subcarriers, respectively. To avoid implementing a bank of oscillators with prohibitive complexity, a discrete-time multicarrier modulation performed by an $M^{(\cdot)}$-point IDFT operation is applied at the transmitter in this chapter. Thus, as mentioned in Chapter 2, the frequency separation between adjacent subcarriers is $\Delta f = \frac{1}{T^{(\cdot)}}$.

The received waveform of the dual-rate MC-CDMA signal can be written as

$$r(t)=\sum_{i=-\infty}^{+\infty}\left[\sum_{n=1}^{M^{(l)}}\sum_{k=1}^{K^{(l)}}\sqrt{a_k^{(l)}}b_k^{(l)}(i)\sum_{m=1}^{M^{(l)}}h_m^{(l)}c_{km}e^{j2\pi\frac{mn}{M^{(l)}}}P^{(l)}(t-(iM^{(l)}+n)T_c^{(l)})\right.$$
$$\left.+\sum_{s=(i-1)N+1}^{iN}\sum_{n=1}^{M^{(h)}}\sum_{k=1}^{K^{(h)}}\sqrt{a_k^{(h)}}b_k^{(h)}(s)\sum_{m=1}^{M^{(h)}}h_m^{(h)}\theta_{km}e^{j2\pi\frac{mn}{M^{(h)}}}P^{(h)}(t-(sM^{(h)}+n)T_c^{(h)})\right]+n(t) \quad (4.1)$$

where $\sqrt{a_k^{(\cdot)}}$ denotes the kth user's transmitted signal amplitude, $b_k^{(\cdot)}(i) \in [1,-1]$ denotes the kth user's ith BPSK-modulated information bit, c_{km} and θ_{km} denote the mth chip of the kth low-rate and high-rate user's spreading code, $\mathbf{c}_k$ and $\boldsymbol{\theta}_k$, respectively. A virtual "chip" interval is defined as $T_c^{(\cdot)} = \frac{T^{(\cdot)}}{M^{(\cdot)}}$. The additive white Gaussian noise process $n(t)$ has zero mean and variance σ_n^2. The rectangular pulse shape function in equation (4.1) is defined as,

$$P^{(\cdot)}(t) = \begin{cases} \frac{1}{\sqrt{T^{(\cdot)}}} & (iM^{(\cdot)}+n-1)T_c^{(\cdot)} \le t < (iM^{(\cdot)}+n)T_c^{(\cdot)} \\ 0 & \text{otherwise} \end{cases} \quad (4.2)$$

Also, in equation (4.1), $h_m^{(\cdot)}$ denotes the amplitude of the channel fading factor on the mth subcarrier $f_m^{(\cdot)}$. This random variable is assumed Rayleigh distributed. The correlation between the different $h_m^{(\cdot)}$ depends on the channel's delay spread and the frequency separation as shown in equation (2.6).

4.2 Fixed Spreading Length (FSL) Scheme

In the FSL scheme, the low-rate and high-rate users share the same set of subcarriers with length $M = M^{(h)} = M^{(l)}$. Given the assumption that the length of the spreading codes is equal to the number of subcarriers, the spreading codes of low-rate users and high-rate users are also of the same length, M. The value of M can be determined[1] according to the total bandwidth BW and the frequency separation Δf as $M = \frac{BW-\Delta f}{\Delta f}$. The frequency separation Δf is chosen to be $\frac{1}{T^{(h)}}$, which is the minimum required frequency separation to maintain orthogonality between adjacent subcarriers for the high-rate users. Thus, the frequency of the mth subcarrier is, $f_m =$

[1]The guard band is ignored for brevity.

$\frac{m-1}{T^{(h)}}$, $m = 1, 2, \ldots, M$. This frequency separation also ensures subcarrier orthogonality for the low-rate users, as $\Delta f = \frac{N}{T^{(l)}}$. An example of the subcarrier assignment of the FSL dual-rate MC-CDMA system with $N = 2$ is shown in Figure 4.1.

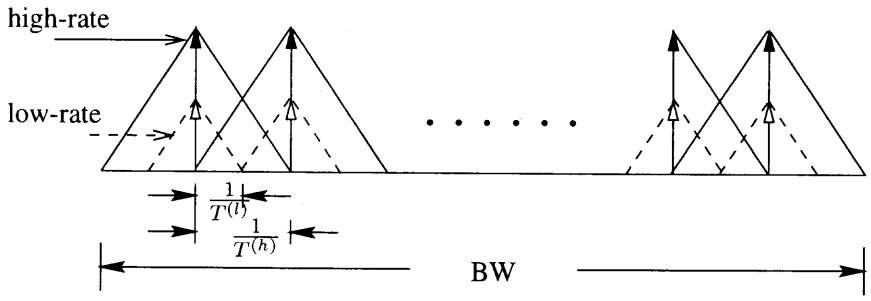

Figure 4.1 The subcarrier assignment of an FSL dual-rate MC-CDMA system.

The general structure of the received dual-rate signal shown in equation (4.1) can be rewritten for the FSL scheme as

$$r_f(t) = \sum_{i=-\infty}^{+\infty} \left[\sum_{n=1}^{M} \sum_{k=1}^{K^{(l)}} \sqrt{a_k^{(l)}} b_k^{(l)}(i) \sum_{m=1}^{M} h_m^{(h)} c_{km} e^{j2\pi \frac{mn}{M}} P^{(l)}(t - (iM+n)T_c^{(l)}) \right.$$
$$\left. + \sum_{s=(i-1)N+1}^{iN} \sum_{n=1}^{M} \sum_{k=1}^{K^{(h)}} \sqrt{a_k^{(h)}} b_k^{(h)}(s) \sum_{m=1}^{M} h_m^{(h)} \theta_{km} e^{j2\pi \frac{mn}{M}} P^{(h)}(t - (sM+n)T_c^{(h)}) \right] + n(t) \quad (4.3)$$

4.2.1 FSL Receiver Design

The received FSL dual-rate signal can be detected by a low-rate-mode (LRM) receiver proposed in [42, 43] for DS-CDMA and [63] for MC-CDMA. The LRM receiver processes the received signal at interval $[(i-1)T^{(l)}, iT^{(l)})$. Within this duration, each low-rate user transmit one bit, while, each high-rate user transmits N successive bits. The nth bit of these N high-rate bits, where $n = 1, 2, \ldots, N$, can be considered as a virtual low-rate bit with duration $T^{(l)}$, in which only the nth subinterval with duration $T^{(h)}$ is non-zero. Thus, the dual-rate system is equivalent to a single rate low-rate system with $K = K^{(l)} + NK^{(h)}$ virtual low-rate users, each transmitting at the rate, $\frac{1}{T^{(l)}}$. In the FSL dual-rate MC-CDMA system, the LRM receiver consists

of N M-point DFTs concatenated in serial. The block diagram of the FSL dual-rate MC-CDMA system is shown in Figure 4.2.

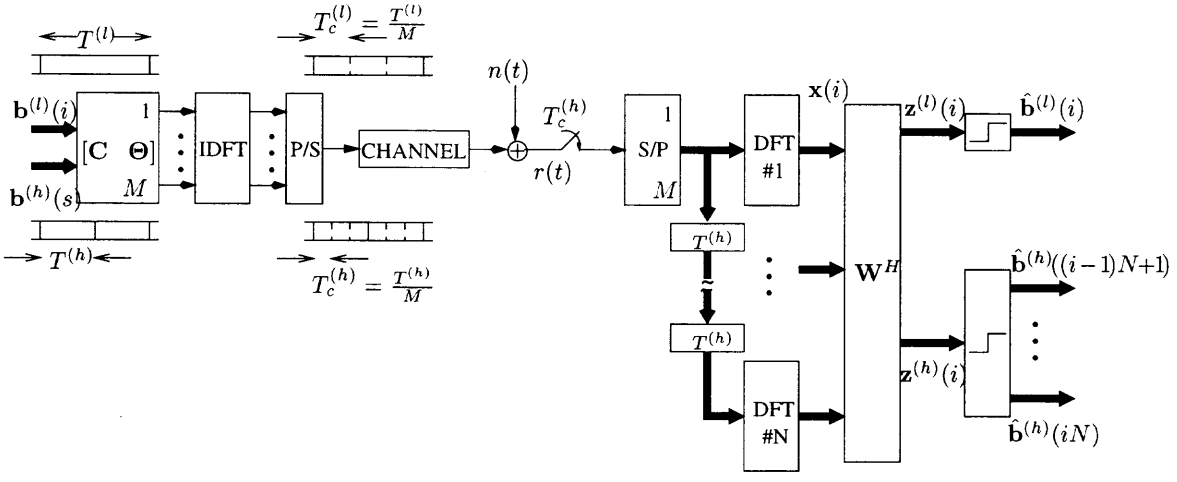

Figure 4.2 The block diagram of the FSL dual-rate MC-CDMA system.

The received FSL signal is first sampled at the virtual chip rate $\frac{1}{T_c^{(h)}}$ and converted into parallel to form an $M \times 1$ vector. The sampling rate is chosen to be $\frac{1}{T_c^{(h)}}$ since it guarantees no modulated information loss for both the high-rate and low-rate signals. The vector that is obtained at the subinterval $[(i-1)T^{(l)} + (n-1)T^{(h)}, (i-1)T^{(l)} + nT^{(h)})$ is processed by the nth M-point DFTs of the LRM receiver to perform multicarrier demodulation. The output of the nth DFT can be described as

$$\boldsymbol{x}_n(i) = \boldsymbol{H} \left[\frac{1}{\sqrt{N}} \boldsymbol{C}_f \quad \boldsymbol{\Theta} \right] \begin{bmatrix} \boldsymbol{A}^{(l)} & \\ & \boldsymbol{A}^{(h)} \end{bmatrix} \begin{bmatrix} \boldsymbol{b}^{(l)}(i) \\ \boldsymbol{b}^{(h)}((i-1)N+n) \end{bmatrix} + \boldsymbol{\eta}_n(i) \qquad (4.4)$$

where the matrix $\boldsymbol{A}^{(\cdot)} = \text{diag}\left[\sqrt{a_1^{(\cdot)}} \ \sqrt{a_2^{(\cdot)}} \ \cdots \ \sqrt{a_{K^{(\cdot)}}^{(\cdot)}}\right]$ contains the amplitudes of all users on the diagonal, the vector $\boldsymbol{b}^{(\cdot)}(i) = \left[b_1^{(\cdot)}(i) \ b_2^{(\cdot)}(i) \ \cdots \ b_{K^{(\cdot)}}^{(\cdot)}(i)\right]^T$ contains the information bits of all users, and the matrix $\boldsymbol{H} = \text{diag}\left[h_1^{(h)}, h_2^{(h)}, \cdots, h_M^{(h)}\right]$ contains the channel fading factors of the M subcarriers on the diagonal. $\boldsymbol{C}_f = [\mathbf{c}_1 \ \mathbf{c}_2 \ \cdots \ \mathbf{c}_{K^{(l)}}]$ and $\boldsymbol{\Theta} = [\boldsymbol{\theta}_1 \ \boldsymbol{\theta}_2 \ \cdots \ \boldsymbol{\theta}_{K^{(h)}}]$ are the spreading code matrices for the low-rate and high-rate users, respectively. Also, in equation (4.4), the

elements of an $(M \times 1)$ white Gaussian noise vector $\boldsymbol{\eta}_n(i)$ have zero mean and variance σ_n^2.

Thus, the output of the LRM receiver at interval $[(i-1)T^{(l)}, iT^{(l)})$ can be formed by stacking N DFT output vector $\boldsymbol{x}_n(i)$ into an $(NM \times 1)$ vector $\boldsymbol{x}_f(i)$ as

$$\begin{aligned}
\boldsymbol{x}_f(i) &= \left[\begin{array}{cccc} \boldsymbol{x}_1(i)^T & \boldsymbol{x}_2(i)^T & \ldots & \boldsymbol{x}_N(i)^T \end{array}\right]^T \\
&= \boldsymbol{H}_f \begin{bmatrix} \frac{1}{\sqrt{N}}\boldsymbol{C}_f & \boldsymbol{\Theta} & \mathbf{0} & \ldots & \mathbf{0} \\ \frac{1}{\sqrt{N}}\boldsymbol{C}_f & \mathbf{0} & \boldsymbol{\Theta} & \ldots & \mathbf{0} \\ \vdots & \vdots & \vdots & \ddots & \vdots \\ \frac{1}{\sqrt{N}}\boldsymbol{C}_f & \mathbf{0} & \mathbf{0} & \ldots & \boldsymbol{\Theta} \end{bmatrix} \begin{bmatrix} \boldsymbol{A}^{(l)} & & & \\ & \boldsymbol{A}^{(h)} & & \\ & & \ddots & \\ & & & \boldsymbol{A}^{(h)} \end{bmatrix} \begin{bmatrix} \boldsymbol{b}^{(l)}(i) \\ \boldsymbol{b}^{(h)}((i-1)N+1) \\ \vdots \\ \boldsymbol{b}^{(h)}(iN) \end{bmatrix} + \boldsymbol{\eta}(i) \\
&\stackrel{\text{def}}{=} \boldsymbol{P}_f \boldsymbol{A} \boldsymbol{b}(i) + \boldsymbol{\eta}(i) \qquad (4.5)
\end{aligned}$$

where $\boldsymbol{H}_f = \text{diag}\left[\underbrace{\boldsymbol{H} \;\; \boldsymbol{H} \;\; \ldots \;\; \boldsymbol{H}}_{N}\right]$ and the $(NM \times 1)$ white Gaussian noise vector $\boldsymbol{\eta}(i) = \left[\begin{array}{cccc} \boldsymbol{\eta}_1(i)^T & \boldsymbol{\eta}_2(i)^T & \ldots & \boldsymbol{\eta}_N(i)^T \end{array}\right]^T$ have zero mean and covariance matrix $\sigma_n^2 \boldsymbol{I}$, where $\boldsymbol{I}$ is an $(NM \times NM)$ identity matrix.

Equation (4.5) shows that the output vector $\boldsymbol{x}_f(i)$ contains the information of the $K^{(l)}$ low-rate users' current bits and the $K^{(h)}$ high-rate users' N successive bits. An MMSEC multiuser detector with an $(NM \times (K^{(l)} + NK^{(h)}))$ coefficient matrix $\boldsymbol{W} = [\boldsymbol{w}_1, \boldsymbol{w}_2, \ldots, \boldsymbol{w}_{K^{(l)}+NK^{(h)}}]$, is applied to form the test statistic of the transmitted bits of the low-rate and high-rate users. Similar to equation (3.11), the kth column of $\boldsymbol{W}$, $\boldsymbol{w}_k$, can be shown as

$$\begin{aligned}
\boldsymbol{w}_k = \arg\min_{\boldsymbol{w}_k} \text{MSE}_k &= \frac{\sqrt{a_k}}{1 + a_k \boldsymbol{p}_{f,k}^H \left(\boldsymbol{P}_{f,k} \boldsymbol{A}_k^2 \boldsymbol{P}_{f,k}^H + \sigma_n^2 \boldsymbol{I}\right)^{-1} \boldsymbol{p}_{f,k}} \times \\
&\qquad \left(\boldsymbol{P}_{f,k} \boldsymbol{A}_k^2 \boldsymbol{P}_{f,k}^H + \sigma_n^2 \boldsymbol{I}\right)^{-1} \boldsymbol{p}_{f,k} \qquad (4.6)
\end{aligned}$$

where $\boldsymbol{P}_{f,k}$ denotes the matrix $\boldsymbol{P}_f$ without the kth column, $\boldsymbol{p}_{f,k}$ denotes the kth column of $\boldsymbol{P}_f$ and $\boldsymbol{A}_k$ denotes the matrix $\boldsymbol{A}$ without the kth column and row. The decision variables for the desired low-rate and high-rate users can be obtained by

the ith bit of the kth low-rate user: $z_k^{(l)}(i) = \boldsymbol{w}_k^H \boldsymbol{x}_f(i)$ (4.7)

the jth bit of the kth high-rate user: $z_k^{(h)}(j) = \boldsymbol{w}_{K^{(l)}+K^{(h)}(j-(i-1)N-1)+k}^H \boldsymbol{x}_f(i)$ (4.8)

4.2.2 Performance of the Low-rate Users

Without loss of generality, assume that low-rate user 1 is the desired user. Using the decision variable defined in equation (4.7), the desired user's ith BPSK-modulated bit can be estimated as

$$\hat{b}_1^{(l)}(i) = \mathrm{sgn}(z_1^{(l)}(i)) \tag{4.9}$$

From equations (3.13) and (3.14), the BER of the desired low-rate user in the FSL scheme using the MMSEC detector with coefficients $\boldsymbol{w}_1$ shown in equation (4.6) is given by

$$\mathrm{BER}_{1,\mathrm{mmsec}}^{f,(l)} = \mathrm{E}_{\boldsymbol{H}}\left[\mathrm{Q}\left(\sqrt{\left\{a_1^{(l)}\boldsymbol{p}_{f1}^H\left(\boldsymbol{P}_{f1}\boldsymbol{A}_1^2\boldsymbol{P}_{f1}^H+\sigma_n^2\boldsymbol{I}\right)^{-1}\boldsymbol{p}_{f1}\right\}}\right)\right] \tag{4.10}$$

When only a single low-rate user is present in the system, the MMSEC receiver achieves the minimum BER, the SUB, defined as

$$\mathrm{BER}_{1,\mathrm{SUB}}(i) = \mathrm{E}_{\boldsymbol{H}}\left[\mathrm{Q}\left(\sqrt{\frac{a_1^{(l)}}{\sigma_n^2}\frac{1}{M^{(h)}}\sum_{m=1}^{M^{(h)}}h_m^{(h)2}}\right)\right] \tag{4.11}$$

4.2.3 Performance of the High-rate Users

For the detection of the high-rate users, again assume, without loss of generality, that high-rate user 1 is the desired user. Using the decision variable defined in equation (4.8), the desired user's jth bit can be estimated as

$$\hat{b}_1^{(h)}(j) = \mathrm{sgn}(z_1^{(h)}(j)) \tag{4.12}$$

Similar to the low-rate user case, the BER of the MMSEC receiver for the desired high-rate user in the FSL scheme is given by

$$\mathrm{BER}_{1,\mathrm{mmsec}}^{f,(h)} = \mathrm{E}_{\boldsymbol{H}}\left[\mathrm{Q}\left(\sqrt{\left\{a_1^{(h)}\boldsymbol{p}_{f,K^{(l)}+1}^H\left(\boldsymbol{P}_{f,K^{(l)}+1}\boldsymbol{A}_{K^{(l)}+1}^2\boldsymbol{P}_{f,K^{(l)}+1}^H+\sigma_n^2\boldsymbol{I}\right)^{-1}\boldsymbol{p}_{f,K^{(l)}+1}\right\}}\right)\right] \tag{4.13}$$

As can be seen from equation (4.5), the outputs of the demodulator at every time instant $T^{(l)}$ contain N successive bits for each high-rate user. Notice that these

N bits are always orthogonal, because they are located at non-overlapping time slots. Thus, there is no ISI present among these N successive bits for each high-rate user. The minimum BER can be achieved by the MMSEC receiver is the same as the low-rate user's SUB[2] shown in equation (4.11).

4.3 Coded Fixed Spreading Length (CFSL) Scheme

The FSL scheme protects the dual-rate signals from ICI. However, the non-overlapping subcarrier spectra of the low-rate signals result in a reduced bandwidth efficiency and hence limited performance for the low-rate users in the FSL scheme. In order to compensate for this disadvantage of the low-rate users, a channel coding scheme is added for the low-rate users in a FSL dual-rate system. The idea of using channel coding in the FSL dual-rate MC-CDMA system is straightforward: in the time domain, one low-rate bit can be seen as equivalent to an N times repeated high-rate bit. Thus, a low-rate MC-CDMA signal is equivalent to a repetitional encoded high-rate signal, as shown in Figure 4.3. Therefore, the performance of the low-rate users can be improved by a coding gain, if other more efficient coding schemes than a repetition code scheme are used. Furthermore, unlike other systems where any channel coding scheme introduces redundancy into the transmitted data bit and hence lowers the transmission data rate, the built-in repetition code structure of the low-rate MC-CDMA signal provides the possibility of adding channel coding to the low-rate users without loss of bandwidth efficiency.

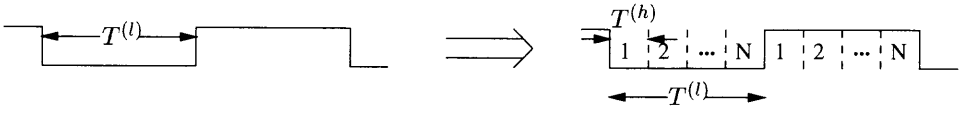

Figure 4.3 The low-rate MC-CDMA signal's timing structure

[2]with $a_1(l)$ replaced by $a_1(h)$.

In the CFSL scheme, before being sent to the multiplexer, the kth low-rate users' information bit sequences with block size N_b, $\mathbf{b}_k^{(l)} = [b_k^{(l)}(1), b_k^{(l)}(2), \ldots, b_k^{(l)}(N_b)]$, are encoded by a channel encoder into a code sequence with block size N_d, $\boldsymbol{d}_k = [d_k(1), d_k(2), \ldots, d_k(N_d)]$, where $N_d = NN_b$. Notice that the code rate $R_c = 1/N$ compensates for the bit rate difference between the high-rate and low-rate users. That is, the coded low-rate bits, $\boldsymbol{d}_k$, has bit rate $\frac{1}{T^{(h)}}$, instead of the original bit rate $\frac{1}{T^{(l)}}$. Hence, after the encoder, the dual-rate system actually becomes a single-rate high-rate system. The waveform of the received dual-rate signal in equation (4.1) can be rewritten for the CFSL scheme as

$$\begin{aligned} r_c(t) &= \sum_{i=-\infty}^{+\infty} \left[\sum_{n=1}^{M} \sum_{k=1}^{K^{(l)}} \sqrt{a_k^{(l)}} d_k(i) \sum_{m=1}^{M} h_m^{(h)} c_{km} e^{j2\pi \frac{mn}{M}} P^{(l)}(t-(iM+n)T_c) \right. \\ &+ \left. \sum_{n=1}^{M} \sum_{k=1}^{K^{(h)}} \sqrt{a_k^{(h)}} b_k^{(h)}(i) \sum_{m=1}^{M} h_m^{(h)} \theta_{km} e^{j2\pi \frac{mn}{M}} P^{(h)}(t-(iM+n)T_c) \right] + n(t) \end{aligned} \quad (4.14)$$

where $d_k(i) \in (1, -1)$ represents the ith coded bit of the kth low-rate user. The time index of the coded bit $d_k(i)$ and the original low-rate bit $b_k(j)$ are related by $j = \lfloor \frac{i}{N_d} \rfloor$.

4.3.1 CFSL Receiver Design

As the transmission rate of the low-rate users after the encoder becomes the same as that of the high-rate users, a high-rate-mode (HRM) receiver is applied in the CFSL scheme. The HRM receiver consists of only one M-point DFT and processes the received signal every $T^{(h)}$. The block diagram of the CFSL dual-rate MC-CDMA system is shown in Figure 4.4.

Like the LRM FSL receiver, the HRM CFSL receiver samples the received signal $r_c(t)$ at the virtual chip rate $\frac{1}{T_c^{(h)}}$. Every M samples are demodulated by an M-point DFT at every $T^{(h)}$ interval. The output of the demodulator at interval $[(i-1)T^{(h)}, iT^{(h)})$ can be written as

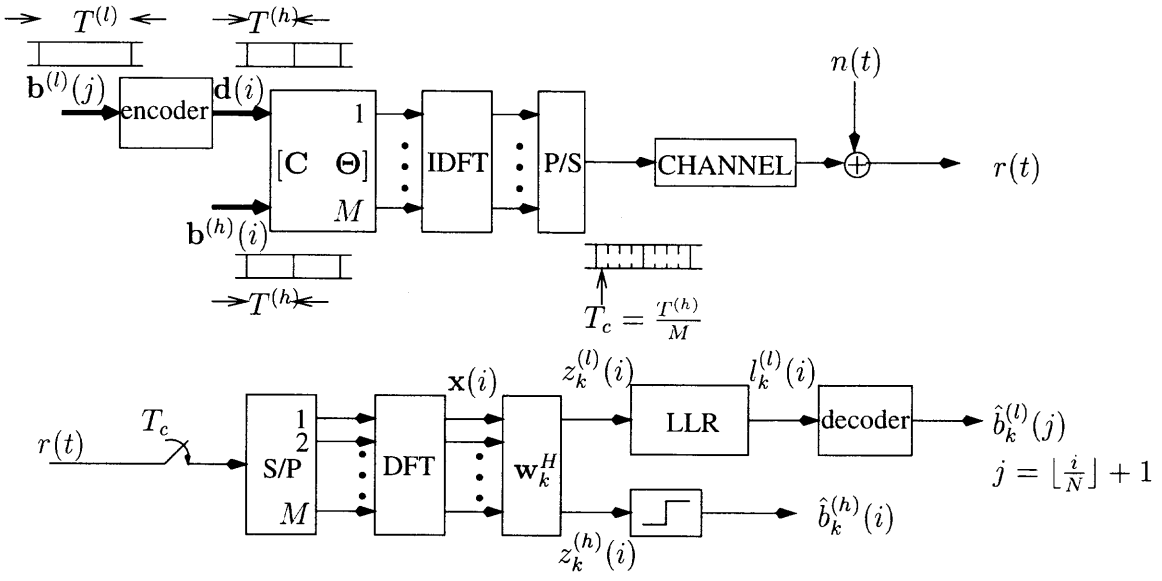

Figure 4.4 The block diagram of the CFSL dual-rate MC-CDMA system

$$\begin{aligned} \boldsymbol{x}_c(i) &= \boldsymbol{H} \left[\begin{array}{cc} \frac{1}{\sqrt{N}}\boldsymbol{C}_f & \boldsymbol{\Theta} \end{array} \right] \left[\begin{array}{cc} \boldsymbol{A}^{(l)} & \\ & \boldsymbol{A}^{(h)} \end{array} \right] \left[\begin{array}{c} \boldsymbol{d}(i) \\ \boldsymbol{b}^{(h)}(i) \end{array} \right] + \boldsymbol{\eta}_c(i) \\ &\stackrel{\text{def}}{=} \boldsymbol{P}_c \boldsymbol{A}_c \boldsymbol{b}_c(i) + \boldsymbol{\eta}_c(i) \end{aligned} \tag{4.15}$$

where

$$\begin{aligned} \boldsymbol{d}(i) &= [d_1(i) \quad d_2(i) \quad \ldots \quad d_{K^{(l)}}(i)]^T \\ \boldsymbol{b}(i) &= \left[\boldsymbol{d}(i)^T \quad \boldsymbol{b}^{(h)}(i)^T\right]^T \end{aligned}$$

and the $(M \times 1)$ white Gaussian noise vector $\boldsymbol{\eta}_c(i)$ has zero mean and covariance matrix $\sigma_n^2 \boldsymbol{I}_c$, where $\boldsymbol{I}_c$ is an $(M \times M)$ identity matrix. Equation (4.15) shows that $\boldsymbol{x}_c(i)$ contains only the high-rate users' current transmitted bits and the low-rate users' current transmitted coded bits. This is different from the output vector $\boldsymbol{x}_f(i)$ of the LRM receiver in the FSL scheme shown in equation (4.5). After the demodulator, the MMSEC multiuser detector, utilized in the FSL scheme, is also applied in the CFSL scheme to obtain the decision variables for the low-rate and high-rate users. Notice that since the decision variables for the low-rate users are encoded, a soft

decision decoder is needed after the MMSEC detector for the low-rate users as shown in Figure 4.4.

4.3.2 MMSEC Multiuser Detector

Without loss of generality, the low-rate user 1 is assumed to be the desired user. Multiplying the MMSEC coefficients $\boldsymbol{w}_{c,1}$, given by equation (4.6)[3], with the output of the HRM demodulator $\boldsymbol{x}_c(i)$, a decision variable for low-rate user 1 is obtained as

$$\begin{aligned} z_1^{(l)}(i) &= \boldsymbol{w}_{c,1}{}^H \boldsymbol{x}(i) \\ &= \underbrace{\boldsymbol{w}_{c,1}{}^H \boldsymbol{p}_{c1} \sqrt{a_1^{(l)}} d_1(i)}_{\text{desired}} + \underbrace{\boldsymbol{w}_{c,1}^H \boldsymbol{P}_{c1} \boldsymbol{A}_{c1} \boldsymbol{b}_{c1}(i)}_{\text{MUI}} + \boldsymbol{w}_{c,1}^H \boldsymbol{\eta}_c(i) \end{aligned} \tag{4.16}$$

where $\boldsymbol{b}_{c1}(i)$ denotes the vector $\boldsymbol{b}_c(i)$ without the first element, $\boldsymbol{P}_{c1}$ denotes the matrix $\boldsymbol{P}_c$ without the 1st column, $\boldsymbol{p}_{c1}$ denotes the 1st column of $\boldsymbol{P}_c$ and $\boldsymbol{A}_{c1}$ denotes the matrix $\boldsymbol{A}_c$ without the 1st column and row. If a sufficient number of users is present, the MUI term in equation (4.16) can be approximated using the central limit theorem by an Gaussian r.v. with zero mean. Therefore, the decision variable $z_1^{(l)}(i)$ can be considered as a Gaussian r.v. with mean μ and variance σ^2, where

$$\begin{aligned} \mu &= \boldsymbol{w}_{c,1}{}^H \boldsymbol{p}_{c1} \sqrt{a_1^{(l)}} d_1(i) \\ \sigma^2 &= \boldsymbol{w}_{c,1}^H \boldsymbol{P}_{c1} \boldsymbol{A}_{c1}^2 \boldsymbol{P}_{c1}^H \boldsymbol{w}_{c,1} + \boldsymbol{w}_{c,1}^H \boldsymbol{w}_{c,1} \sigma_n^2 \end{aligned} \tag{4.17}$$

This statistic will be used in the reliability estimator shown in Figure 4.4 to generate the log-likelihood ratios (LLR) of the decision variables of the low-rate users. LLR is the optimum soft decision value based on the maximum likelihood (ML) rule.

4.3.3 Soft Decision Decoding

A sequence of decision variables for the desired low-rate user 1,

$$\boldsymbol{z}_1^{(l)} = [z_1^{(l)}(1), z_1^{(l)}(2), \ldots, z_1^{(l)}(N_d)] \tag{4.18}$$

[3]The matrices $\boldsymbol{P}_f$, $\boldsymbol{A}$ and $\boldsymbol{I}$ are replaced by $\boldsymbol{P}_c$, $\boldsymbol{A}_c$ and $\boldsymbol{I}_c$

is used to calculate the log-likelihood ratio (LLR) of each element of $\boldsymbol{z}_1^{(l)}$,

$$\mathbf{l}_1 = [l_1(1), l_1(2), \ldots, l_1(N_d)] \tag{4.19}$$

The vector $\mathbf{l}_1$ contains the optimum soft decisions to be used at the decoder. As defined in [68], the LLRs are given by,

$$l_1(n) = \ln\left(\frac{\mathrm{p}\left(z_1^{(l)}(n)|d_1(n)=+1\right)}{\mathrm{p}\left(z_1^{(l)}(n)|d_1(n)=-1\right)}\right) \tag{4.20}$$

where $\mathrm{p}\left(z_1^{(l)}(n)|d_1(n)\right)$ denotes the pdf of $z_1^{(l)}(n)$ given $d_1(n)$ and can be written as

$$\mathrm{p}\left(z_1^{(l)}(n)|d_1(n)\right) = \frac{1}{\sqrt{2\pi\sigma^2}}\exp\left(-\frac{\left(z_1^{(l)}(n)-\mu\right)^2}{\sigma^2}\right) \tag{4.21}$$

where μ and σ^2 are given in equation (4.17). Thus, the LLRs for low-rate user 1 can be written as,

$$l_1(n) = \frac{4\boldsymbol{w}_{c,1}{}^H\boldsymbol{p}_{c1}\sqrt{a_1^{(l)}}}{\boldsymbol{w}_{c,1}^H\boldsymbol{P}_{c1}\boldsymbol{A}_{c1}^2\boldsymbol{P}_{c1}^H\boldsymbol{w}_{c,1} + \boldsymbol{w}_{c,1}^H\boldsymbol{w}_{c,1}\sigma_n^2} z_1^{(l)}(n) \stackrel{\text{def}}{=} \lambda(n) z_1^{(l)}(n) \tag{4.22}$$

Following the maximum likelihood (ML) rule, the decoder determines the most likely transmitted code sequence $\hat{\boldsymbol{d}}_1$ by choosing $\hat{\boldsymbol{d}}_1 = \boldsymbol{d}^p$, where $\boldsymbol{d}^p$ is the pth possible code sequence, if the pth correlation metric $c_p = \boldsymbol{d}^p\mathbf{l}_1^T$ is the maximum of 2^{N_b} possible correlation metrics. The low-rate user 1's transmitted bit $b_1(i)$ can be decided from $\hat{\boldsymbol{d}}_1$.

Notice that, if channel fading is slow, the factor $\lambda(n)$ in equation (4.22) is a fixed value for $n = 1, 2, \cdots, N_d$. Furthermore, this value is always positive when the MMSEC coefficients $\boldsymbol{w}_{c,1}$ are used at the detector. This can be shown as follows. The numerator in equation (4.22) can be written as

$$\begin{aligned} 4\boldsymbol{w}_{c,1}{}^H\boldsymbol{p}_{c1}\sqrt{a_1^{(l)}} &= \frac{4a_1^{(l)}\boldsymbol{p}_{c1}^H\left(\boldsymbol{P}_{c1}\boldsymbol{A}_{c1}^2\boldsymbol{P}_{c1}^H + \sigma_n^2\boldsymbol{I}_c\right)^{-1}\boldsymbol{p}_{c1}}{1 + a_1^{(l)}\boldsymbol{p}_{c1}^H\left(\boldsymbol{P}_{c1}\boldsymbol{A}_{c1}^2\boldsymbol{P}_{c1}^H + \sigma_n^2\boldsymbol{I}_c\right)^{-1}\boldsymbol{p}_{c1}} \\ &= \frac{4\text{MSNIR}}{1+\text{MSNIR}} \end{aligned} \tag{4.23}$$

where MSNIR is the maximum SNIR achieved by the MMSEC detector as defined in equation (3.13). Since the MSNIR is assumed to have a positive value, the numerator in equation (4.22) is positive. The denominator in equation (4.22) is also a positive number because it is the sum of two variances. Therefore,

$$\lambda(n) > 0 \tag{4.24}$$

Thus, in this case, the sign and magnitude of $l_1(n)$ will only depend on $z_1^{(l)}(n)$, which means equation (4.22) can be reduced to $l_1(n) = z_1^{(l)}(n)$. Hence, the LLR block shown in Figure 4.4 can be omitted.

4.3.4 Performance of the Low-rate Users

A linear binary Hadamard block code with block length N_d can be generated by an $N_d \times N_d$ Hadamard matrix and its complement [20]. This Hadamard block coding scheme has a code rate $R_c = \frac{\log_2 2N_d}{N_d}$. Applying the MMSEC multiuser detector, followed by the soft decision decoder, the probability of choosing a correct code sequence $\boldsymbol{d}_1$ for the desired low-rate user 1, P_c, can be described by a joint probability as

$$\mathrm{P}_c = \int_{-\infty}^{\infty} \prod_{\substack{i=1 \\ i \neq p}}^{2N_d} \mathrm{P}(c_i < c_p | c_p) p(c_p) dc_p \tag{4.25}$$

where c_i denotes the correlation metric between user 1's LLRs, $\mathbf{l}_1$, and the ith possible code sequence. $p(c_p)$ denotes the pdf of the correlation metric c_p. Thus, the BER of low-rate user 1 in the CFSL scheme can be derived as

$$\begin{aligned} \mathrm{BER}_{1,\mathrm{mmsec}}^{c,(l)} &= \mathrm{E}_{\boldsymbol{H}}\left[\frac{N_d}{2N_d - 1}(1 - \mathrm{P}_c)\right] \\ &= \mathrm{E}_{\boldsymbol{H}}\left[\frac{N_d}{2N_d - 1}\left\{1 - \frac{1}{\sqrt{2\pi}}\int_{-\infty}^{+\infty} e^{-\frac{y^2}{2}}\left[\mathrm{Q}\left(-y - \frac{\mu_c}{\sigma_c}\right)\right]^{2N_d - 2} \times \mathrm{Q}\left(-y - \frac{2\mu_c}{\sigma_c}\right) dy\right\}\right] \end{aligned} \tag{4.26}$$

where

$$\begin{aligned} \mu_c &= N_d \boldsymbol{w}_{c,1}^H \boldsymbol{p}_{c1} \sqrt{a_1^{(l)}} \\ \sigma_c^2 &= N_d \boldsymbol{w}_{c,1}^H \left(\boldsymbol{P}_{c1} \boldsymbol{A}_{c1}^2 \boldsymbol{P}_{c1}^H + \sigma_n^2 \boldsymbol{I}_c\right) \boldsymbol{w}_{c,1} \end{aligned}$$

As the signal structure of the high-rate users is the same in both the CFSL and FSL systems, the performance of the high-rate users remains the same as that of the FSL system.

4.4 Variable Spreading Length (VSL) Scheme

The VSL scheme is another approach to improve the performance of the low-rate users in a dual-rate MC-CDMA system. With this scheme, the low-rate and high-rate users use different sets of subcarriers. The frequencies of the low-rate users' subcarriers, $\mathbf{f}^{(l)} = [f_1^{(l)}, f_2^{(l)}, \ldots, f_{M^{(l)}}^{(l)}]$, are related by $f_m^{(l)} = (m-1)\frac{1}{T^{(l)}}$; while the frequencies of the high-rate users' subcarriers, $\mathbf{f}^{(h)} = [f_1^{(h)}, f_2^{(h)}, \ldots, f_{M^{(h)}}^{(h)}]$, are related by $f_m^{(h)} = (m-1)\frac{1}{T^{(h)}}$. The $\frac{1}{T^{(l)}}$ and $\frac{1}{T^{(h)}}$ are the minimum required frequency separation to maintain orthogonality between adjacent subcarriers for the low-rate and high-rate users, respectively. Given the assumption that the length of the spreading codes is equal to the number of subcarriers, the low-rate and high-rate users are assigned with the spreading codes of different length. That is, when $BW \gg \frac{1}{T^{(\cdot)}}$, $M^{(l)} \approx NM^{(h)}$. Since $\frac{T^{(l)}}{M^{(l)}} = \frac{T^{(h)}}{M^{(h)}}$, the virtual chip interval for both low and high-rate signals is $T_c = \frac{T^{(\cdot)}}{M^{(\cdot)}}$. The subcarrier assignment of the proposed VSL dual-rate MC-CDMA system with $N = 2$ is shown in Figure 4.5.

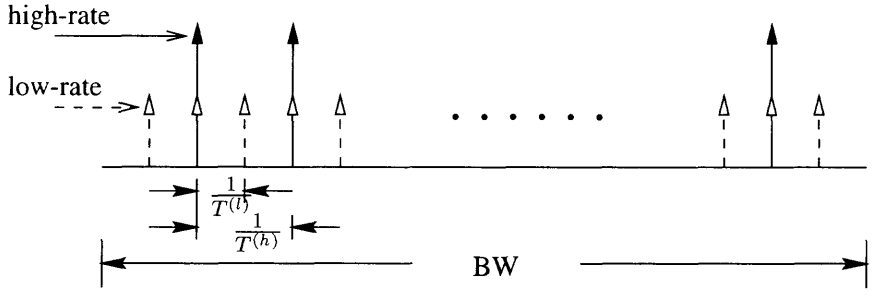

Figure 4.5 The subcarrier assignment of a VSL dual-rate MC-CDMA system.

The bandwidth efficiency of a low-rate user in the VSL scheme is much greater than in the FSL scheme since the subcarrier spectra of the low-rate users are much

more densely spaced in the VSL scheme. Also, due to a longer spreading length, the low-rate users will have a stronger interference suppression capability than in the FSL scheme. This is because longer codes usually have better cross-correlation property. However, since the subcarrier sets $\mathbf{f}^{(l)}$ and $\mathbf{f}^{(h)}$ are not orthogonal, i.e.,

$$\int_{(i-1)T^{(h)}}^{iT^{(h)}} \cos 2\pi f_m^{(l)} t \cos 2\pi f_n^{(h)} t dt \neq \delta(m-n) \tag{4.27}$$

the VSL scheme introduces ICI between signals with different rates.

The waveform of the received dual-rate signal in equation (4.1) can be rewritten for the VSL scheme as

$$\begin{aligned} r_v(t) = \sum_{i=-\infty}^{+\infty} \Bigg[& \sum_{n=1}^{M^{(l)}} \sum_{k=1}^{K^{(l)}} \sqrt{a_k^{(l)}} b_k^{(l)}(i) \sum_{m=1}^{M^{(l)}} h_m^{(l)} c_{km} e^{j2\pi \frac{mn}{M^{(l)}}} P^{(l)}(t-(iM^{(l)}+n)T_c) \\ & + \sum_{s=(i-1)N+1}^{iN} \sum_{n=1}^{M^{(h)}} \sum_{k=1}^{K^{(h)}} \sqrt{a_k^{(h)}} b_k^{(h)}(s) \sum_{m=1}^{M^{(h)}} h_m^{(h)} \theta_{km} e^{j2\pi \frac{mn}{M^{(h)}}} P^{(h)}(t-(sM^{(h)}+n)T_c) \Bigg] + n(t) \end{aligned} \tag{4.28}$$

Notice that by using the VSL scheme, every N subcarriers of the low-rate users, $f_i^{(l)}$, $i=(m-1)N+1,(m-1)N+2,\ldots,mN$, where $m=1,2,\ldots,M^{(h)}$, are located inside the same spectrum of the mth subcarrier of the high-rate signal, $f_m^{(h)}$. Since subchannels of the high-rate users are assumed frequency-flat faded, the subchannel fading of these N low-rate subcarriers is highly correlated. Without loss of generality, these N subcarriers are assumed to undergo the same fading, i.e.

$$h_n^{(l)} = h_{\lfloor \frac{n-1}{N} \rfloor + 1}^{(h)}, \quad n=1,2,\ldots,M^{(l)} \tag{4.29}$$

4.4.1 VSL Receiver Design

An LRM receiver is proposed for the VSL scheme. This receiver consists of a $M^{(l)}$-point DFT to perform the multicarrier demodulation every $T^{(l)}$. The block diagram of the proposed VSL dual-rate MC-CDMA system with an LRM receiver is shown in Figure 4.6.

The received signal is sampled by the LRM receiver at the virtual chip rate $\frac{1}{T_c}$. The sample obtained at the instant $t=(i-1)T+sT_c$ for $s=1,2,\ldots,M^{(l)}$ can be

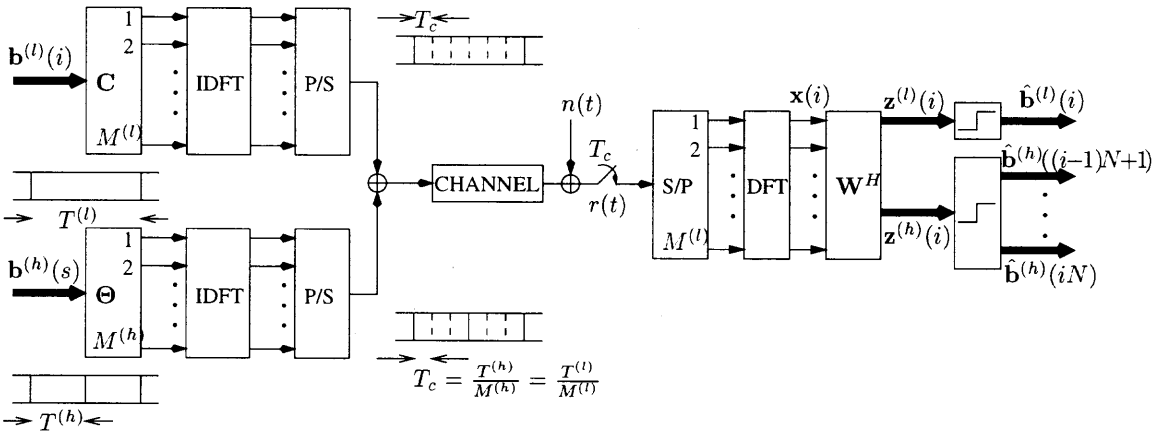

Figure 4.6 The block diagram of the VSL dual-rate MC-CDMA system.

described by

$$\begin{aligned} r_s(i) &= \frac{1}{\sqrt{M^{(l)}}} \sum_{k=1}^{K^{(l)}} \sqrt{a_k^{(l)}} b_k^{(l)}(i) \sum_{m=1}^{M^{(l)}} h_m^{(l)} c_{km} e^{j2\pi \frac{ms}{M^{(l)}}} \\ &+ \frac{1}{\sqrt{M^{(h)}}} \sum_{m=1}^{M^{(h)}} \sum_{k=1}^{K^{(h)}} \sqrt{a_k^{(h)}} b_k^{(h)}(p) \sum_{m=1}^{M^{(h)}} h_m^{(h)} \theta_{km} e^{j2\pi \frac{ms}{M^{(h)}}} + n_s(i) \end{aligned} \tag{4.30}$$

where $p = \lfloor \frac{s}{M^{(h)}} \rfloor + N(i-1) + 1$ is the index of the high-rate users' bits, which are transmitted during the pth high-rate bit interval $[(p-1)T^{(h)}, pT^{(h)})$. The factors $\frac{1}{\sqrt{M^{(l)}}}$ and $\frac{1}{\sqrt{M^{(h)}}}$ denote the amplitude of the normalized pulse shape functions $P^{(l)}(t)$ and $P^{(h)}(t)$. Also, $n_s(i)$ denotes a white Gaussian noise sample with zero mean and variance σ_n^2. $M^{(l)}$ samples of the received signal at the interval $[(i-1)T^{(l)}, iT^{(l)})$, are processed by the $M^{(l)}$-point DFT. The qth output of the DFT can then be shown as

$$\begin{aligned} x_q(i) &= \frac{1}{M^{(l)}} \sum_{s=1}^{M^{(l)}} r_s(i) e^{-j2\pi \frac{sq}{M^{(l)}}} \\ &= \frac{1}{\sqrt{M^{(l)}}} \sum_{k=1}^{K^{(l)}} \sqrt{a_k^{(l)}} b_k^{(l)}(i) h_q^{(l)} c_{kq} \\ &+ \frac{1}{\sqrt{M^{(l)}}} \sum_{k=1}^{K^{(h)}} \sqrt{a_k^{(h)}} \sum_{n=1}^{N} b_k^{(h)}(n) \sum_{m=1}^{M^{(h)}} h_m^{(h)} \frac{\theta_{km}}{\sqrt{N}} \mathbf{\Gamma}_{q,m}(n) + \eta_q(i) \end{aligned} \tag{4.31}$$

where

$$\mathbf{\Gamma}_{q,m}(n) = \frac{1}{M^{(h)}} e^{j2\pi \frac{q}{N}(n-1)} \sum_{s=1}^{M^{(h)}} e^{j2\pi \frac{m-\frac{q}{N}}{M^{(h)}} s} \tag{4.32}$$

$$\eta_q(i) = \frac{1}{M^{(l)}} \sum_{s=1}^{M^{(l)}} n_s(i) e^{-j2\pi \frac{sq}{M^{(l)}}} \sim \mathcal{N}(0, \frac{\sigma_n^2}{M^{(l)}}) \tag{4.33}$$

$q = 1, 2, \ldots, M^{(l)}$, $m = 1, 2, \ldots, M^{(h)}$ and $n = p - (i-1)N \in \{1, 2, \ldots, N\}$ is the index of the subinterval $[(i-1)T^{(l)} + (n-1)T^{(h)}, (i-1)T^{(l)} + nT^{(h)})$. The first term of equation (4.31) contains the information of the low-rate users that is transmitted through the qth subcarrier. The second term contains the information of the high-rate users that is demodulated by the qth low-rate users' subcarrier. It can be seen that there exists interference between the qth subcarrier of the low-rate users and the mth subcarrier of the high-rate users at the nth subinterval $T^{(h)}$. This ICI, represented by the transformation $\mathbf{\Gamma}_{q,m}(n)$ defined in equation (4.32), is introduced due to the non-orthogonality between the high-rate and low-rate users' subcarriers depicted by equation (4.27)[4]. As a result of the presence of ICI, the spreading code of the kth high-rate user at the nth subinterval is transformed into

$$\tilde{\theta}_{kq}(n) = \sum_{m=1}^{M^{(h)}} h_m^{(h)} \frac{\theta_{km}}{\sqrt{N}} \mathbf{\Gamma}_{q,m}(n) = \frac{1}{M^{(h)}} e^{j2\pi \frac{qn}{N}} \sum_{m=1}^{M^{(h)}} h_m^{(h)} \frac{\theta_{km}}{N} \sum_{s=1}^{M^{(h)}} e^{j2\pi \frac{m-\frac{q}{N}}{M^{(h)}} s} \tag{4.34}$$

Equation (4.34) shows that this ICI may cause severe MUI even in an ideal non-faded AWGN channel, $h_m(h) = 1$ for $m = 1, 2, \ldots, M^{(h)}$, as the orthogonality between the spreading codes may have been impaired by the transformation. Hence, in the VSL system, the performance of both low-rate and high-rate users may be degraded. However, it can be proven that in an ideal non-faded AWGN channel, the transformed spreading codes $\tilde{\boldsymbol{\theta}}_k(n) = [\tilde{\theta}_{k1}(n), \tilde{\theta}_{k2}(n), \ldots, \tilde{\theta}_{kM^{(l)}}(n)]^T$ have the following properties, which will assure the feasibility of the proposed VSL scheme.

- **Property 1.** The transformed spreading codes of the high-rate users maintain the same correlation properties of the original ones and the transformed spreading codes at different subintervals are orthogonal:

$$\tilde{\boldsymbol{\theta}}_k^H(i)\tilde{\boldsymbol{\theta}}_l(i') = \begin{cases} \boldsymbol{\theta}_k^T \boldsymbol{\theta}_l & \text{if } i = i' \\ 0 & \text{if } i \neq i' \end{cases} \quad i, i' = 1, 2, \ldots, N \tag{4.35}$$

[4]Notice that when $M^{(h)} = M^{(l)} = M$, as in the FSL scheme, the $\mathbf{\Gamma}_{q,m}(n) = \delta(q-m)$ for all n's. Thus, the ICI vanishes.

- **Property 2.** If the spreading code of the kth low-rate user $\boldsymbol{c}_k$ is a vector consisting of N repetitive $(M^{(h)} \times 1)$ sub-vectors $\bar{\boldsymbol{c}}_k$, i.e., $\boldsymbol{c}_k = [\bar{\boldsymbol{c}}_k^T, \bar{\boldsymbol{c}}_k^T, \ldots, \bar{\boldsymbol{c}}_k^T]^T$, and the sub-vector $\bar{\boldsymbol{c}}_k$ is orthogonal to the original spreading code of the lth high-rate user, i.e. $\bar{\boldsymbol{c}}_k^T \boldsymbol{\theta}_l = 0$ then, the spreading code of the kth low-rate user is orthogonal to the transformed spreading code of the lth high-rate user at any subinterval, i.e.,

$$\boldsymbol{c}_k^T \tilde{\boldsymbol{\theta}}_l(n) = 0, \quad \forall\, n = 1, 2, \ldots, N \tag{4.36}$$

Therefore, by choosing a set of codes, whose structure satisfied the requirement of **Property 2**, as spreading codes, the MUI caused by ICI due to the non-orthogonality between subcarriers of the low-rate and high-rate users can be eliminated in the VSL system. The details of the proofs of these properties are given in Appendix B. It is worthwhile to note that although the above properties are valid only in the non-faded AWGN channel, the VSL scheme can still be applied in a frequency-selective fading channel, just like other schemes. This is because the invalidity of the properties can be viewed as the impaired orthogonality between orthogonal spreading codes solely due to the channel fading.

The codes that meet the requirement of **Property 2** can be chosen from the Walsh-Hadamard codes. Thus, the Walsh-Hadamard codes are used as spreading codes for the low-rate and high-rate users in this chapter.

After normalizing by $\frac{1}{M^{(l)}}$, equation (4.31) is rewritten as

$$x_q(i) = \sum_{k=1}^{K^{(l)}} \sqrt{a_k^{(l)}}\, b_k^{(l)}(i) h_q^{(l)} c_{kq} + \sum_{k=1}^{K^{(h)}} \sqrt{a_k^{(h)}} \sum_{n=1}^{N} b_k^{(h)}(n) \tilde{\theta}_{kq}(n) + \eta_q(i) \tag{4.37}$$

where $\eta_q(i)$ has variance σ_n^2. In order to estimate the desired user's information, the outputs of the DFT shown in equation (4.37) are stacked into an $(M^{(l)} \times 1)$ vector $\boldsymbol{x}_v(i)$

$$\begin{aligned}\boldsymbol{x}_v(i) &= [x_1(i), x_2(i), \ldots, x_{M^{(l)}}(i)]^T \\ &= \left[\boldsymbol{H}_v\boldsymbol{C}_v\ \tilde{\boldsymbol{\Theta}}(1)\ \ldots\ \tilde{\boldsymbol{\Theta}}(N)\right]\begin{bmatrix}\boldsymbol{A}^{(l)} & & & \\ & \boldsymbol{A}^{(h)} & & \\ & & \ddots & \\ & & & \boldsymbol{A}^{(h)}\end{bmatrix}\begin{bmatrix}\boldsymbol{b}^{(l)}(i) \\ \boldsymbol{b}^{(h)}((i-1)N+1) \\ \vdots \\ \boldsymbol{b}^{(h)}(iN)\end{bmatrix} + \boldsymbol{\eta}(i) \\ &\stackrel{\text{def}}{=} \boldsymbol{P}_v\boldsymbol{A}\boldsymbol{b}(i) + \boldsymbol{\eta}(i) \end{aligned} \tag{4.38}$$

where $(M^{(l)} \times K^{(l)})$ matrix $\boldsymbol{C}_v = [\mathbf{c}_1\ \ \mathbf{c}_2\ \ \ldots\ \ \mathbf{c}_{K^{(l)}}]$ contains the spreading codes of the low-rate users and $(M^{(l)} \times K^{(h)})$ matrix $\tilde{\boldsymbol{\Theta}}(n) = \boldsymbol{\Gamma}(n)\boldsymbol{H}\boldsymbol{\Theta}$ denotes the transformed spreading codes matrix of the high-rate users at the nth subinterval. Also in equation (4.38), the $(M^{(l)} \times M^{(l)})$ diagonal matrix $\boldsymbol{H}_v = [\boldsymbol{H} \otimes \boldsymbol{I}]$ contains the channel fading factors on the $M^{(l)}$ subcarriers. The symbol $\otimes$ denotes the Kronecker tensor product and $\boldsymbol{I}_N$ is an $(N \times N)$ identity matrix. The diagonal elements of $\boldsymbol{H}_v$ are defined in equation (4.29). Equation (4.38) shows that the vector $\boldsymbol{x}_v$ contains the low-rate users' current bits and the high-rate users' N successive bits, which is the same as in the FSL scheme. The outputs of the demodulator in equation (4.38) are multiplied by the MMSEC coefficients, derived similar as equation (4.6)[5], to generate the decision variables as shown in equations (4.7) and (4.8) for the low-rate and high-rate users, respectively.

4.4.2 Performance of the Low-rate Users

As before, low-rate user 1 is assumed to be the desired user. The desired low-rate user 1 can be estimated using equation (4.9)[6]. The BER of low-rate user 1, using the MMSEC detector is given by,

$$\text{BER}^{v,(l)}_{1,\text{mmsec}} = \text{E}_{\boldsymbol{H}}\left[\text{Q}\left(\sqrt{\left\{a_1^{(l)}\boldsymbol{p}_{v1}^H\left(\boldsymbol{P}_{v1}\boldsymbol{A}_1^2\boldsymbol{P}_{v1}^H + \sigma_n^2\boldsymbol{I}\right)^{-1}\boldsymbol{p}_{v1}\right\}}\right)\right] \tag{4.39}$$

[5]with $\boldsymbol{P}_f$ replaced by $\boldsymbol{P}_v$.

[6]with $\boldsymbol{x}_f$ replaced by $\boldsymbol{x}_v$.

where $\boldsymbol{P}_{v1}$ denotes the matrix $\boldsymbol{P}_v$ without the 1st column and $\boldsymbol{p}_{v1}$ denotes the 1st column of $\boldsymbol{P}_v$

4.4.3 Performance of the High-rate Users

The high-rate user 1 is assumed to be the desired user. Similar to the FSL scheme, the output of the demodulator in the VSL scheme contains N successive bits for each high-rate user. Therefore, user 1's jth bit can also be estimated using equation (4.12)[7]. The BER of high-rate user 1 using an MMSEC receiver is given by,

$$\mathrm{BER}_{1,\mathrm{mmsec}}^{v,(h)} = \mathrm{E}_{\boldsymbol{H}}\left[\mathrm{Q}\left(\sqrt{\left\{a_1^{(h)}\boldsymbol{p}_{v,K^{(l)}+1}^H\left(\boldsymbol{P}_{v,K^{(l)}+1}\boldsymbol{A}_{K^{(l)}+1}^2\boldsymbol{P}_{v,K^{(l)}+1}^H+\sigma_n^2\boldsymbol{I}\right)^{-1}\boldsymbol{p}_{v,K^{(l)}+1}\right\}}\right)\right] \tag{4.40}$$

where $\boldsymbol{P}_{v,K^{(l)}+1}$ denotes the matrix $\boldsymbol{P}_v$ without the $(K^{(l)}+1)$th column and $\boldsymbol{p}_{v,K^{(l)}+1}$ denotes the $(K^{(l)}+1)$th column of $\boldsymbol{P}_v$.

In the FSL scheme, the N successive bits of the high-rate users do not interfere with each other because they are orthogonal in time as shown in equation (4.5). However, the orthogonality among these N bits in the VSL scheme is dependent on the correlation of the transformed spreading codes as shown in equation (4.38). If the dual-rate signal is transmitted through an ideal non-faded AWGN channel, the transformed spreading codes from different subintervals are orthogonal, $\tilde{\boldsymbol{\theta}}_k(i)^H\tilde{\boldsymbol{\theta}}_k(i') = 0$ for $i \neq i'$, as given in equation (4.35). Thus, there is no interference between these N bits. However, in a frequency-selective fading channel, equation (4.35) does not hold due to the channel impairment, hence, the transformed spreading codes are no longer orthogonal, i.e. $\tilde{\boldsymbol{\theta}}_k(i)^T\tilde{\boldsymbol{\theta}}_k(i') \neq 0$ for $i \neq i'$, and ISI will be introduced into these N successive high-rate bits. Therefore, the single user performance of the high-rate users using the VSL scheme cannot reach the SUB.

[7] with $\boldsymbol{x}_f$ replaced by $\boldsymbol{x}_v$.

4.5 Simulation Results

To evaluate the performance of the FSL, CFSL and VSL dual-rate MC-CDMA access schemes, numerical results are presented in this section. These results are obtained for a dual-rate MC-CDMA system with a rate ratio $N = 2$. In addition, the high-rate BPSK-modulated signal is transmitted at a bit rate $\frac{1}{T^{(h)}} = 62$kbps and the low-rate BPSK-modulated signal is transmitted at a bit rate $\frac{1}{T^{(l)}} = 31$kbps. Hence, with a total bandwidth $BW = 1.06$MHz, the number of subcarriers for the high-rate users is $M^{(h)} = 16$ in all three schemes, while the number of subcarriers for the low-rate users is $M^{(l)} = 16$ in the FSL/CFSL scheme and $M^{(l)} = 32$ in the VSL scheme. For the high-rate users, Hadamard codes with length 16 are selected as spreading codes. For the low-rate users, Hadamard codes with lengths 16 and 32 are selected in the FSL/CFSL and VSL schemes, respectively. In the CFSL scheme, an $(8, 4)$ block code is generated at the encoder by an 8×8 Hadamard matrix and its complement. The 1/2-rate coding scheme compensates for the rate difference between the high-rate and low-rate users in the CFSL dual-rate system. A soft decision decoder is used to determine the transmitted code with maximal correlation metric and decode it according to the Hadamard matrix. Simulations have been carried out in the correlated Rayleigh fading channel modeled in section 3.5.2, whose rms channel delay spread τ_d was selected as $\tau_d = 0.5\mu s$. The subcarriers with length 16 are spaced by $\Delta f = 62$kHz. The correlation between the fading factors on these subcarriers, $h_m^{(h)}$, can be calculated using equation (2.6). The 32 subcarriers of the low-rate users in the VSL scheme are spaced by $\Delta f = 31$kHz. The correlated fading factors on these subcarriers, $h_m^{(l)}$, are related to the fading factors, $h_m^{(h)}$, as defined in equation (4.29). Since the BER depends on channel realization, all the BER curves are the results of averaging over 200 Monte-Carlo runs.

Figure 4.7 shows the near-far performance of low-rate user 1 using the FSL, CFSL and VSL schemes in a correlated Rayleigh fading channel with $\text{SNR}_1 = 15$dB.

Eight low-rate and eight high-rate users are assumed. In the low interference region, the VSL and FSL schemes approach the same single user performance, because the frequency diversity that can be utilized by a MC-CDMA signal consisting of one low-rate user is assumed the same for two schemes as shown in equation (4.29). In the high interference region, the VSL scheme significantly outperforms the FSL scheme. Thus, in the VSL scheme, the low-rate users possess a stronger interference suppression capability than in the FSL scheme. This is because the spreading codes of the low-rate users are longer in the VSL scheme than in the FSL scheme, and hence have a much better cross-correlation property. It can also be notice that because of the coding gain, the CFSL scheme outperforms both the FSL and VSL schemes in the low interference region. In the high interference region, however, the BER of the CFSL scheme increases more rapidly than the other two schemes. As a result, the CFSL scheme depicts the worst performance among three proposed schemes in the high interference region. This is because, when the SNIR decreases below a certain level, the coded system will suffer from error propagation.

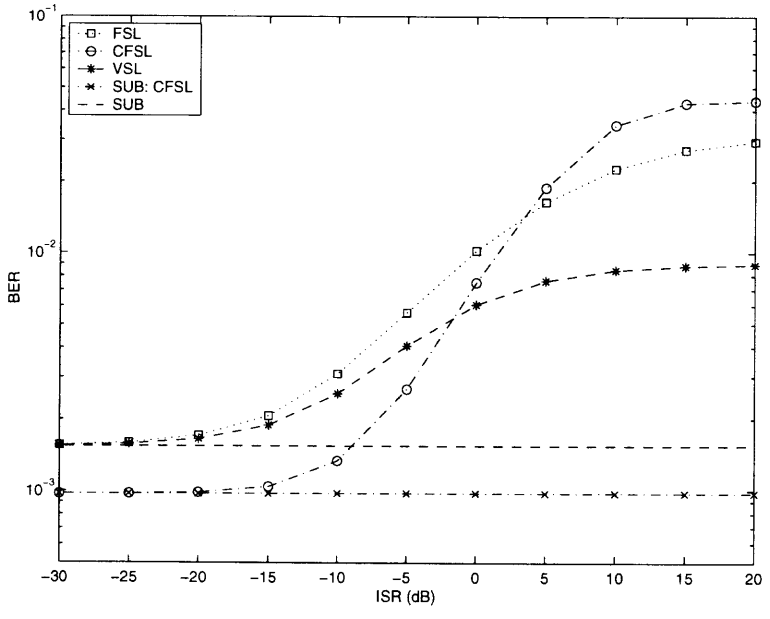

Figure 4.7 BER of low-rate user 1 for FSL, CFSL and VSL vs. ISR, $\mathrm{SNR}_1 = 15\mathrm{dB}$, $K^{(h)} = 8$ and $K^{(l)} = 8$

To avoid error propagation in the CFSL scheme, the desired user's SNR must be increased, as shown in Figure 4.8. In this figure, the BER of low-rate user 1 using the FSL, CFSL and VSL schemes vs. SNR_1 with ISR= 8dB and ISR= −8dB is presented. Eight low-rate and eight high-rate users are assumed. It shows that in the low interference case (ISR= −8dB), the required SNR for the CFSL scheme to outperform the FSL scheme is about 7dB. While, in the high interference case (ISR= 8dB), the required SNR is about 27dB. To improve the performance of the CFSL scheme in the high interference region, another possible solution can be suggested is to apply a more efficient channel coding scheme, such as convolutional code. This might be a topic for future investigation. Also, as expected, the performance of low-rate user1 in the VSL scheme has a performance that is superior to in the FSL scheme, especially when a severe near-far problem exists. In the low interference case, the VSL scheme has a slight SNR gain about 1dB, at BER=10^{-3}, in comparison to the FSL scheme. While, in the high interference case (severe near-far problem), the VSL scheme shows significant SNR gain of about 9dB at BER=10^{-3}.

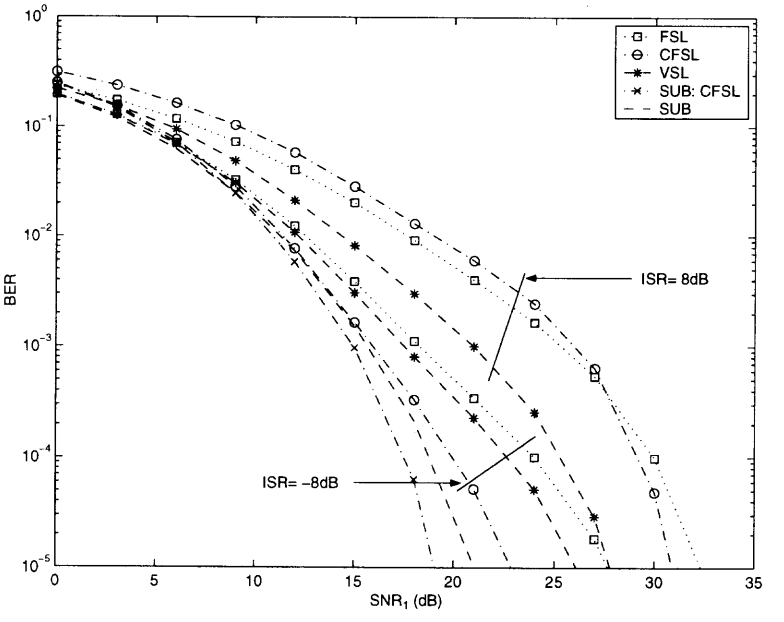

Figure 4.8 BER of low-rate user 1 for FSL, CFSL and VSL vs. SNR_1 for ISR= 8dB and ISR= −8dB, $K^{(h)} = 8$ and $K^{(l)} = 8$

The BER performance of high-rate user 1 vs. ISR using the FSL and VSL schemes is shown in Figure 4.9. Eight low-rate and eight high-rate users are assumed. The high-rate user 1 has $\mathrm{SNR}_1 = 10\mathrm{dB}$. First, note that the VSL scheme has a worse single user performance than that of the FSL scheme. This is due to ISI among each N successive bits of high-rate user 1 at the output of the LRM receiver, since the frequency-selective fading channel impairs the orthogonality among the transformed high-rate user 1's spreading codes of these N bits. Second, notice that for the high-rate user, just as for the low-rate users, the VSL scheme still outperforms the FSL scheme in the high interference region. This is because the transformed high-rate users' spreading codes is longer than the original ones and hence provide stronger interference suppression capability.

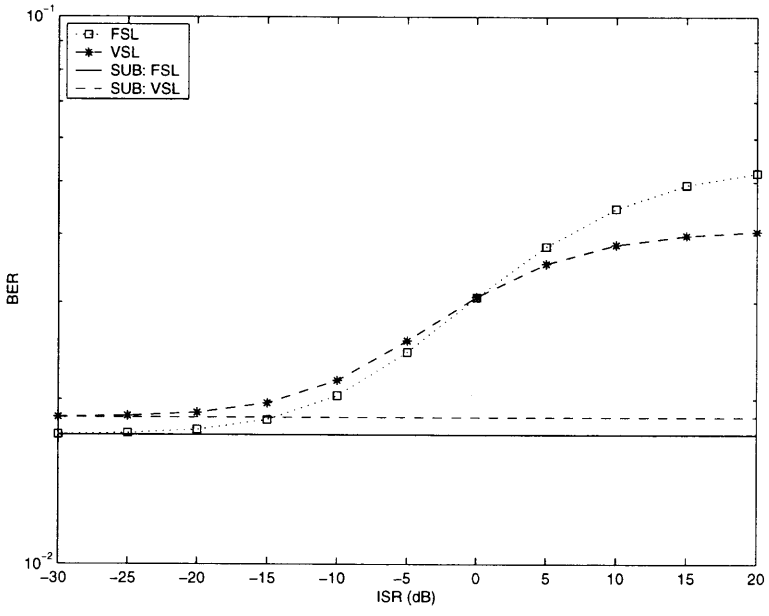

Figure 4.9 BER of high-rate user 1 for FSL and VSL vs. ISR, $K^{(h)} = 8$ and $K^{(l)} = 8$

In Figure 4.10, the required SNR_1 for low-rate user 1 to achieve a BER of 10^{-2} using the FSL, CFSL and VSL schemes are shown vs. the number of active users. The number of users is increased from one (single low-rate user) to sixteen (eight low-rate and eight high-rate users). All active users have equal signal power, i.e.

ISR= 0dB, and the required SNR_1 was determined through Monte-Carlo simulation. In comparison to the FSL scheme, the CFSL scheme shows a better performance for low-rate user 1, in terms of requiring less SNR_1, with any number of active users. The difference between the required SNR_1 for the CFSL and FSL schemes becomes larger when the number of active users increases: from about 0.3dB in a single low-rate user system to about 0.8dB in a 16-user system. When the number of active users is small (less than 4), the VSL scheme requires about the same SNR_1 as the FSL scheme, which is more than the CFSL scheme, for low-rate user 1 to achieve 10^{-2} BER. However, the performance of low-rate user 1 is degraded much faster in the FSL and CFSL schemes than in the VSL scheme with the increase of the user number. As a result, after the number of active users becomes larger than eight, low-rate user 1 in the VSL scheme requests the least SNR_1 among three schemes to obtain BER= 10^{-2}. This is as expected, since in the VSL scheme the low-rate users, assigned with the longer spreading codes, have a stronger interference suppression capability than in other two schemes.

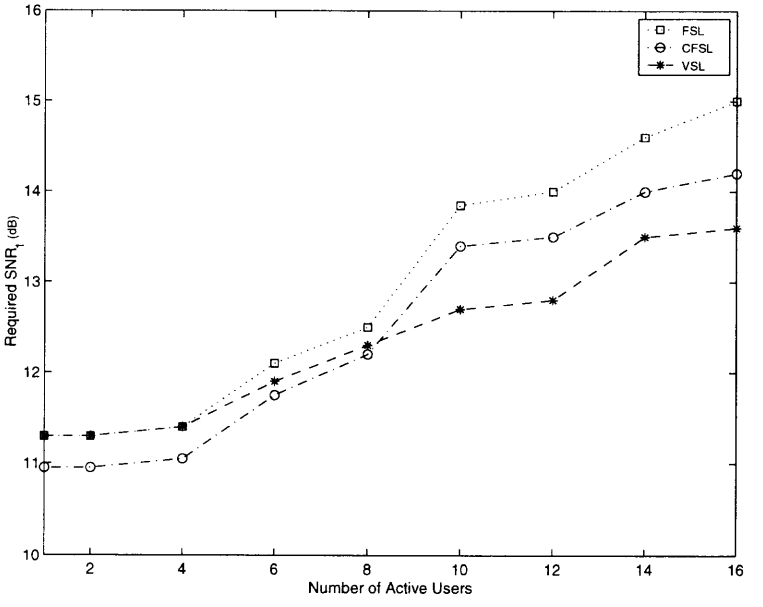

Figure 4.10 Required SNR_1 of low-rate user 1 to obtain a BER of 10^{-2} for FSL, CFSL and VSL vs. number of active users, ISR= 0dB.

4.6 Discussion

In this chapter, three novel multi-rate access schemes for an MC-CDMA system, FSL, CFSL and VSL, were presented. These schemes provide the MC-CDMA system with the flexibility and capability to handle multimedia traffic with variable data rates and QoS requirements. For each access scheme, the performance of the low-rate and high-rate users was derived analytically. In addition, the performance was evaluated numerical using a correlated frequency-selective Rayleigh fading channel. The FSL scheme does not suffer from ICI. However, this scheme introduces a loss of spectrum efficiency for the low-rate users, because the spectra of the adjacent subcarriers of the low-rate users are not overlapping. Therefore, the FSL scheme results in limited performance of the low-rate users and consequently degrades the system capacity. Both CFSL and VSL schemes were proposed to improve the performance of the low-rate users. The CFSL scheme uses channel coding for the low-rate users to compensate for the loss of spectrum efficiency by a channel coding gain. The performance of the low-rate users was shown to be improved in the CFSL scheme. However, a performance degradation due to error propagation may appear, when the SNIR is weak. Further research on a stronger coding scheme was suggested to alleviate the error propagation. In the VSL scheme, by allowing the subcarrier spectra of the low-rate users to be overlapping, the spectrum efficiency of the low-rate users is retained. However, ICI is introduced and causes loss of orthogonality among spreading codes, which may severely degrade both high-rate and low-rate users' performance. It was shown that spreading codes with a special structure, such as the Walsh-Hadamard codes, can maintain the orthogonality in the presence of ICI in a non-faded AWGN channel. Thus, the feasibility of the FSL scheme was ensured. Additionally, in the VSL scheme, the low-rate users' spreading codes are longer than in the FSL and CFSL schemes. With a better cross-correlation property, the longer

spreading codes provide a stronger interference suppression capability. As a result, VSL outperforms both FSL and CFSL in the presence of strong interference.

CHAPTER 5

CONCLUSIONS

In the preceding chapters, multiuser detection and multi-rate access in an MC-CDMA system operating in a frequency-selective fading channel have been studied.

Receivers with a multi-shot structure for asynchronous MC-CDMA were developed in Chapter 2. It was shown that the multi-shot MMSE receiver suppresses interference caused by the asynchronous reception of different users in an uplink scenario. The performance of the MMSE receiver and the conventional decorrelating receiver is sensitive to the accuracy of the delay estimation. The near-far resistance of these receivers is impaired in the presence of a timing error. A blind adaptive decorrelating receiver based on the bootstrap algorithm was shown to offer significant performance improvement in a channel with time-varying transmission delays. This blind adaptive bootstrap receiver consists of two stages that jointly perform multiuser interference (MUI) cancellation and inter-rail interference cancellation. However, the performance of the inter-rail interference cancellation of the second stage is degraded by possible phase ambiguity. As a result, this blind adaptive two-stage bootstrap receiver has a limited working range, which depends on the type of modulation, frequency offset and/or timing mismatch. A blind differential bootstrap algorithm was proposed to avoid phase ambiguity. This algorithm compensates for the effects of a frequency offset and/or timing mismatch by transmitting differentially encoded symbol, and thus, eliminates the need of the second stage (inter-rail interference canceler) in the bootstrap receiver.

The multi-shot receivers use a demultiplexer to extract the users' information preceding the multiuser detection. This is particularly important for the adaptive receivers based on the bootstrap algorithm, since this algorithm separates active users by forcing decorrelation at the detector's output. Choosing the type of the

demultiplexer affects the performance of the receivers. The receiver with an MRC-weighted demultiplexer is superior to the one with an EGC-weighted demultiplexer in a frequency-selective fading channel. However, the former must be accompanied by channel estimation and tracking.

In Chapter 3, a novel partial sampling MMSEC (PS-MMSEC) receiver was proposed to remove the timing knowledge requirement for conventional uplink receivers. This receiver does not require synchronization with the desired signal. To capture one complete symbol of the desired user, an extended observation interval of at least two symbol durations must be used. In this receiver, the received signal is demodulated at a partial sampling rate, i.e. at a rate exceeding the symbol rate. As a result, the partial sampling demodulator quantizes the timing uncertainty of the received signal into a finite set of hypotheses. The sufficient statistic provided by the partial sampling demodulator is used by an optimal MMSEC multiuser detector to estimate the desired user's information. The MMSEC detector, which performs demultiplexing and detection together, has equal or better performance than the MMSE detector preceded by a demultiplexer. However, this superior performance is achieved at the expense of a higher system complexity. Because the partial sampling provides more degrees of freedom to suppress MUI, the PS-MMSEC receiver showed a stronger interference suppression capability than the symbol MMSEC receiver with known timing and the same extended observation length. It was shown that the complexity of the PS-MMSEC receiver, in terms of the number of detector coefficients, can be decreased by choosing a lower partial sampling rate. Furthermore, the partial sampling rate can be significantly reduced with negligible performance loss. However, because the number of detector coefficients are also directly related to the number of the subcarriers, the complexity is still dependent on the number of the subcarriers even with a low partial sampling rate. The complexity increases exponentially with the number of the subcarriers increasing. To avoid an excessive

number of detector coefficients, the reduced complexity PS-MMSEC (RPS-MMSEC) structure was proposed. The RPS-MMSEC receiver groups several carrier elements together before multiuser detection. Thus, an MMSEC detector with fewer coefficients, independent of the number of the subcarriers, can be implemented. Numerical results showed that with a proper grouping parameter, the complexity of the RPS-MMSEC can be reduced dramatically, without significant performance loss. The flexible choice of complexity provides a trade-off with the performance and makes the RPS-MMSEC receiver more convenient and suitable for practical applications. In addition, the MMSEC detector coefficients can be obtained adaptively using the LMS algorithm. The adaptive PS/RPS-MMSEC receivers, with no need of timing acquisition, showed a faster convergence and better symbol error rate performance than the symbol MMSEC receiver with known timing, which is due to more degrees of freedom provided by the partial sampling demodulator.

Chapter 4 presented several dual-rate access schemes that enable an MC-CDMA system to integrate users with different data rates and/or QoS requirements. The simplest and most straightforward dual-rate access scheme is the fixed spreading length (FSL) scheme. In the FSL scheme, users with different rates are assigned spreading codes of the same length and modulated onto the same set of subcarriers. The subcarriers are spaced by the reciprocal of the high-rate users' bit duration, which maintains subcarrier orthogonality for both the high-rate and low-rate users. Therefore, the FSL scheme does not suffer from ICI. However, this scheme results in a loss of spectrum efficiency for the low-rate users, because the frequency separation of the adjacent subcarriers is not as small as possible. Therefore, the FSL scheme degrades the system capacity. Two other schemes, coded FSL (CFSL) and variable spreading length (VSL), were proposed to combat the loss of spectrum efficiency for the low-rate users. Both the CFSL and VSL scheme were shown to improve the performance of the low-rate users in terms of bit error rate and hence, system

capacity. The CFSL scheme uses channel coding for the low-rate users to compensate for the loss spectrum efficiency by a channel coding gain. The performance of the low-rate users was shown to improve significantly in the CFSL scheme. However, when the power of the desired signal is too weak compared to the power of noise and interference, a performance degradation may appear due to error propagation in the coded system. Further research on a stronger coding scheme was suggested to alleviate the error propagation. In the VSL scheme, the high-rate and low-rate users are allowed to transmit information through two different sets of subcarriers. Thus, the spectrum efficiency of the low-rate users is maintained as the subcarrier spectra of the low-rate users are also overlapping. However, ICI is introduced, since the two sets of subcarriers are no longer orthogonal. Moreover, ICI results in a loss of orthogonality among the spreading codes. As a result, the performance of the VSL scheme may be severely degraded by MUI. To avoid this degradation, codes with a special structure, such as the Walsh-Hadamard codes must be used as the spreading codes in the VSL scheme. It was shown that spreading codes based on Walsh-Hadamard codes maintain their orthogonality properties in the presence of ICI in a non-faded AWGN channel. Additionally, in the VSL scheme, the low-rate users' spreading codes are longer than in the FSL and CFSL schemes. The longer spreading codes have a better cross-correlation property and thus provide a stronger interference suppression capability. As a result, the VSL scheme outperforms the FSL and CFSL schemes for the low-rate users in the presence of strong MUI.

APPENDIX A

SNR OF BOOTSTRAP ALGORITHM UNDER THE LIMITING CONDITION

In this appendix, the signal-to-noise ratio (SNR) of the bootstrap algorithm under the limiting condition is shown to be identical to the SNR of the conventional decorrelating detector in a frequency-selective fading channel.

The output vector of the matched filter with dimension $K \times 1$ can be described as

$$\boldsymbol{x} = \boldsymbol{P}\boldsymbol{A}\boldsymbol{b} + \boldsymbol{n} \tag{A.1}$$

Without losing generality, the user 1 is chosen as the desired user. Thus, the matrices in equation (A.1) can be expanded as

$$\begin{aligned}
\boldsymbol{P} &= \begin{bmatrix} p_{11} & p_{12} & \cdots & p_{1K} \\ p_{21} & p_{22} & \cdots & p_{2K} \\ \vdots & \vdots & \ddots & \vdots \\ p_{K1} & p_{K2} & \cdots & p_{KK} \end{bmatrix} = \begin{bmatrix} p_{11} & \boldsymbol{q}_1 \\ \boldsymbol{p}_1 & \boldsymbol{P}_1 \end{bmatrix} \\
\boldsymbol{A} &= \begin{bmatrix} \sqrt{a_1} & 0 & \cdots & 0 \\ 0 & \sqrt{a_2} & \cdots & 0 \\ \vdots & \vdots & \ddots & \vdots \\ 0 & 0 & \cdots & \sqrt{a_K} \end{bmatrix} = \begin{bmatrix} \sqrt{a_1} & \boldsymbol{0} \\ \boldsymbol{0} & \boldsymbol{A}_1 \end{bmatrix} \\
\boldsymbol{b} &= \begin{bmatrix} b_1 & b_2 & \cdots & b_K \end{bmatrix}^T = \begin{bmatrix} b_1 & \boldsymbol{b}_1 \end{bmatrix}^T
\end{aligned} \tag{A.2}$$

The Gaussian noise vector has zero mean and covariance matrix $\boldsymbol{R}_n = \begin{bmatrix} r_{11} & \boldsymbol{r}_1^H \\ \boldsymbol{r}_1 & \boldsymbol{R}_1 \end{bmatrix}$.

Using the conventional decorrelating detector $\boldsymbol{P}^{-1}$, the decision variables can be expressed as

$$\boldsymbol{z} = \boldsymbol{P}^{-1}\boldsymbol{x} = \boldsymbol{A}\boldsymbol{b} + \boldsymbol{\eta} \tag{A.3}$$

where $\boldsymbol{\eta} = \boldsymbol{P}^{-1}\boldsymbol{n} \sim \mathcal{N}(\boldsymbol{0}, \boldsymbol{R}_\eta)$, with $\boldsymbol{R}_\eta = \boldsymbol{P}^{-1}\boldsymbol{R}_n(\boldsymbol{P}^{-1})^H$. The SNR of the desired user using a conventional decorrelating detector is

$$\mathrm{SNR_d} = \frac{a_1}{\boldsymbol{R}_\eta(1,1)} \tag{A.4}$$

Applying the block matrix inversion lemma,

$$\begin{bmatrix} A & B \\ C & D \end{bmatrix}^{-1} = \begin{bmatrix} (A-BD^{-1}C)^{-1} & -(A-BD^{-1}C)^{-1}BD^{-1} \\ -(D-CA^{-1}B)^{-1}CA^{-1} & (D-CA^{-1}B)^{-1} \end{bmatrix}$$

the inverse of the correlation matrix $\boldsymbol{P}^{-1} = \begin{bmatrix} u & \boldsymbol{v} \\ \boldsymbol{y} & \boldsymbol{Z} \end{bmatrix}$ can be expanded as

$$\begin{aligned} u &= (p_{11} - \boldsymbol{q}_1\boldsymbol{P}^{-1}\boldsymbol{p}_1)^{-1} \\ \boldsymbol{v} &= -(p_{11} - \boldsymbol{q}_1\boldsymbol{P}^{-1}\boldsymbol{p}_1)^{-1}\boldsymbol{q}_1\boldsymbol{P}_1 = -u\boldsymbol{q}_1\boldsymbol{P}_1 \end{aligned}$$

Therefore

$$\boldsymbol{R}_\eta(1,1) = |u|^2 r_{11} + u^*\boldsymbol{v}\boldsymbol{r}_1 + u\boldsymbol{r}_1^H\boldsymbol{v}^H + \boldsymbol{v}\boldsymbol{R}_1\boldsymbol{v}^H = |u|^2[r_{11} - 2\boldsymbol{q}_1\boldsymbol{P}^{-1} + \boldsymbol{q}_1\boldsymbol{P}^{-1}\boldsymbol{R}_1(\boldsymbol{P}^{-1})^H(\boldsymbol{q}_1)^H] \tag{A.5}$$

Substituting with the steady state value of the bootstrap weight of user 1 under the limiting condition, $\boldsymbol{w}_1 = (\boldsymbol{P}^{-1})^H(\boldsymbol{q}_1)^H$, the decorrelating detector's SNR can be shown as

$$\mathrm{SNR_d} = \frac{a_1|u^2|}{r_{11} - 2\boldsymbol{w}_1^H\boldsymbol{r}_1 + \boldsymbol{w}_1^H\boldsymbol{R}_1\boldsymbol{w}_1} \tag{A.6}$$

Using the bootstrap weight $\boldsymbol{w}_1$, the decision variable of the desired user 1 can be shown as

$$\begin{aligned} z_1 &= x1 - \boldsymbol{w}_1^H\boldsymbol{x}_1 \\ &= (p_{11} - \boldsymbol{p}_1\boldsymbol{P}_1^{-1}\boldsymbol{p}_1)a_1b_1 + n_b = \alpha_1\sqrt{a_1}b_1 + n_b \end{aligned} \tag{A.7}$$

where $\alpha_1 = u^{-1}$ and $\sigma_b^2 = \mathrm{E}[n_b n_b^*] = r_{11} - 2\boldsymbol{w}_1^H\boldsymbol{r}_1 + \boldsymbol{w}_1^H\boldsymbol{R}_1\boldsymbol{w}_1$. The SNR of user 1 under the limiting condition using the bootstrap detector is shown to be identical to that of the decorrelating detector,

$$\mathrm{SNR_b} = \frac{a_1|\alpha_1|^2}{\sigma_b^2} = \frac{a_1|u|^{-2}}{r_{11} - 2\boldsymbol{w}_1^H\boldsymbol{r}_1 + \boldsymbol{w}_1^H\boldsymbol{R}_1\boldsymbol{w}_1} = \mathrm{SNR_d} \tag{A.8}$$

Therefore, the bootstrap detector's performance and the decorrelating detector's performance are identical under the limiting condition.

APPENDIX B

CORRELATION OF THE TRANSFORMED SPREADING CODES IN VSL DUAL-RATE MC-CDMA

B.1 Correlation between High-Rate Users

The transformation $\mathbf{\Gamma}(n)$, caused by ICI, does not change the correlation properties of the high-rate users' spreading codes. The transformed spreading codes for different high-rate bits are orthogonal:

$$\tilde{\boldsymbol{\theta}}_k^H(i)\tilde{\boldsymbol{\theta}}_k(i') = \begin{cases} \boldsymbol{\theta}_k^T\boldsymbol{\theta}_k & \text{if } i = i' \\ 0 & \text{if } i \neq i' \end{cases} \qquad i, i' = 1, 2, \ldots, N \tag{B.1}$$

Proof: $\tilde{\boldsymbol{\theta}}(i)$ can be rewritten as,

$$\tilde{\boldsymbol{\theta}}_k(i) = \mathbf{\Gamma}(i)\boldsymbol{\theta}_k \tag{B.2}$$

where

$$\mathbf{\Gamma}(i) = [\boldsymbol{\gamma}_1(i) \;\; \boldsymbol{\gamma}_2(i) \;\; \ldots \;\; \boldsymbol{\gamma}_{M^{(h)}}(i)] \tag{B.3}$$

The column vector $\boldsymbol{\gamma}_n(i)$ can be shown has the following property,

$$\begin{aligned} \boldsymbol{\gamma}_n^H(i)\boldsymbol{\gamma}_m(i') &= \frac{1}{M^{(h)^2}} \sum_{q=1}^{M^{(l)}} e^{j2\pi\frac{i'-i}{N}q} \sum_{s=1}^{M^{(h)}} e^{-j2\pi\frac{n-\frac{q}{N}}{M^{(h)}}s} \sum_{t=1}^{M^{(h)}} e^{j2\pi\frac{m-\frac{q}{N}}{M^{(h)}}t} \\ &= \frac{1}{M^{(h)^2}} \sum_{s=1}^{M^{(h)}} \sum_{t=1}^{M^{(h)}} e^{j2\pi\frac{mt-ns}{M^{(h)}}} \sum_{q=1}^{M^{(l)}} e^{j2\pi\frac{(t-s)+M^{(h)}(i'-i)}{M^{(l)}}q} \\ &= \frac{1}{M^{(h)^2}} \sum_{s=1}^{M^{(h)}} \sum_{t=1}^{M^{(h)}} e^{j2\pi\frac{mt-ns}{M^{(h)}}} \delta\left[(t-s) + M^{(h)}(i'-i)\right] \\ &= N\delta(m-n)\delta(i'-i) \end{aligned} \tag{B.4}$$

Notice term

$$(t-s) \in [1 - M^{(h)}, \ldots, -1, 0, 1, \ldots, M^{(h)} - 1]$$

and term

$$M^{(h)}(i'-i) \in [(1-N)M^{(h)}, \ldots, -M^{(h)}, 0, M^{(h)}, \ldots, (N-1)M^{(h)}]$$

Thus, the forth equality in equation (B.4) is valid as

$$\delta\left[(t-s)+M^{(h)}(i'-i)\right]=\delta(t-s)\cdot\delta(i'-i) \tag{B.5}$$

From equation (B.4),it can be shown

$$\mathbf{\Gamma}^H(i)\mathbf{\Gamma}(i')=\begin{cases} N\boldsymbol{I}^{M^{(h)}} & i=i' \\ \mathbf{0} & i\neq i' \end{cases} \tag{B.6}$$

Therefore

$$\tilde{\boldsymbol{\theta}}_k^H(i)\tilde{\boldsymbol{\theta}}_k(i')=\frac{1}{N}\boldsymbol{\theta}_k^T\left[\mathbf{\Gamma}^H(i)\mathbf{\Gamma}(l)\right]\boldsymbol{\theta}_k=\boldsymbol{\theta}_k^T\boldsymbol{\theta}_k\delta(i-i')$$

B.2 Correlation between High-Rate and Low-Rate Users

The transformed spreading codes of the kth low-rate and k'th high-rate users after transformation are orthogonal, i.e. $\boldsymbol{c}_k^T\tilde{\boldsymbol{\theta}}_{k'}(n)=0,\ \forall\ n=1,2,\ldots,N$, if the spreading codes satisfy the condition

$$\bar{\boldsymbol{c}}_k^T\boldsymbol{\theta}_{k'}=0\ \text{ and }\ \boldsymbol{c}_k=[\bar{\boldsymbol{c}}_k^T,\bar{\boldsymbol{c}}_k^T,\ldots,\bar{\boldsymbol{c}}_k^T]^T \tag{B.7}$$

where, $\bar{\boldsymbol{c}}_k$ is an $(M^{(h)}\times 1)$ sub-vector of the kth low-rate user's spreading code $\boldsymbol{c}_k$.

Proof: By applying equation (4.34), the cross-correlation between the kth low-rate user's spreading code $\boldsymbol{c}_k$ and the k'th high-rate user's transformed spreading code $\tilde{\boldsymbol{\theta}}_{k'}$ becomes

$$\mathbf{c}_k^T\tilde{\boldsymbol{\theta}}_{k'}(n)=\frac{1}{M^{(h)}}\sum_{q=1}^{M^{(l)}}c_{kq}e^{j2\pi\frac{qn}{N}}\sum_{m=1}^{M^{(h)}}\theta_{k'm}\sum_{s=1}^{M^{(h)}}e^{j2\pi\frac{m-\frac{q}{N}}{M^{(h)}}s} \tag{B.8}$$

Replacing q in the equation above with $q=iM^{(h)}+m$ and substituting $c_{kq}=c_{k,q-iM}$, gives

$$\begin{aligned}
\mathbf{c}_k^T\tilde{\boldsymbol{\theta}}_{k'}(n) &= \frac{1}{M^{(h)}}\sum_{m=1}^{M^{(h)}}\sum_{s=1}^{M^{(h)}}\sum_{i=0}^{N-1}c_{km}\theta_{k'm}e^{j2\pi\frac{iM^{(h)}+m}{N}n}e^{j2\pi\frac{m-\frac{iM^{(h)}+m}{N}}{M^{(h)}}s} \\
&= \frac{1}{M^{(h)}}\sum_{m=1}^{M^{(h)}}\sum_{s=1}^{M^{(h)}}c_{km}\theta_{k'm}e^{j2\pi\frac{mn}{N}}e^{j2\pi\frac{ms-\frac{m}{N}s}{M^{(h)}}}\sum_{i=0}^{N-1}e^{j2\pi\frac{M^{(h)}n-s}{N}i} \\
&= \frac{1}{M^{(h)}}\sum_{m=1}^{M^{(h)}}\sum_{s=1}^{M^{(h)}}c_{km}\theta_{k'm}e^{j2\pi\frac{mn}{N}}e^{j2\pi\frac{ms-\frac{m}{N}s}{M^{(h)}}}\delta(M^{(h)}n-s)
\end{aligned} \tag{B.9}$$

Since $s \in [1, M^{(h)}]$, $\delta(\cdot)$ is nonzero only when $s = M^{(h)}$ and $n = 1$. Equation (B.9) can then be rewritten as

$$\mathbf{c}_k^T \tilde{\boldsymbol{\theta}}_{k'}(n) = \frac{1}{M^{(h)}} \sum_{m=1}^{M^{(h)}} c_{km}\theta_{k'm} \qquad (B.10)$$

If $\mathbf{c}_k$ and $\boldsymbol{\theta}_{k'}$ satisfies the condition shown in equation (B.7), equation (B.10) is equal to 0. Thus, the low-rate users' spreading codes are orthogonal to the transformed high-rate users' spreading codes.

REFERENCES

1. D. Knisely, Q. Li, and N. Ramesh, "CDMA2000: a third-generation radio transmission technology," *Bell Labs Technical Journal*, 1998.

2. M. Zeng, A. Annamalai, and V. Bhargava, "Recent advances in cellular wireless communications," *IEEE Communications Magazine*, 1999.

3. R. Nee, G. Awater, M. Morikura, H. Takanashi, M. Webster, and K. Halford, "New high-rate wireless LAN standards," *IEEE Communications Magazine*, 1999.

4. S. Zeisberg, M. Bauling, and A. Finger, "WLAN evolution from HIPERLAN type 2 to MEDIAN," in *Proceeding of the IEEE Vehicular Technology Conference*, pp. 2656–2660, July 1999.

5. T. Rappaport, *Wireless Communications Principles & Practice*, Prentice Hall, Upper Saddle River, NJ, U.S.A, 1996.

6. N. Morinaga, M. Nakagawa, and R. Kohno, "New concepts and technologies for achieving highly reliable and high-capacity multimedia wireless communications system," *IEEE Communications Magazine*, 1997.

7. J. Bingham, "Multicarrier modulation for data transmission: An idea whose time has come," *IEEE Communication Magazine*, pp. 5–14, May 1990.

8. M. Russell and G. Stüber, "Terrestrial digital video broadcasting for mobile reception using OFDM," *Wireless Personal Communications*, vol. 2, no. 1&2, pp. 45–65, 1995.

9. M. Alard and R. Lasalle, "Principles of modulation and channel coding for digital broadcasting for mobile receivers," *EBU Review*, 1987.

10. S. Weinstein and P. Ebert, "Data transmission by frequency-division multiplexing using the discrete fourier transform," *IEEE Tran. on Comm. Tech.*, vol. COM-19, no. 5, pp. 626–634, October 1971.

11. R. W. Chang, "Synthesis of band-limited orthogonal signals for multichannel data transmission," *Bell System Technical Journal*, vol. 45, pp. 1775–1796, Dec. 1966.

12. L. Cimini, Jr., "Analysis and simulation of a digital mobile channel using orthogonal frequency division multiplexing," *IEEE Transactions on Communications*, vol. COM-33, no. 7, pp. 665–675, July 1985.

13. S. Slimane, "Bandwidth efficiency of MC-CDMA signals," *Electronics Letters*, vol. 35, no. 21, pp. 1797–1798, Oct. 1999.

14. E. Sourour and M. Nakagawa, "Performance of orthogonal multicarrier CDMA in a multipath fading channel," *IEEE Transactions on Communications*, vol. 44, 1996.

15. L. Vandendorpe, "Multitone spread spectrum multiple access communications system in a multipath Rician fading channel," *IEEE Transactions on Vehicular Technology*, vol. 44, 1995.

16. N. Yee, J. Linnartz, and G. Fettweis, "Multi-carrier CDMA indoor wireless radio networks," in *Proceeding of IEEE Personal Indoor and Mobile Radio Communications Conference*, Japan, pp. 109–113, Sept. 1993.

17. S. Verdú, "Minimum probability of error for asynchronous Gaussian multiple access channels," *IEEE Transactions on Information Theory*, vol. 32, 1986.

18. R. Lupas and S. Verdú, "Linear multiuser detector for synchronous code division multiple access channels," *IEEE Transactions on Information Theory*, vol. 35, no. 1, pp. 123–136, Jan. 1989.

19. R. Lupas and S. Verdú, "Near-far resistance of multiuser detectors in asynchronous channels," *IEEE Transactions on Communications*, vol. 38, no. 4, pp. 496–508, Apr. 1990.

20. J. Proakis, *Digital Communications*, Mc-Graw Hill, New York, NY, U.S.A., 3rd ed., 1995.

21. S. Haykin, *Adaptive Filter Theory*, Prentice Hall, Upper Saddle River, NJ, U.S.A, third ed., 1996.

22. U. Madhow and M. Honig, "MMSE interference suppression for direct-sequence spread-spectrum CDMA," *IEEE Transactions on Communications*, vol. 42, no. 12, pp. 3178–3188, Dec. 1994.

23. M. Honig, U. Madhow, and S. Verdú, "Blind adaptive multiuser detection," *IEEE Transactions on Information Theory*, vol. 41, no. 4, pp. 994–960, July 1995.

24. S. Miller, "An adaptive direct-sequence code-division multiple-access receiver for multiuser interference rejection," *IEEE Transactions on Communications*, vol. 43, no. 2, pp. 1746–1755, Feb. 1995.

25. H. Ge, "Adaptive schemes of implementing the LMMSE multiuser detector for CDMA," in *Proceeding of IEEE International Conference on Communications*, Montreal, Canada, June 1997.

26. Y. Bar-Ness, "The bootstrap decorrelating algorithm: A promising tool for adaptive separation of multiuser CDMA signals," in *Proceeding of the 7th*

Tyrrhenian International Workshop on Digital Communication, invited paper, Viareggio, Italy, Sept. 1995.

27. Y. Bar-Ness and J. B. Punt, "Adaptive bootstrap multi-user CDMA detector," *special issue on "Signal Separation and Interference Cancellation for Personal, Indoor and Mobile Radio Communications," Wireless Personal Communications*, vol. 3, no. 1-2, pp. 55–71, 1996.

28. Y. Bar-Ness and N. Waes, "The complex bootstrap algorithm for blind separation of QAM multiuser CDMA signals," *Wireless Personal Communications*, vol. 12, 2000.

29. A. Haimovich, Y. Bar-Ness, and R. Manzo, "A stochastic gradient-based decorrelation algorithm with applications to multicarrier-CDMA," in *Proceeding of IEEE Vehicular Technology Conference*, pp. 464–468, 1995.

30. M. Visser and Y. Bar-Ness, "Adaptive reduced complexity multi-carrier CDMA (MC-CDMA) structure for downlink PCS," *European Transactions on Telecommunications*, 1999.

31. M. Visser and Y. Bar-Ness, "Joint multiuser detection and frequency offset correction for downlink MC-CDMA," in *Proceeding of IEEE Global Telecommunications Conference*, Brazil, Dec. 1999.

32. N. Yee and J. Linnartz, "Wiener filtering of Multi-Carrier CDMA in a Rayleigh fading channel," in *Proceeding of IEEE Personal Indoor and Mobile Radio Communications Conference*, The Hagues, The Netherlands, Sept. 1994.

33. A. Chouly, A. Brajal, and S. Jourdan, "Orthogonal multicarrier techniques applied to direct sequence spread spectrum CDMA systems,"

34. P. Jung, F. Berens, and J. Plechinger, "Joint detection for multicarrier CDMA mobile radio systems - part I: system model, part II: Detection techniques," in *Proceeding of IEEE International Symposium on Spread Spectrum Techniques and Applications*, pp. 991–995,996–1000, 1996.

35. S. Kaiser, *Multi-Carrier CDMA mobile radio systems-analysis and optimization of detection, decoding, and channel estimation*, PhD thesis, Germany, 1998.

36. S. Hara and R. Prasad, "Design and performance of multicarrier CDMA system in frequency-selective Rayleigh fading channels," *IEEE Transactions on Vehicular Technology*, vol. 48, no. 5, pp. 1584–1595, Sept. 1999.

37. T. Ottosson and A. Svensson, "Multi-rate schemes in DS/CDMA systems," in *Proceeding of the IEEE Vehicular Technology Conference*, pp. 1006–1010, July 1995.

38. T.-H. Wu and E. Geraniotis, "CDMA with multiple chip rates for multi-media communications," in *Proceeding of the 28th Annual Conference on Information Sciences and Systems*, U.S.A., pp. 992–997, Mar. 1994.

39. C.-L. I and R. Gitlin, "Multi-code CDMA wireless personal communications networks," in *Proceeding of the IEEE International Conference on Communications*, pp. 1060–1064, June 1995.

40. C.-L. I and R. Gitlin, "Performance of multi-code CDMA wireless personal communications networks," in *Proceeding of the IEEE Vehicular Technology Conference*, pp. 907–911, July 1995.

41. U. Mitra, "Comparison of ML-based detection for two multi-rate access schemes for CDMA communications," *IEEE Transactions on Communications*, vol. 47, no. 1, pp. 64–77, Jan. 1999.

42. M. Saquib, R. Yates, and N. Mandayan, "Decorrelating detectors for a dual rate synchronous DS/CDMA channel," *Wireless Personal Communications*, pp. 197–216, May 1999.

43. J. Chen and U. Mitra, "Analysis of decorrelator-based receivers for multi-rate DS/CDMA communications," *IEEE Transactions on Vehicular Technology*, vol. 48, no. 6, pp. 1966–1983, Nov. 1999.

44. H. Ge, "Multiuser detection for intergrated multi-rate CDMA," in *Proceeding of the IEEE International Conference on Information, Communications and Signal Processing*, Singapore, pp. 858–862, Sept. 1997.

45. J. Ma and H. Ge, "Modified multi-rate detection for frequency selecitve rayleigh fading CDMA channels," in *Proceeding of IEEE Personal Indoor and Mobile Radio Communications Conference*, Boston, MA, pp. 1304–1308, Sept. 1998.

46. J. Ma and H. Ge, "Multi-rate LMMSE detectors for asynchronous multi-rate CDMA systems," in *Proceeding of the IEEE International Conference on Communications*, pp. 714–718, June 1998.

47. N. Yee and J. Linnartz, "Wiener filtering of Multi-Carrier CDMA in a Rayleigh fading channel," in *Proceeding of IEEE Personal Indoor and Mobile Radio Communications Conference*, The Netherlands, Sept. 1994.

48. Y. Bar-Ness, J. Linnartz, and X. Liu, "Synchronous multi-user multi-carrier CDMA communications system with decorrelating interference canceler," in *Proceeding of IEEE Personal Indoor and Mobile Radio Communications Conference*, The Netherlands, pp. 184–188, Sept. 1994.

49. A. Bahai and G. Fettweis, "Results on multi-carrier CDMA receiver design," in *Proceeding of IEEE International Conference on Communications*, vol. 2, U.S.A., pp. 915–918, Jun. 1995.

50. M. Visser and Y. Bar-Ness, "Adaptive Multi-Carrier CDMA (MC-CDMA) structure for downlink PCS," in *Proceeding of the 9th Tyrrhenian International Workshop on Digital Communication*, Italy, Sept. 1997.

51. M. Visser, *Adaptive Interference Cancellation Techniques for Multicarrier Modulated Systems*, PhD thesis, New Jersey Institute of Technology, 1999.

52. S. Wijayasuriya, G. Norton, and J. McGeehan, "A sliding window decorrelating receiver for multiuser DS-CDMA mobile radio networks," *IEEE Transactions on Vehicular Technology*, vol. 45, no. 3, pp. 503–521, 1996.

53. M. Juntti and B. Aazhang, "Finite memory-length linear multiuser detection for asynchronous CDMA communications," *IEEE Transactions on Communications*, vol. 45, no. 5, pp. 611–622, May 1997.

54. H. Ge and Y. Bar-Ness, "Multi-shot approach to multiuser separation and interference suppression in asynchronous CDMA," *Wireless Personal Communications*, pp. 15–16, 2000.

55. N. van Waes and Y. Bar-Ness, "Adaptive algorithm for the multishot matched filtering multiuser detector in a multipath Rayleigh fading environment," in *Proceeding of IEEE Vehicular Technology Conferencethe*, Canada, pp. 184–188, May 1998.

56. U. Madhow, "Blind adaptive interference suppression for the near-far resistant acquisition and demodulation of direct-sequence CDMA signals," *IEEE Transactions on Communications*, vol. 45, no. 1, pp. 124–136, Jan. 1997.

57. U. Madhow, "MMSE interference suppression for timing acquisition and demodulation in direct-sequence CDMA systems," *IEEE Transactions on Communications*, vol. 46, no. 8, pp. 1065–1075, Aug. 1998.

58. P. Zong, Y. Bar-Ness, and J. Chan, "Adaptive multi-shot multiuser detection for asynchronous MC-CDMA using bootstrap algorithm," in *Proceeding of International Workshop On Multi-Carrier Spread-Spectrum*, Germany, Sept 1999.

59. P. Zong, Y. Bar-Ness, and J. Chan, "Joint adaptive multi-user detection and time tracking in the uplink of MC-CDMA system," in *Proceeding of 34th Annual Conference on Information Sciences and Systems*, Princeton, NJ, Mar 2000.

60. P. Zong, K. Wang, and Y. Bar-Ness, "Partial sampling MMSE interference suppression in asynchronous multi-carrier CDMA system," to appear in *IEEE Journal on Selected Areas in Communicatioins.*

61. P. Zong, K. Wang, and Y. Bar-Ness, "A novel partial sampling MMSE receiver for uplink multi-carrier CDMA," in *Proceeding of IEEE Vehicular Technology Conference*, Rhodes, Greece, May 6-9 2001.

62. K. Wang, P. Zong, and Y. Bar-Ness, "A reduced complexity partial sampling MMSE receiver for asynchronous MC-CDMA systems," submitted to *IEEE Global Telecommunications Conference*, 2001.

63. P. Zong, Y. Bar-Ness, and J. Chan, "Performance analysis of a dual-rate synchronous MC-CDMA system," in *Proceeding of IEEE Global Telecommunications Conference*, San Francisco, CA, Nov 2000.

64. P. Zong and Y. Bar-Ness, "Performance of a variable spreding length (VSL) dual-rate MC-CDMA system," in *Proceeding of 35th Annual Conference on Information Sciences and Systems*, Baltimore, MD, Mar 2001.

65. P. Zong, K. Wang, and Y. Bar-Ness, "Performance improvement for low-rate signal in a dual-rate MC-CDMA system with frequency-selective Rayleigh fading channel," submitted to *the 4th International Symposium on Wireless Personal Multimedia Communications*, Aalborg, Denmark, Sept. 2001.

66. W. Jakes, Jr., *Microwave Mobile Communications*, John Wiley and Sons, New York, NY, U.S.A., 1974.

67. C. Lee and Y. Bar-Ness, "Convergence and stability analysis of the adaptive bootstrap CDMA multi-user detector," in *IEEE Communication Theory Mini-Conference*, pp. 168–171, 1999.

68. J. Hagenauer, "Source-controlled channel decoding," *IEEE Transactions on Communications*, vol. 43, no. 9, pp. 2449–2457, Sept. 1995.